



THE HONG KONG
POLYTECHNIC UNIVERSITY

香港理工大學

Pao Yue-kong Library

包玉剛圖書館

Copyright Undertaking

This thesis is protected by copyright, with all rights reserved.

By reading and using the thesis, the reader understands and agrees to the following terms:

1. The reader will abide by the rules and legal ordinances governing copyright regarding the use of the thesis.
2. The reader will use the thesis for the purpose of research or private study only and not for distribution or further reproduction or any other purpose.
3. The reader agrees to indemnify and hold the University harmless from and against any loss, damage, cost, liability or expenses arising from copyright infringement or unauthorized usage.

IMPORTANT

If you have reasons to believe that any materials in this thesis are deemed not suitable to be distributed in this form, or a copyright owner having difficulty with the material being included in our database, please contact lbsys@polyu.edu.hk providing details. The Library will look into your claim and consider taking remedial action upon receipt of the written requests.

MODELLING AND ANALYSIS OF
MATERIAL REMOVAL
CHARACTERISTICS IN COMPUTER
CONTROLLED ULTRA-PRECISION
POLISHING

CAO ZHONGCHEN

Ph.D

The Hong Kong Polytechnic University

2016

The Hong Kong Polytechnic University

Department of Industrial and Systems Engineering

**Modelling and Analysis of Material Removal
Characteristics in Computer Controlled
Ultra-precision Polishing**

CAO Zhongchen

A thesis submitted in partial fulfilment of the requirements
for the degree of Doctor of Philosophy

September 2015

CERTIFICATE OF ORIGINALITY

I hereby declare that this thesis is my own work and that, to the best of my knowledge and belief, it reproduces no material previously published or written, nor material that has been accepted for the award of any other degree or diploma, except where due acknowledgement has been made in the text.

_____ (Signed)

CAO ZHONGCHEN (Name of student)

ABSTRACT

Abstract of thesis entitled "Modelling and Analysis of Material Removal Characteristics in Computer Controlled Ultra-precision Polishing" submitted by CAO ZHONGCHEN in September 2015 for a doctor of philosophy degree at The Hong Kong Polytechnic University.

Computer Controlled Ultra-precision Polishing (CCUP) based on fluid jet polishing (FJP) and bonnet polishing (BP) with multi-axis machining is an enabling technology which can fabricate ultra-precision freeform surfaces with sub-micrometre form accuracy and surface roughness in the nanometre range, especially for the fabrication of difficult-to-machine and ferrous materials, which are not amenable using other ultra-precision machining technologies such as single-point diamond turning and raster milling. However, CCUP is a complex process which relies heavily on the planning of the process steps in terms of the use of the polishing conditions and polishing fluid on specific materials being cut. It is found that the material removal analysis is clearly a fundamental element in achieving the corrective polishing and optimization of the polishing process.

Nowadays, the acquisition of tool influence functions still depends largely on the expensive trial-and-error approach when new materials, new surface designs or new polishing parameters are used. Although studies on polishing mechanisms and nano-mechanics are still sparse, there is a need for methods and tools for modelling and simulation which can simulate and predict the effect of different polishing

parameters on the material removal characteristics and surface generation in CCUP.

To meet this need, this thesis describes a theoretical and experimental study of material removal characteristics and surface generation in CCUP. It is divided into three parts. Firstly, Taguchi trials were conducted to identify the optimal level of combination and the significance of the individual operational parameters in fluid jet polishing and bonnet polishing. Hence, a series of experiments was performed to investigate the effects of the process parameters on the material removal characteristics in fluid jet polishing (FJP) as well as the material removal mechanism in bonnet polishing. The results not only provide an important means for better understanding the effect of the factors affecting the polishing process, but also provide the basis for the establishment of theoretical models for the prediction and simulation of the material removal characteristics and surface generation in CCUP.

Secondly, a comprehensive computational fluid dynamic (CFD)-based erosion model was developed by a combination of CFD simulation, erosion model, and experimental research so as to predict the material removal characteristics and surface generation in fluid jet polishing. In the computational fluid dynamic simulations, an Eulerian-Eulerian-Lagrangian method is used which treats the water and air as an Eulerian phase and the particles as Lagrangian particles. The coupled discrete phase model (DPM) and the volume of fluid (VOF) model are used to describe the multiphases in the FJP process. This CFD model also presents the application of the $k-\omega$ model, together with the level set method, to describe the slurry/air interface in the commercial finite element analysis package FLUENT. After solving the stream

flow characteristics, the motion of individual particles is also calculated in order to obtain more accurate predictions of the trajectories of individual particles impacting on the surface. The predicted results are used to integrate with the developed erosion model for the prediction of the material removal characteristics. Hence, the polishing path planning is determined based on the desired surface integrity of the optical surface to be generated using the data of the material removal characteristics. Finally, a theoretical model is built for predicting and simulating the surface generation in FJP. A series of spot and pattern polishing tests as well as simulation experiments by the theoretical model were conducted. The results not only show that the theoretical model predicts well for the surface generation under different polishing conditions but also helps to gain a better understanding of the polishing process in FJP.

In the third part, a multi-scale theoretical model was established for predicting and characterizing the material removal characteristics and surface generation in bonnet polishing based on contact mechanics, kinematics theory and abrasive wear mechanism. Specifically, the pressure and velocity distributions are determined based on the kinematics theory and contact mechanics at the macro scale, and the pad topography which affects the contact ratio and hence the material removal rate at the micro scale, while the micro- or nano-sized abrasive particles scratch the surface at the nano scale. The model developed in this study attempts to capture much of the basic physics of the polishing process including the tool radius, polishing depth, head speed, *precess* angle, pad topography, polishing time, particle shape, slurry concentration, and the mechanical properties of the pad and workpiece. Experimental

results show that the theoretical model predicts well that the material removal amount which increases with increasing *precess* angle and tool offset, depends linearly on the head speed and slurry concentration. A pattern test was also conducted to validate the surface generation model.

The originality and significance of this research lies in the provision of CFD-based modelling of the material removal characteristics and surface generation for fluid jet polishing and multi-scale modelling of the material removal characteristics and surface generation for bonnet polishing. The successful development of the theoretical model helps greatly to make the CCUP process more predictive, so as to further optimize the manufacturing process for different work materials without the need for costly trial and error polishing tests. Moreover, this is the first of its kind in which the deterministic model has been successfully built which acquires much of the basic physics of the polishing process. This contributes significantly to form the theoretical basis for the better understanding of the polishing process.

PUBLICATIONS ARISING FROM THE THESIS

Journal Papers

[1] **Cao, Z.C.** and Cheung C.F., “Theoretical Modelling and Analysis of the Material Removal Characteristics in Fluid Jet Polishing”, *International Journal of Mechanical Sciences*, Vol.89, pp.158–166 (2014).

[2] **Cao, Z.C.**, Cheung, C.F. and Kong, L.B. “Computational fluid dynamics–based analysis of material removal characteristics in fluid jet polishing”, *Proceeding of IMechE, Part B, Journal of Engineering Manufacture*, in press (2014).

[3] **Cao, Z.C.** and Cheung, C.F. "An Experimental Study of Effect of Process Parameters on the Tool Influence Function for Fluid Jet Polishing", *Key Engineering Materials*, Vol.679, pp.91-96 (2016)..

[4] **Cao, Z.C.**, Cheung, C.F. and Ren M.J. “Modelling and Characterization of Surface Generation in Fluid Jet Polishing”, *Precision Engineering - Journal of the International Societies for Precision Engineering and Nanotechnology*, Vol. 43, pp. 406-417 (2016).

[5]. **Cao, Z.C.** and Cheung, C.F. “Multi-scale Modelling and Simulation of Material Removal Characteristics in Computer-controlled Bonnet Polishing”, *International Journal of Mechanical Sciences*, Vol. 106, pp.147-156 (2016).

[6] **Cao, Z.C.**, Cheung, C.F. and Zhao X., “A theoretical and experimental

investigation of material removal characteristics and surface generation in bonnet polishing”, *Wear* , Vol. 360-361, pp.137-146 (2016).

Conference Papers

[1] **Cao, Z.C.** and Cheung, C.F. “A Study of Finite Element Analysis of Materials Removal Characteristics in Fluid Jet Polishing”, Proceedings of the 2nd International Conference on Abrasive Processes (ICAP 2014), Sept 9 – Sept 10, Cambridge, UK, (2014).

[2] **Cao, Z.C.** and Cheung, C.F. “A Study of Materials Removal Mechanisms for Fluid Jet Polishing Using Computational Fluid Dynamics Modelling”, Proceedings of the 29th ASPE Annual Meeting, Nov 9- Nov 14, Boston, Massachusetts, USA,, pp.496-501 (2014).

[3] Cheung, C.F., **Cao Z.C.** and Ho L.T. “A Study of Factors Affecting Material Removal in Computer-controlled Bonnet Polishing”, Proceedings of the 30th ASPE Annual Meeting, Austin, TX, pp.547-550 (2015).

ACKNOWLEDGEMENTS

I would like to express my sincerely thanks to my supervisor, Prof. Benny C.F. Cheung, Professor of the Department of Industrial and Systems Engineering and Associate Director of the Partner State Key Laboratory of Ultra-precision Machining Technology of The Hong Kong Polytechnic University, for his valuable guidance, encouragement, instruction, and support. Without his consistent and professional guidance, this thesis could not have been completed.

Many thanks are also due to the Research Grants Council (RGC) of the Government of the Hong Kong Special Administrative Region (HKSAR) for the financial support of the research work under Project No.: PolyU 5132/11E. Moreover, I would also like to express my gratitude to the staff in the Partner State Key Laboratory of Ultra-precision Machining Technology of The Hong Kong Polytechnic University, especially Dr Lingbao Kong, Dr Mingjun Ren and Dr Lai Ting Ho, for their sharing of invaluable research experience and providing kind technical support throughout my study. Many thanks are also due to my friends, Dr Shaojian Zhang, Dr Haitao Wang, Dr Hao Wang, Dr Sujuan Wang, Dr Guoqing Zhang, Dr Gaobo Xiao, Mr Da Li, Mr Mingyu Liu, Mr Peng Huang and Mr Zhiwei Zhu, for their kind encouragement and support during the research study.

Finally, my heartfelt thanks are due to my beloved family: my wife Ms. Yongtong Chen and my parents for their loving consideration and support given to me throughout my study. Without their understanding and patience, this study could not have been successfully completed.

TABLE OF CONTENTS

ABSTRACT	i
PUBLICATIONS ARISING FROM THE THESIS.....	v
ACKNOWLEDGEMENTS.....	vii
TABLE OF CONTENTS	viii
LIST OF FIGURES	xiv
LIST OF TABLES.....	xix
CHAPTER 1 INTRODUCTION	2
1.1 Background of the Study	2
1.2 Research Objectives and Significance.....	4
1.3 Organization of the Thesis.....	5
CHAPTER 2 LITERATURE REVIEW	7
2.1 Overview of the Polishing Processes.....	7
2.1.1 Computer Numerical Control Polishing	8
2.1.2 Float Polishing	9
2.1.3 Elastic Emission Machining.....	10
2.1.4 Stressed Lap Polishing	11
2.1.5 Chemical Mechanical Polishing.....	12

2.1.6 Magneto-rheological Finishing	14
2.2 Computer Controlled Ultra-precision Polishing (CCUP)	15
2.2.1 Fluid Jet Polishing (FJP)	16
2.2.2 Bonnet Polishing (BP)	19
2.2.3 Polishing Machine and Accessories	22
2.2.4 Polishing Process Parameters	25
2.3 Material Removal Mechanisms in Polishing Processes	27
2.3.1 Process Components affecting Material Removal in Polishing	29
2.3.1.1 <i>Work Materials</i>	29
2.3.1.2 <i>Polishing Slurry</i>	31
2.3.1.3 <i>Polishing Tool</i>	32
2.3.2 Material Removal Mechanisms involving Brittle Fracture	33
2.3.2.1 <i>Models for Abrasion by Brittle Fracture</i>	35
2.3.2.2 <i>Models for Erosion by Brittle Fracture</i>	36
2.3.3 Material Removal Mechanisms without Brittle Fracture	37
2.3.3.1 <i>Models for Abrasion by Plastic Deformation</i>	39
2.3.3.2 <i>Models for Erosion by Plastic Deformation</i>	40
2.4 Surface Measurement and Characterization Methods	42
2.4.1 Surface Topography	43
2.4.2 Surface Integrity	45
2.5 Modelling and Simulation of Polishing Processes	47

2.5.1 Computational Fluid Dynamics	47
2.5.2 Finite Element Methods	49
2.5.3 Discrete Element Method.....	50
2.5.4 Kinematic Models	51
2.5.5 Molecular Dynamic Models.....	52
2.6 Summary	54
 CHAPTER 3 EXPERIMENTAL INVESTIGATION OF FACTORS	
AFFECTING MATERIAL REMOVAL IN COMPUTER CONTROLLED	
ULTRA-PRECISION POLISHING	
57	
3.1 Introduction	57
3.2 Taguchi Approach for Material Removal Analysis in Fluid Jet Polishing.....	58
3.2.1 Experimental Design.....	58
3.2.2 Results and Discussion.....	59
3.2.2.1 <i>Optimal Process Parameters</i>	59
3.2.2.2 <i>Confirmatory Experiments</i>	62
3.3 Effect of Polishing Parameters on Material Removal Rate in Fluid Jet	
Polishing.....	63
3.3.1 Experimental Design.....	63
3.3.2 Results and Discussion.....	65
3.3.2.1 <i>Effect of Polishing Time</i>	65
3.3.2.2 <i>Effect of Slurry Pressure</i>	66

3.3.2.3 <i>Effect of Standoff Distance</i>	67
3.3.2.4 <i>Effect of Impingement Angle</i>	68
3.3.2.5 <i>Effect of Slurry Concentration</i>	70
3.3.2.6 <i>Effect of Particle Size</i>	71
3.4 Taguchi Approach for Material Removal Analysis in Bonnet Polishing.....	73
3.4.1 Experimental Design.....	73
3.4.2 Results and Discussion.....	75
3.4.2.1 <i>Optimal Process Parameters</i>	75
3.4.2.2 <i>Confirmatory Experiments</i>	78
3.5 A Study of Material Removal Mechanisms in Bonnet Polishing	79
3.5.1 Experimental Design.....	79
3.5.2 Results and Discussion.....	82
3.5.2.1 <i>Pad-abrasive-workpiece Interactions</i>	82
3.5.2.2 <i>Hydrodynamic Lubrication</i>	84
3.5.2.3 <i>Effect of Polishing Time</i>	86
3.6 Summary	87
CHAPTER 4 CFD-BASED MODELLING OF MATERIAL REMOVAL	
CHARACTERISTICS AND SURFACE GENERATION IN FLUID JET	
POLISHING	91
4.1 Introduction	91
4.2 Polishing Mechanisms.....	92

4.2.1 Material Removal Mechanism	92
4.2.2 Surface Generation Mechanism	93
4.3 Theoretical Modelling of Material Removal in FJP	94
4.3.1 Computational Fluid Dynamics Modelling.....	95
4.3.1.1 <i>Dynamic Flow Description</i>	97
4.3.1.2 <i>Turbulence Flow Description</i>	98
4.3.1.3 <i>Multiphase Flow Description</i>	98
4.3.1.4 <i>Lagrangian Particle Phase</i>	99
4.3.1.5 <i>Boundary Conditions and Other Numerical Settings</i>	100
4.3.2 Spatial Distribution of Abrasive Particles	101
4.3.3. Erosion Model for a Single Particle	103
4.3.3.1. <i>The Normal Component of Kinetic Energy</i>	105
4.3.3.2. <i>The Tangential Component of Kinetic Energy</i>	106
4.3.3 Polishing Tool Path Planning	109
4.4 Experimental and Simulated Results	112
4.4.1 Experimental Verification of the Material Removal Model using Various Polishing Conditions	112
4.4.2 Experimental Verification of the Surface Generation Model for the Various Materials	119
4.5 Summary	127

CHAPTER 5 MULTI-SCALE MODELLING OF MATERIAL REMOVAL

CHARACTERISTICS AND SURFACE GENERATION IN BONNET	
POLISHING	129
5.1 Introduction	129
5.2 Multi-scale Material Removal Model.....	130
5.2.1. Modelling of Surface Velocity Distribution	131
5.2.2. Modelling of Pressure Distribution.....	133
5.2.3. Single-particle Wear Model	136
5.2.4. Active Number of Abrasive Particles	139
5.3 Surface Generation Model	141
5.4 Results and Discussion.....	143
5.4.1. Experimental Verification of the Multi-scale Material Removal Model ..	143
5.4.2. Experimental Verification of the Surface Generation Model by the Pattern Test	148
5.5 Conclusions	151
CHAPTER 6 OVERALL CONCLUSIONS	153
CHAPTER 7 SUGGESTIONS FOR FUTURE RESEARCH	159
REFERENCES.....	162

LIST OF FIGURES

Figure 2.1 Schematic of the float polishing apparatus using a diamond turned thin lap (Namba et al., 1987).....	10
Figure 2.2 Schematic model of elastic emission machining (EEM) (Mori et al., 1990)	11
Figure 2.3 Top view of the 60-cm stressed lap; 12 actuators are attached to the periphery of the plate, and twisting and bending moments are produced by the arrangement of the tension bands in sets of equilateral triangles (West et al., 1994).	12
Figure 2.4 Schematic diagram of the chemical mechanical polishing.....	14
Figure 2.5 Schematic diagram of MRF machine (Harris, 2011).....	15
Figure 2.6 Schematic illustration of Fluid Jet Polishing (FJP)	17
Figure 2.7 Schematic illustration of bonnet polishing (BP).....	21
Figure 2.8 Key components of a CCUP system (for case Zeeko polishing machine) .	23
Figure 2.9 Configure of polishing tools in CCUP	24
Figure 2.10 Factors affecting surface generation in CCUP	26
Figure 2.11 Illustration of the wear behaviors in the polishing process (Hutchings, 1993).....	28
Figure 2.12 A schematic diagram of vent crack formation under point indentation, showing plastic deformation and median vent form during loading (+) half-cycle, lateral vents during unloading (-) half-cycle (Lawn and Wilshaw, 1975).....	34

Figure 2.13 Schematic illustration of material removal in a brittle material by the extension of lateral cracks from beneath a plastic groove (Evans, 2011).	.35
Figure 2.14 Slip line fields for the deformation of a perfectly plastic deformation caused by the sliding of a rigid two-dimensional wedge from right to left (Challen and Oxley, 1979).	38
Figure 2.15 Approximate current capabilities of various residual stress measurement techniques-the destructive tech are shaded grey (Withers et al., 2008).	46
Figure 3.1 S/N ratio factor response graphs for the volumetric material removal rate	62
Figure 3.2 Mean factor response graphs for the volumetric material removal rate	62
Figure 3.3 The effect of the polishing time on: (a) the width; (b) the maximum depth and (c) the volumetric removal of the polished spot	65
Figure 3.4 The effect of the slurry pressure on: (a) the width; (b) the maximum depth and (c) the volumetric material removal rate of the tool influence function	67
Figure 3.5 The effect of the standoff distance on: (a) the width; (b) the maximum depth and (c) the volumetric material removal rate of the tool influence function	68
Figure 3.6 The 3D surface topography of the influence function for the different impingement angle	69
Figure 3.7 The effect of the impingement angle on: (a) the maximum depth and (b) the volumetric material removal rate of the tool influence function	70
Figure 3.8 The effect of the slurry concentration on: (a) the width; (b) the maximum	

depth and (c) the volumetric material removal rate of the tool influence function.....	71
Figure 3.9 The effect of the particle size on: (a) the width; (b) the maximum depth and (c) the volumetric material removal rate of the tool influence function (TIF)	72
Figure 3.10 S/N ratio factor response graphs for the volumetric material removal rate	77
Figure 3.11 Mean factor response graphs for the volumetric material removal rate ...	77
Figure 3.12 Schematic diagram of bonnet polishing and workpiece-pad interactions	81
Figure 3.13 The effect of polishing time and on the surface generation.....	87
Figure 4.1 Material removal mechanism in the FJP process: (a) fluid conditions in the case of perpendicular impact and (b) abrasive particles' erosion conditions	93
Figure 4.2 Flowchart of theoretical modelling of the material removal characteristics and surface generation by FJP	95
Figure 4.3 (a) Boundary conditions of the CFD model and (b) experimental setup of fluid jet polishing.....	101
Figure 4.4 Schematic illustration of erosion behaviour of impacting particle	104
Figure 4.5 Tool path planning for Fluid Jet Polishing	110
Figure 4.6 Schematic diagram of the theoretical modelling of the surface generation in the raster and cross polishing.....	111
Figure 4.7 (Colour online) Distribution of normal impact fluid field (for 10 bar): (a)	

phase field, (b) pressure field (Pa), (c) velocity field (m/s) and (d) concentration field (kg/m ³)	115
Figure 4.8 Comparison between the measured and simulated results for the maximum depth of the influence function	116
Figure 4.9 Surface matching and error evaluation process for case C3.....	118
Figure 4.10 Comparison between the measured and simulated results of TIF for various materials.....	122
Figure 4.11 Comparison between the experimental and simulated results for NiCu.	123
Figure 4.12 Comparison between the experimental and simulated results for steel..	124
Figure 4.13 Comparison between the experimental and simulated results for BK7..	125
Figure 4.14 Schematic diagram of the error evaluation process for the pattern test..	126
Figure 4.15 Evaluated form error of the testing patterns for different materials	127
Figure 5.1 Flowchart of the theoretical modelling process of the material removal characteristics and surface generation for bonnet polishing	131
Figure 5.2 (a) Graphical illustration and (b) detailed geometry in the polishing area by the polishing bonnet on flat surface.....	132
Figure 5.3 Sketch of pressure distribution for the rolling bonnet	135
Figure 5.4 Geometry of contact between an abrasive particle and a surface: (a) and (b) in elevation; (c) in plan view	138
Figure 5.5 Schematic diagram of the surface generation model in raster polishing ..	142
Figure 5.6 Results of the simulation and experiment in terms of 3D topography, X-Z profile and Y-Z profile (for the case of B3).....	146

Figure 5.7 Comparison of experimental data and predicted data under different polishing conditions.....	147
Figure 5.8 Comparison between the measured and simulated results of the pattern test	149
Figure 5.9 Evaluated prediction error of the testing pattern for bonnet polishing	150

LIST OF TABLES

Table 2.1 Typical parameters in FJP system (Beaucamp et al., 2014c)	26
Table 2.2 Typical parameters in BP system (Zeng and Blunt, 2014).....	27
Table 2.3 Comparison of salient feature of ductile metals and brittle non-metals (Komanduri et al., 1997).....	30
Table 2.4 Resolution and range of some surface measurement instruments (Lonardo et al., 1996; Whitehouse, 1994).....	44
Table 3.1 The fixed process parameters in Taguchi design of experiments.....	58
Table 3.2 The control factors and levels in the Taguchi design of experiments	59
Table 3.3 Experimental results for the volumetric material removal rate.....	60
Table 3.4 S/N ratio factor response data for material removal rate	61
Table 3.5 Results of confirmation trials	63
Table 3.6 The parameter settings for studying the effect of individual parameter on the material removal in fluid jet polishing	64
Table 3.7 The fixed process parameters in Taguchi design of experiments.....	74
Table 3.8 The control factors and levels in Taguchi design of experiments	74
Table 3.9 Experimental results for the volumetric material removal rate.....	76
Table 3.10 S/N ratio factor response data for material removal rate	78
Table 3.11 Results of confirmation trials	79
Table 3.12 Polishing parameters used in the experimental studies.....	81
Table 3.13 Experimental results for studying interactions between the pad, workpiece and particles	83

Table 3.14 Experimental results used to study hydrodynamic conditions in the contact area.....	85
Table 4.1 The experimental parameters used for validation of theoretical modelling	113
Table 4.2 Evaluated results of polished spots under different polishing conditions ..	119
Table 4.3 Parameters for tool influence function tests and pattern tests of FJP.....	120
Table 5.1 The process parameters of polishing experiments	144
Table 5.2 Parameters used in the present simulation	145
Table 5.3 Parameters for generating surface pattern	149

CHAPTER 1 INTRODUCTION

1.1 Background of the Study

Nowadays, ultra-precision freeform surfaces are widely used in various applications, such as photonics, optics, opto-mechanics-electronics, biomedical engineering, etc. (Cheung et al., 2012). The application of freeform surfaces is moving swiftly in the automotive industry from aesthetics of car body panels and interiors (Qin et al., 2006) to advanced optical reflectors for use with LED lighting (Hu et al., 2012). Freeform femoral knee components are used together with matching freeform tibial insets in biomedical engineering to create a load-bearing surface that imitates the action of the human knee joint (Curodeau et al., 2000). The compliance between these bearing surfaces, their geometry accuracy, and surface finish of such components can improve the wear resistance, and hence increases the lifetime of the medical implant (Blunn et al., 1997). The aforementioned components are commonly composed of difficult-to-machine materials such as Ti-6Al-4V ELI, titanium, and, in the case of optical moulds, NiCu alloys that have a hardness and tensile strength enabling them to withstand the press forces applied to the mould during the manufacture of components.

To meet the optical surface requirements for a wide range of freeform optics, these surfaces are usually fabricated by ultra-precision machining technologies with sub-micrometre form accuracy and nanometric surface finish (Cheung et al., 2007). However, the geometrical complexity of freeform surfaces brings considerable challenges for precision manufacturing of them. Currently, many ultra-precision

machining technologies can be potentially applied to produce complex freeform surfaces, such as ultra-precision diamond machining technologies (Brinksmeier et al., 2012), ultra-precision grinding (Brinksmeier et al., 2010), Magneto-Rheological Finishing (MRF) (Kordonski et al., 2004), Ion Beam Figuring (IBF) (Yongqi and Bryan, 2000), etc. However, freeform machining technologies based on diamond machining are susceptible to significant tool wear problems due to the high hardness and brittle nature of most difficult-to-machine materials being cut. Although ultra-precision grinding and milling methods are developed to suit the fabrication of some kinds of freeform optics or difficult-to-machine materials, they cannot meet the surface requirements for a wide variety of optical applications (Fang et al., 2013). MRF is not suitable for magnetic materials while IBF has a relatively low material removal rate. As a result, the fabrication of these complex surfaces with sub-micrometric form accuracy and nanometric surface finish, especially for hard and difficult-to-machine materials, has always been a challenge to the optics industry. There is a need for the development of more economic and controllable methods to fabricate these complex surfaces.

Computer Controlled Ultra-precision Polishing (CCUP) based on fluid jet polishing and bonnet polishing is an enabling multi-axis machining technology which is capable of fabricating ultra-precision freeform surfaces with sub-micrometre form accuracy and surface roughness in the nanometre range. They are especially useful for machining difficult-to-machine and ferrous materials, which are not amenable using other ultra-precision machining technologies such as single-point diamond turning

and raster milling (Cheung et al., 2010a). The advantage of CCUP over the conventional multi-axis CNC mechanical machining such as micro-milling include: (a) CCUP can machine difficult-to-machine materials and brittle materials; (b) high surface accuracy with sub-micrometre form error and nanometre surface finish; (c) less tool wear; (d) different structure generation by modifying the tool influence function instead of changing the cutting tool to have different geometries. CCUP provides an important means for machining difficult-to-machine materials such as Ti-6Al-4V Steel and Titanium with sub-micrometre form accuracy and surface finish in the nanometric range.

The process control of the surface roughness and form accuracy of the polishing process is indispensable for achieving the ever increasing tolerances and to meet the demand for high-precision optical, biomedical, and automotive components (Hilerio et al., 2004; Jacobs, 2007). Although polishing is one of the machining processes with the longest history, research on the polishing mechanics, especially nano-mechanics, during the polishing process has received relatively little attention. As a result, in-depth research work on the polishing mechanics is indispensable to gain a better understanding of the surface generation mechanism for CCUP.

1.2 Research Objectives and Significance

CCUP is a complex process and our understanding of the material removal characteristics, surface generation and the factors affecting the surface generation of CCUP is far from complete. As a result, the research study aimed to conduct extensive

experimental and theoretical investigations on the material removal and surface generation mechanisms in CCUP and the research objectives are summarized as follows:

- (i) To identify the optimal level combination and the significance of the individual operational parameters on the material removal and surface generation in CCUP.
- (ii) To investigate the material removal and surface generation mechanisms in CCUP.
- (iii) To establish a theoretical model for the prediction and simulation of the material removal characteristics and surface generation in the CCUP process.
- (iv) To verify the established model through a series of simulation and polishing experiments.

1.3 Organization of the Thesis

The thesis is divided into seven chapters. In Chapter 1, an introduction about the background, research motivation and objectives of the study is given. In Chapter 2, a literature review is conducted to review and summarize the state-of-the-art and up-to-date research in the field of Computer Controlled Ultra-precision Polishing (CCUP). It focuses on an overview of the polishing process, and hence highlights computer numerical control polishing, material removal mechanisms in polishing processes, surface analysis and measurement methods, as well as the state-of-the-art research on modelling and simulation of polishing processes.

In Chapter 3, the Taguchi method is used to design experiments to investigate the

factors affecting the material removal rate in fluid jet polishing and bonnet polishing, and a series of experiments was also performed to investigate the effect of the polishing parameters on the material removal characteristics in fluid jet polishing and study the material removal mechanism in bonnet polishing.

A theoretical model is built for predicting and characterizing the materials removal characteristics and surface generation in FJP based on an appropriate combination of computational fluid dynamics (CFD) modelling, erosion model and experimental study in Chapter 4. A series of spot and pattern polishing tests as well as simulation experiments were also conducted. Chapter 5 presents a multi-scale theoretical model for the prediction and simulation of the material removal characteristics and surface generation in bonnet polishing. The model is established based on the study of contact mechanics, kinematics theory, wear mechanisms, as well as the relative and cumulative removal process of surface generation in bonnet polishing. Finally, an overall conclusion to the thesis is presented in Chapter 6 while some suggestions for future work are made in Chapter 7.

CHAPTER 2 LITERATURE REVIEW

2.1 Overview of the Polishing Processes

Polishing is commonly accomplished without allowing fine abrasive particles to produce brittle fractures on the target surfaces, while the material is removed little by little only by means of plastic deformation, to finally produce a super mirror surface (Toshiro, 2006). Due to increasing surface requirements for functional enhancement, polishing is well-known as a critical technology for the manufacturing of functional materials within various components, such as optical components, electronic components and precision machinery components. During the past few decades, much research has been performed on the study of surface figuring in computer controlled polishing (CCP) (Schinhaerl et al., 2008b and 2008c; Xi and Zhou, 2005), as well as the polishing mechanics (Evans et al., 2003a; Gee, 1996; Xie and Bhushan, 1996), and the analysis methods which include finite element methods (FEM), quasi-static model, fluid dynamic when analyzing the slurries and probability statistics.

For polishing process, most of the techniques involve case-based expert planning systems, neural networks and data mining (Su et al., 2005), fuzzy logic, neuro-fuzzy (Wu and Wang, 2009) and the neuro-Taguchi-based method (Wang and Chou, 2005). However, most previous research on the polishing process has focused on studying the processing of surface roughness, while the study of the effect of geometrical or form accuracy has received relatively few attention. Moreover, our current understanding of the material removal characteristics and mechanisms is still far away

from complete. This is particularly true for ultra-precision, multi-axis, freeform polishing, which is used for finishing ultra-precision freeform components requiring precise control across the polished surface to maintain high form accuracy and good surface finish so as to enhance the functionality of the polished components. The following is a brief review of various types of Computer Controlled Polishing (CCP) implemented for optical fabrication, including CCP with small and large rotating tools, float polishing, elastic emission machining (EEM), stressed lap polishing, ion beam figuring (IBF), chemical-mechanical polishing (CMP), magneto-rheological finishing (MRF), etc.

2.1.1 Computer Numerical Control Polishing

Computer numerical control (CNC) polishing has been developed for polishing large aspheric optics (Beckstette et al., 1989; Jones and Rupp, 1990). Jones and Plante (1987) reported on a computer numerical control (CNC) polishing machine that uses a small rotating tool with a diameter of 75-100 mm, constructed the desired optical contour in an iterative process and then carried out an interferometric inspection. The form error of the large optic (up to four metres in size) was reduced from 24 μm to 1.9 μm . The surface roughness of a 1 metre diameter optic could be achieved at 1.6 nm root-mean-square value. Despite the fact that CCP can be used for grinding or polishing aspheric optics, the polishing process still requires a lot of iterations of craft polishing and measurement. The fundamental problem is that CCP requires a range of sub-aperture tools of decreasing size to change the mismatch between polishing tool

and the workpiece. Each tool can be designed to correct form errors in general but in turn then superimposes its own signature and leaves a spatial-frequency signature.

2.1.2 Float Polishing

In 1977, Namba and Tsuwa (1977) first reported on the float polishing technique as shown in Figure 2.1. The rotational sample and ultra-precision diamond turned tin lap are submerged in a slurry composed of free abrasives and deionized water. A suitable amount of polishing slurry is supplied and stored in a circular-shaped frame along the outer edge of the thin tip. Polishing is advanced by pressing the workpiece against the tool surface. Both of them are submerged in the polishing slurry and the flatness of the workpiece is copied from the thin tip. Relatively soft materials (e.g. Sn, Cu, nylon) are commonly used for the polishing lap, and a hydrodynamic film should be maintained between the polished surface and the lap. Float polishing gradually came to be used for polishing single crystal and polycrystalline Mn-Zn ferrites for magnetic heads (Namba and Tsuwa, 1978), metals (e.g. Steel, NiCu, iron) (Namba and Tsuwa, 1980) and optical materials (e.g. glasses, quartz, fused silica) (Bennett et al., 1987; Namba et al., 1987; Namba et al., 1989). Despite floating polishing succeeding in making atomically flat surfaces on various materials without subsurface damage, it still encompasses lots of problems for float polishing spherical or aspherical shapes as well as polycrystalline and composite materials.

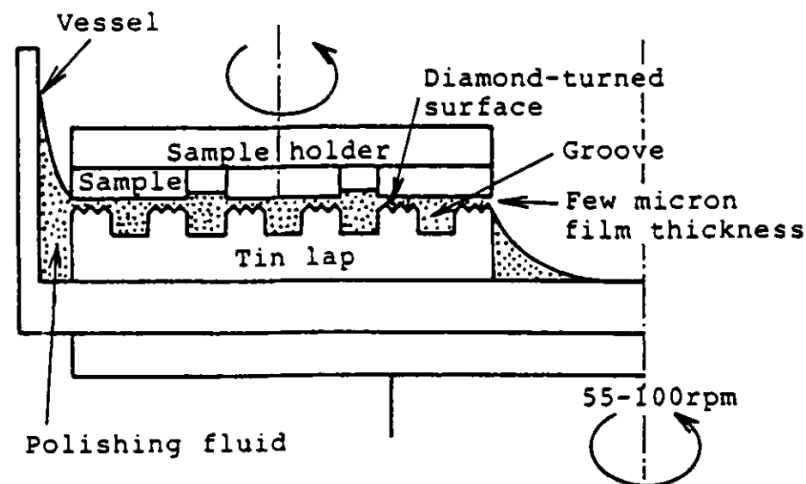


Figure 2.1 Schematic of the float polishing apparatus using a diamond turned thin lap

(Namba et al., 1987)

2.1.3 Elastic Emission Machining

Mori et al. (1976) of Osaka University suggested that the impact of ultrafine particles on the target surface may possibly cause material removal at the atomic level. Hence, the surface finish of the polished workpiece can be in close proximity to the order of atomic dimensions. They termed this noncontact machining process Elastic Emission Machining (EEM) which makes use of a rotating polyurethane ball to bring fine powder particles to the workpiece surface for shaping and polishing as shown in Figure 2.2. The workpiece is submerged in slurry made up of sub-micrometre sized abrasive particles and pure water. A fluid gap of about $1\ \mu\text{m}$ is maintained between the bottom of the sphere and the workpiece (Mori et al., 1987, 1988). The abrasive particles are accelerated by the flow of fluid in the gap, but gradually leave the fluid flow lines to intercept the workpiece surface. With a negligible contribution to the material removal associated with the mechanical energies of the power particles and

the abrasive pad, the chemical reaction between the polished surface and the abrasive particles cause the removal of surface atoms from the target surface and then atomic-order surface roughness without crystallographic damage can be achieved (Kanaoka et al., 2008; Mori et al., 1990).

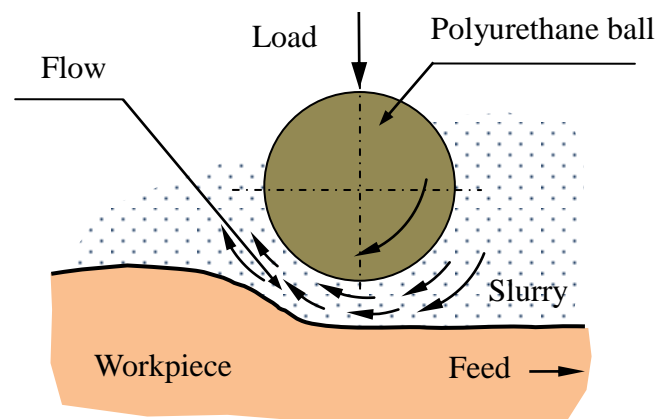


Figure 2.2 Schematic model of elastic emission machining (EEM) (Mori et al., 1990).

2.1.4 Stressed Lap Polishing

Since the mid-1980s stressed lap polishing has been developed by the Steward Observatory Mirror Laboratory for large astronomical telescope mirrors (Martin et al., 1990). The stressed-lap polishing tool is about 1/3 the size of the polished part and actively deformed by on-board electromechanical actuators to conform to the local target surface. The deformation of the stressed-lap tool is changed by the application of bending and twisting edge moments as shown in Figure 2.3. In principle, the large stiff tool used in stressed lap polishing is advantageous since it produces high material removal rates and natural smoothing over a wide range of spatial frequencies, and it

also provides one solution to the fundamental problem of the mismatch between large polishing tools and highly aspheric optical surfaces. However, the tool is complex and has to be re-built for new jobs which can only be warranted for high capital-value jobs.

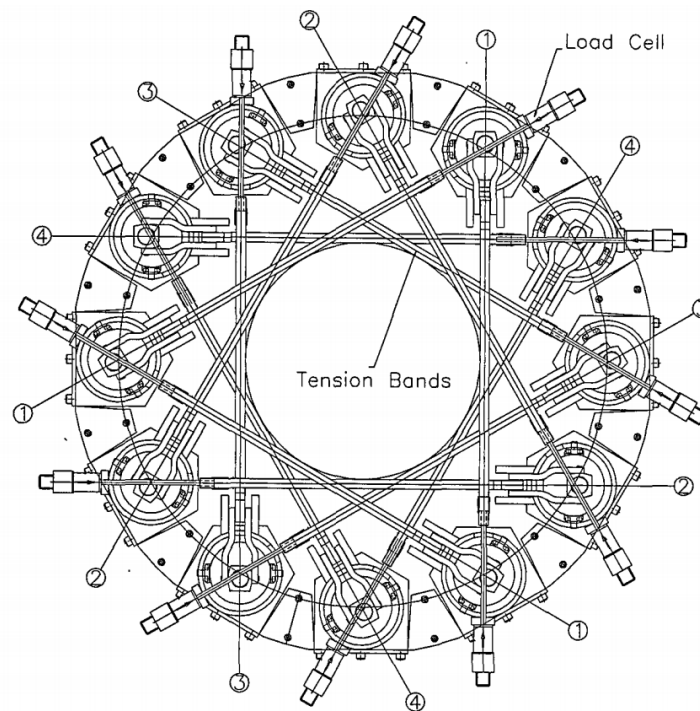


Figure 2.3 Top view of the 60-cm stressed lap; 12 actuators are attached to the periphery of the plate, and twisting and bending moments are produced by the arrangement of the tension bands in sets of equilateral triangles (West et al., 1994).

2.1.5 Chemical Mechanical Polishing

Several terms are found to describe the process of chemical mechanical polishing (CMP) which include chemo-mechanical, mechano-chemical polishing (Vora et al., 1982) and chemical-mechanical polishing (Nanz and Camilletti, 1995). These

distinctions are created by researchers to highlight the major factor resulting from the material removal in the polishing process. In chemo-mechanical polishing, the key factor removing the material is chemical action and then the reaction product is removed by the following mechanical action. In contrast, mechano-chemical polishing emphasizes mechanical action followed by chemical action. In chemical mechanical polishing, a specific fluid is used to generate chemical reaction with the workpiece surface and this reaction product is later removed by the mechanical action of the abrasive particles. The difference between chemo-mechanical polishing and chemical mechanical polishing is that the chemical reaction that occurs between the abrasives and the work material in chemo-mechanical polishing is different from that formed between the fluid and the work material in chemical mechanical polishing.

CMP introduced by IBM has been widely accepted as the manufacturing technology for planarization in submicron integrated circuit manufacturing and the ultra-fine finishing of electronic materials (Venkatesh et al., 1995). In the CMP process, a rotating wafer is pressed face-down by a carrier against a rotating, compliant, polishing pad flooded with a polishing slurry as shown in Figure 2.4. The polishing slurry including abrasive particles and chemical reagents is dragged into the interface between the pad and the workpiece. The assorted action of chemical reagents, polishing pad and abrasive particles leads to material removal and polishing of the workpiece surface (Zhao and Chang, 2002). Many problems with CMP come up including low productivity, uncontrollable removal rate, non-uniformity and defects (Tichy et al., 1999). There are a number of physical mechanisms at work in CMP, and

the improvement of the process requires a study from a number of perspectives of science and engineering.

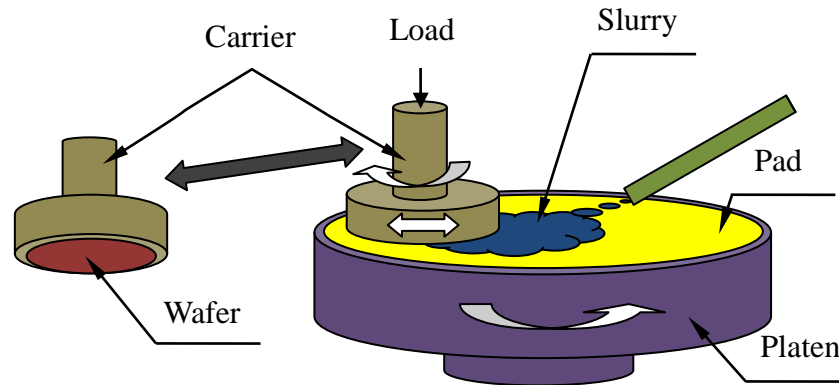


Figure 2.4 Schematic diagram of the chemical mechanical polishing

2.1.6 Magneto-rheological Finishing

Magneto-rheological finishing (MRF) invented by Kordonsky et al. (1995) is a computer-controlled polishing process. As shown in Figure 2.5, MRF makes use of the property of magneto-rheological (MR) fluid to change the viscosity in the presence of a magnetic field. The MR fluid (consisting of iron particles, deionized water and stabilizing agents) is firstly mixed, pumped, and conditioned in their liquid states. After that, it is converted into a semi-solid state to create a stable and conformable polishing pad. This polishing pad is applied to polishing the workpiece surface (Jacobs et al., 1995).

The magneto-rheological polishing fluid is jetted on the rim of a rotating wheel, which transports the fluid to the polishing zone. The workpiece to be polished is controlled precisely by the motion controller and immersed into the ribbon of fluid.

The wheel rim and the polished surface form a converging gap which is exposed to the magnetic field, and the rotating wheel generates a flow of magnetically stiffened MR polishing fluid through the converging gap. Such flow results in high shear stress in the contact zone and material removal over a portion of the workpiece surface. MRF is a deterministic and flexible figuring and polishing process that has a relatively high, stable and controllable removal rate while creating a smooth, damage-free surface finish for a wide variety of materials (Dumas, 2005).

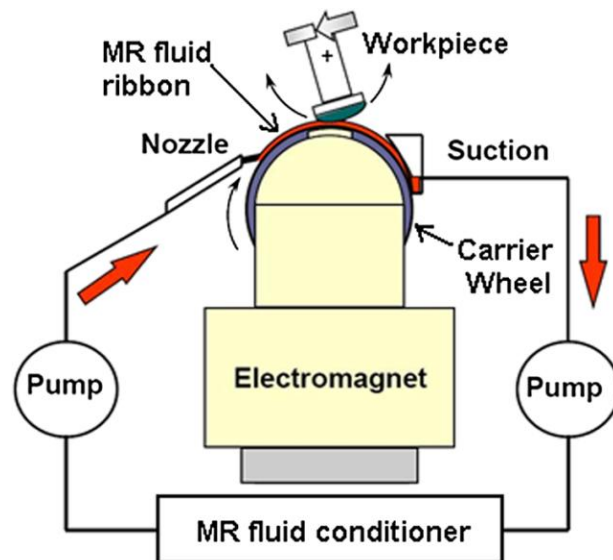


Figure 2.5 Schematic diagram of MRF machine (Harris, 2011)

2.2 Computer Controlled Ultra-precision Polishing (CCUP)

To meet the optical surface requirements for a wide variety of freeform optics, these surfaces are usually fabricated by ultra-precision machining technologies with sub-micrometre form accuracy and nanometric surface finish (Cheung et al., 2007). At present, CCUP is an enabling technology which is capable of fabricating

ultra-precision freeform surfaces with sub-micrometre form accuracy and surface roughness in the nanometre range. CCUP is used to machine difficult-to-machine and ferrous materials, which are not amenable to be machined by other ultra-precision machining technologies such as single-point diamond turning and raster milling (Cheung et al., 2010a).

In this study, CCUP was undertaken on a 7-axis CNC platform which allows bonnet polishing (BP) and fluid jet polishing (FJP) to be conducted. Both these processes can produce similar surface roughness but differences in surface texture after polishing (Ho et al., 2012). Fluid jet polishing is found to be effective in removing scratches and/or machine marks produced by other machining processes. It has the advantage of localized force and less heat generation, and the stable and controllable material removal function with very little tool wear and no edge effect problem, while bonnet polishing has the advantage of high polishing efficiency, mathematically tractable influence function, and flexibly controllable spot size with variable tool hardness (Bingham et al., 2000). As a result, the CCUP system combining the FJP and BP processes is an effective polishing method which shows great potential with regard to the application value in the fabrication of freeform components with sub-micrometre form accuracy and nanometric surface finish.

2.2.1 Fluid Jet Polishing (FJP)

Fluid jet polishing (FJP) was presented by Fahnle et al. (1998) in the 1990s with the advent of demands in optical finishing methods that can be applied locally to

polish optical surfaces of complex shapes. The principle of the FJP setup originated from two completely different techniques: abrasive slurry jet machining and bowl feed polishing. As shown in Figure 2.6, FJP is an intermediate method that bears a resemblance to the kinetic process engaged in abrasive water jet machining to guide a premixed slurry to the surface at low pressures for shaping and polishing (Fahnle and Brug, 1999a). Due to the low pressure applied, the material is removed little by little in the ductile mode and the less heat generated is promptly taken away by the jet fluid in the FJP process (Fahnle and Brug, 1999b). As a result, FJP is a promising technology which is becoming more widely used in the superfinishing of complex optical lenses, mirrors and moulds on a number of materials from glass to nickel (Beaucamp and Namba, 2013; Cheung et al., 2010a; Cheung et al., 2010b).

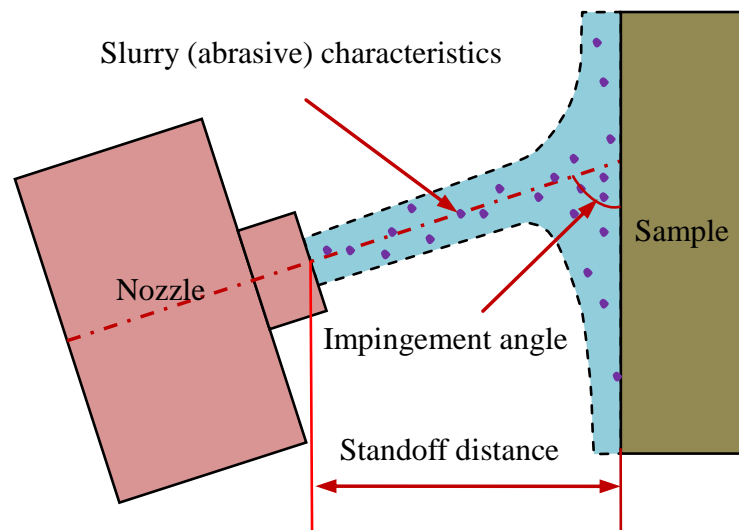


Figure 2.6 Schematic illustration of Fluid Jet Polishing (FJP)

It has been found that most of research carried out in the field of Fluid Jet Polishing has focused on the following areas:

- (i) Process modelling such as material removal mechanism modelling (Li et al., 2010), understanding the erosion mechanisms in the process (Shi et al., 2010) and surface characterization models (Fang et al., 2006a; Jafar et al., 2013a, 2013b).
- (ii) Introducing new operations for the FJP such as integrating with bonnet polishing to optimize the polishing process chain (Ho et al., 2012), selecting polishing parameters to optimize the FJP process (Tsai et al., 2008), machining and polishing of difficult-to-machine materials such as glass (Booij et al., 2002), stainless steel (Tsai et al., 2008; Yan et al., 2008), Electroless Nickel (ENi) and binderless Tungsten Carbide (WC) (Beaucamp et al., 2011).
- (iii) Development of new systems for the FJP process, such as stable pressure systems (Beaucamp et al., 2012), online monitoring systems (Brug et al., 2003; Brug et al., 2002) and nozzle shape optimization.
- (iv) Development of new applications for the FJP process such as Jules Verne (Booij et al., 2003) and submerged jet polishing (Shi et al., 2011). Although many researchers have carried out scientific research which attempts to improve the surface finish of polished surface and gain a fundamental understanding of the polishing process involved in FJP (Beaucamp et al., 2012; Cheung et al., 2010a; Tsai et al., 2008), our understanding of polishing mechanisms is still far from complete. Moreover, relatively little attention has been received regarding the theoretical modelling of surface generation for FJP.

Due to the complex machining mechanisms, it is still difficult to model the

material removal characteristics and simulate the surface generation for FJP. Nowadays, the generation of a desired surface integrity of high-performance optical surface still depends largely on the expensive trial-and-error approach. As the optimal machining conditions and polishing strategy for ensuring good surface quality depend largely on the polishing environment as well as the work materials and the geometry of surfaces being polished, there is a need for the development of modelling and simulation methods and tools which can simulate and predict the effect of different factors on the surface generation in FJP.

2.2.2 Bonnet Polishing (BP)

Bonnet polishing was originally invented at London's Optical Sciences Laboratory and was then further developed by Zeeko Ltd. It has been exploited for commercial production of the IRP robotic polishing system (Walker et al., 2001). As shown in Figure 2.7, bonnet polishing is a computer controlled sub-aperture polishing process that actively controls the position and orientation of a spinning, inflated, membrane tool (the 'bonnet') as it sweeps through the polished surfaces (Walker et al., 2002a, 2002b). The polishing bonnet is covered with the polishing pad and the slurry is dragged by the porous polishing pad into the interface between the pad and workpiece. Bonnet polishing has the advantage of high polishing efficiency, mathematically tractable influence function, and flexibly controllable spot size with variable tool hardness (Bingham et al., 2000). As a result, bonnet polishing is one of the promising computer controlled ultra-precision polishing technologies which

shows great potential with regard to the application value in the fabrication of freeform surfaces with sub-micrometre form accuracy and nanometric surface finish.

Previous research work has always focused on the development and application of precess polishing processes (Walker et al., 2001, 2002a), edge control (Beaucamp et al., 2014a; Li et al., 2011), and tool path and dwell time optimization (Chaves-Jacob et al., 2013; Wang et al., 2014b). Since the surface generation of bonnet polishing can be considered as the convolution of the influence function and the dwell time map along the pre-specific tool path, a predictable and stable tool influence function and an optimized path generator are of paramount importance for a successful deterministic bonnet polishing process. For this reason, there is much recent research work focusing on the modelling of the influence function based on Preston's equation (Preston, 1927). Cheung et al. (2011) established a predictive model for the determination of the material removal characteristics with the assumption of a modified Gaussian distribution of the contact pressure in bonnet polishing. Li et al. (2013) and Wang et al. (2014a) calculated the pressure distribution in the contact area by the axisymmetric elastic solid model with finite element analysis (FEA). However the pressure on the polished surface is only related to the elastic deformation of the polishing tool in their model. Zeng and Blunt (2014) not only conducted experiments to understand the effects of process parameters on the material removal rate but also created a model by modifying the Preston equation based on experimental data so as to predict the volumetric material removal rate. In their model, the contact pressure was described by the Hertz solution with a correction

term. However, the pressure distribution and surface deformation predicted by Hertz's equations must be modified, when a slurry film is present and the polishing pad slides over the surface in the actual polishing process.

Moreover, the material removal characteristics in bonnet polishing are affected by various parameters which include tool radius, *precess* angle, polishing depth, head speed, tool pressure, polishing time, polishing cloth, slurry concentration, particle size and type, etc. However, the prediction model based on Preston's equation is only concerned with the velocity of polishing tool relative to the workpiece and the contact pressure between the polishing tool and the workpiece. Despite intensive research on theoretical and experimental investigation of bonnet polishing (Song et al., 2008), studies on the polishing mechanisms, especially on establishing deterministic models with consideration of all these operational parameters, are still far from complete.

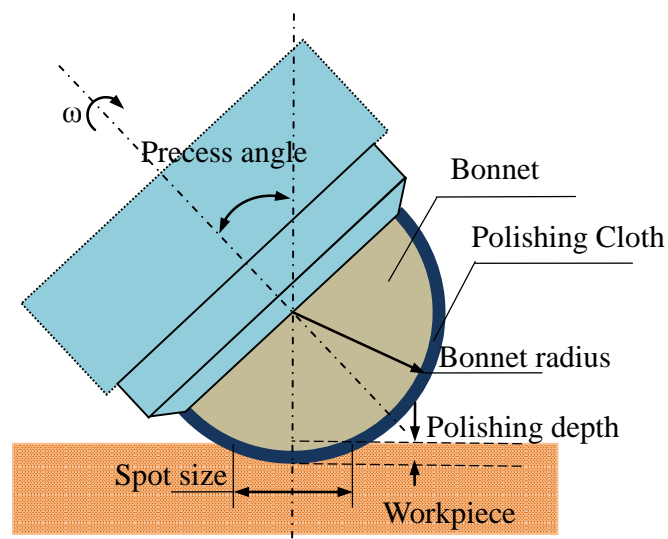


Figure 2.7 Schematic illustration of bonnet polishing (BP)

2.2.3 Polishing Machine and Accessories

Recently, the research and development of some freeform polishing machines have been reported in the manufacturing industry. Tam et al. (1999) used a PUMA 562 6-axis articulated robot with a 4 kg payload to polish a cylindrically shaped specimen for the verification of their tool path generation method. Zhao et al. (2000) developed an integrated robotic polishing system which is composed of a 'RV-M1' industrial robot, a force sensor and other ultrasonic vibration devices for machining free-form surfaces. However, due to the open-chain architecture, many freeform polishing systems established based on open architectural industrial robots possess quite poor dynamic performance and precision (Dong-Fang et al., 1995; Wang et al., 1999).

Since the parallel manipulators are well-known for high speed, high structural rigidity and high precision, they have been increasingly used in the innovative development of machining equipment for freeform polishing. Roswell et al. (2006) described a polishing system established at Ryerson University which contains an active polishing end effector and a hybrid robot. This system has five axes, including a gantry with two axes and a tripod with three axes. Kakinuma et al. (2013) developed a portable 5-axis parallel mechanism polishing machine which independently controls the x-y trajectory, tool posture and polishing force.

The success of ultra-precision freeform polishing technologies relies on high-precision polishing tools, an advanced control system and an excellent slurry delivery system. As shown in Figure 2.8, a conventional CCUP system is normally

composed of four major modules: the polishing tools unit, slurry management unit, motion control system and software unit.

The polishing tools unit contains the jet nozzle for fluid jet polishing and the polishing bonnet for bonnet polishing. Figure 2.9(a) shows a configuration of polishing nozzle in FJP. The polishing nozzle is responsible for transferring the kinetic energy of the abrasive slurry to the target surfaces for shaping and polishing. The size, the shape and the orientation of polishing nozzle can be used to control the material removal rate and hence the surface generation in FJP. Figure 2.9(b) shows a standard detachable polishing cloth stuck on the bonnet and slurry is sprayed on the workpiece surface. The material removal in bonnet polishing is accomplished by the interactions between the polishing pad, workpiece and abrasive particles.

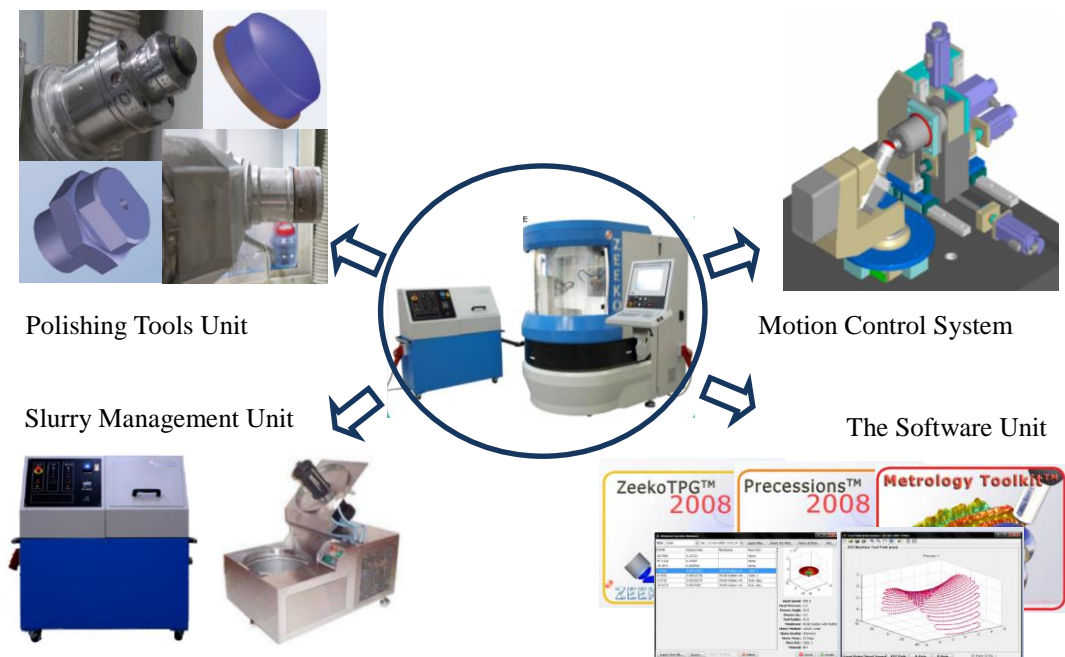


Figure 2.8 Key components of a CCUP system (for case Zeeko polishing machine)

In the slurry management unit, water, oil, or octanol are used frequently as liquid in the optical fabrication industry, and various concentrations of silicon carbide, aluminium oxide, diamond, glass beads or steel shot could be used as the abrasive particles. They are mixed with water to become a slurry by mechanically stirring in a tank. Hence this slurry is pumped from the tank using a low-pressure pump and then guided through a nozzle to the workpiece or polishing pad. After polishing the surface, the slurry is collected and guided back to the tank for re-use.

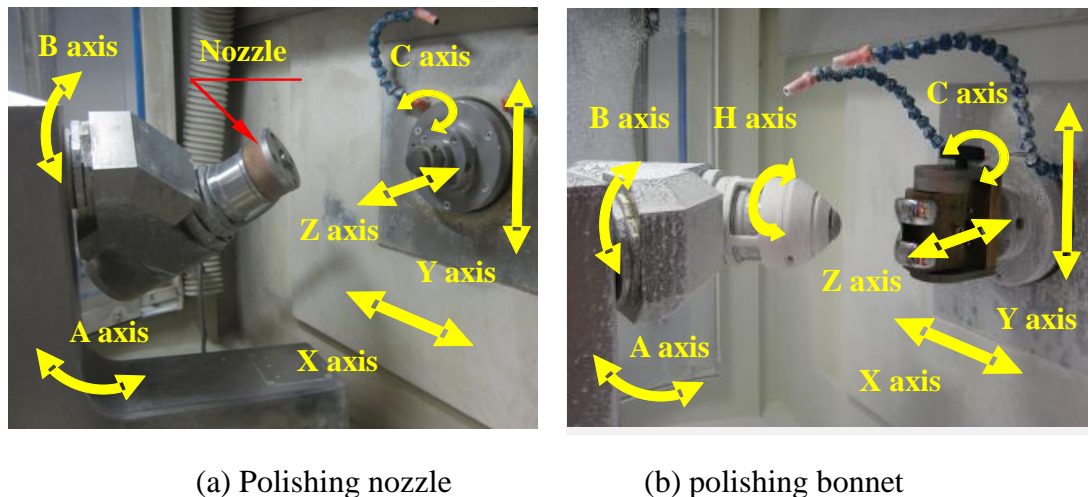


Figure 2.9 Configuration of polishing tools in CCUP

The motion control system is used to perform the defined polishing motion and to control the prescribed operational parameters. Small deviations in the prescribed values of these parameters must be corrected by the control system. In general, the machine structure motion is also controlled by a computerized numerical controller (CNC), which is programmed using standardized numerical control (NC) language.

The software unit is used to calculate the optimum dwell-time and spot-size map

by the input of the measurement data, the designed form, and the influence function data. The calculated results characterizing the footprint of the polishing tool are interpreted by the CNC controller as a varying speed along a predetermined tool path for the corrective polishing.

2.2.4 Polishing Process Parameters

The efficiency of the polishing process is related to polishing load, rotational velocity, polishing time, material property of the target surface and the polishing tool, and polishing medium (Aurich et al., 2013). A larger polishing load leads to a higher material removal rate (Su et al., 2001), but lower surface quality (Sun et al., 2000). The material removal process is more efficient when using a polishing medium with a higher viscosity (Fang et al., 2009). The initial state of the workpiece is also an important factor affecting the efficiency of the polishing process (Liu et al., 2010). In the CCUP system, the polishing process is affected by various parameters as shown in Figure 2.10. The typical parameters used in the CCUP system are listed in Table 2.1 and Table 2.2.

With the increasing demands for functional enhancement, it is of paramount importance to better understand how various polishing process parameters affect the ability to accurately produce a super-finished mirror surface with geometrically dimensional shapes in the nanometre order (Cheung et al., 2010a). The analysis of material removal characteristics is clearly a fundamental element in achieving the corrective polishing and optimization of the polishing process. Nowadays, the

acquisition of tool influence functions still depends mainly on the experience and skill of the machine operator through an expensive trial-and-error approach when the new materials and new surface designs or new machine tools are used.

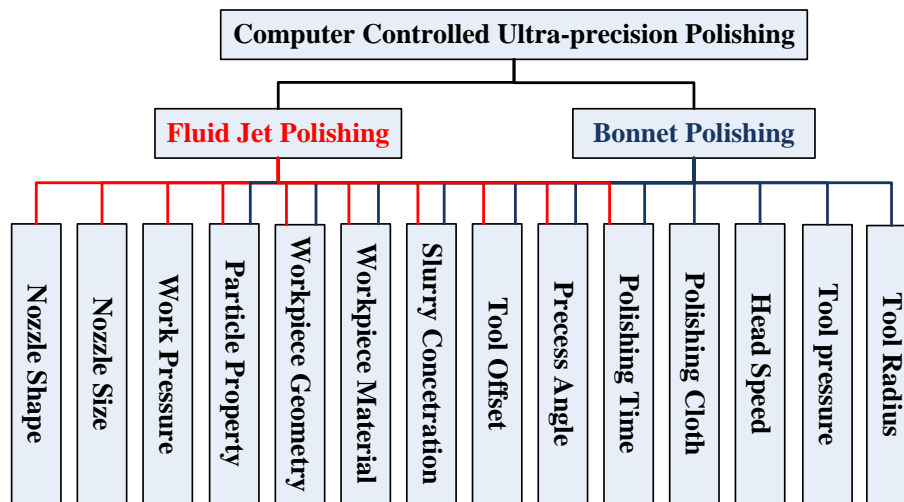


Figure 2.10 Factors affecting surface generation in CCUP

Table 2.1 Typical parameters in FJP system (Beaucamp et al., 2014c)

Parameters	Value
Pressure at nozzle	4-20 bar
Nozzle diameter	0.1-2.0 mm
Abrasive type	CeO ₂ , SiC, Al ₂ O ₃
Abrasive grit	0.2-50μm

It is interesting to note that studies on polishing mechanisms and nano mechanics are still sparse due to the nearly impossible observation of the interface between the polishing pad and the workpiece surface during the process. As the optimal cutting

conditions and polishing strategy for ensuring good surface quality depend largely on the environment of machining, work materials, and the geometry of surfaces being polished, there is a need for the research and development of modelling and simulation methods and tools which can simulate and predict the effect of polishing process parameters on surface generation.

Table 2.2 Typical parameters in BP system (Zeng and Blunt, 2014)

Parameters	Value
<i>Precess</i> angle	5-30 °
Head speed	300-1800 rpm
Tool offset	0.1-0.6 mm
Tool pressure	0.4-2 bar

2.3 Material Removal Mechanisms in Polishing Processes

Polishing is known as the process of macro-flattening and micro-smoothing of non-uniform surfaces using mechanical, chemical, electrolytic or thermal methods, or a synergistic combination of these methods (Chen, 2007). Kasai et al. (1990) simply summarized that material removal is caused with two things. One is a mechanical action including mechanically removing (cutting, scratching) and friction. The other one is a chemical action which includes dissolving and film formation. According to the relationship between the polishing tool and the workpiece during the process, the polishing methods can be classified under two conditions:

- (i) Contact condition which is similar to chemical mechanical polishing and bonnet polishing. A polishing pad is pressured against the target surface to contact directly or maintain a slurry film by controlling the polishing load.
- (ii) Noncontact condition which is similar to fluid jet polishing and ion beam figuring. The workpiece and the polishing tool have no contact and the material removal is controlled by the kinetic energy of the polishing medium.

In general, every polishing method can involve four components which include the work materials, polishing slurry and polishing tool. From the view of the mechanical behaviour, the wear of materials in the polishing process is mainly caused by the abrasive wear due to the abrasive-workpiece and abrasive-pad contact and/or erosion caused by hard particles striking the surface as shown in Figure 2.11. Since the material removal is extremely small in the order of sub-micrometres or less, mechanisms of abrasive wear or erosion in the polishing process can involve both plastic flow and brittle fracture owing to the polishing process parameters, even for brittle materials.

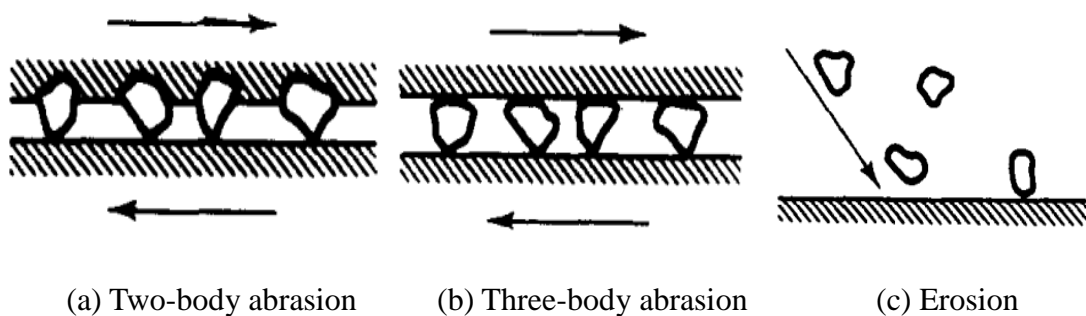


Figure 2.11 Illustration of the wear behaviors in the polishing process (Hutchings,

2.3.1 Process Components affecting Material Removal in Polishing

2.3.1.1 *Work Materials*

A broad range of work materials (e.g. ceramics, metals and their alloys and glasses) can be polished to a specified form error, surface accuracy and surface integrity to reach service requirements (Komanduri et al., 1997). As shown in Table 2.3, a qualitative comparison between ductile metals and brittle non-metals reveals the differences and complexities in polishing of the non-metals with fine abrasive particles as compared to metals and their alloys. The major differences in mechanical behaviour between the ceramics and metals arise from the different nature of the interatomic forces, i.e. ionic or covalent in ceramics, rather than metallic bonding. Ionic bonding, in ceramics such as MgO or Al₂O₃, leads to crystal structures with only a small number of independent slip systems available for dislocations, fewer than the five necessary to accommodate a general plastic strain. Covalent bonding, as in SiC, TiC or diamond, leads to very narrow dislocations which move only under high stress, even though five independent slip systems may exist.

As a result, the material removal of metals predominantly by plastic deformation is quite different from that of ceramics by microchipping or microcleavage, grain boundary cracking, grain dislodgments, etc. (Komanduri et al., 1999) during the finishing process. Although glass has similar brittleness to ceramics, the amorphous structure makes it possess different manufacturing characteristics as compared with metals and ceramics. As a result, many models developed based on the polishing of metals should be inappropriate for finishing of glass and ceramics.

Table 2.3 Comparison of salient feature of ductile metals and brittle non-metals
(Komanduri et al., 1997)

Property	Metals	Non-metals
Type of atomic bond	metallic no directionally	ionic/covalent bond directional
Crystal structure	high symmetry	low symmetry
Thermal expansion	high	low
Thermal conductivity	high	low
Density	high	low
Mode of deformation	high	low
Microstructure		
Intergranular structure	relative sample	complex
Porosity	Practically no pores	Generally pores remain because of the consolidation processes used
Purity	high purity can be obtained	high purity is difficult
Heat resistance	low to moderate	moderate to high
Chemical resistance	low	high
Strength considerations		
Toughness (MN/m ²)	210(carbon steel) 34 (Al alloys)	5.3 (Si ₃ N ₄)
Strain at fracture	5%	0.2%
Weibull index	20	5-20
Failure mechanism	Plastic deformation	Brittle fracture
Breaking energy (J/cm ²)	10	10 ⁻²
Thermal shock resistance	high	low

2.3.1.2 *Polishing Slurry*

A wide range of abrasive particles can be used extensively in the polishing process which include conventional abrasives (e.g. alumina, SiC, ZrO₂, B₄C) and superabrasives (e.g. diamond and cubic boron nitride) as well as soft abrasives for promoting chemo-mechanical action (e.g. MgO, ceria, fumed silica). These abrasive particles are used to chemically and/or mechanically remove the material from the target surface. The abrasive particles can be differentiated by a lot of factors which include chemical composition, particle hardness, particle shape, particle size and concentration. The effect of each of these factors may be significant or insignificant (Evans et al., 2003b).

It is well-known that erosion or abrasion in relation to polishing leads to higher wear rates when the particles have more than about 1.2 times the hardness of the surface (Hutchings, 1992). The shapes of abrasive particles also strongly affect the wear rates in the polishing process, with angular particles causing greater wear than rounded particles. The sizes of abrasive particles used in polishing cover a wide range from tens of nanometres to tens of micrometres. For a given weight percent, slurry with small diameter particles contains more particles than slurry with larger ones. The agglomeration of small particles also affects the average particle size and shape, and hence more or less affects the material removal.

Besides the abrasive particles, the fluid phase of the polishing slurry is also an important factor affecting the polishing efficiency and precision. Chemical

composition and physical properties are commonly used to characterize the fluid phase of the polishing slurry. The chemical compositions of fluids include water, oil, octanol, hydrocarbons and/or alcohols. Physical properties of the fluids including density, thermal conductivity and viscosity, is able to affect both material transport and fluid dynamics in the polishing process. These properties can be affected by pressure, temperature and changes in the chemical composition of the fluid (Evans et al., 2003b).

2.3.1.3 Polishing Tool

In contact polishing, a relatively soft pad is commonly used as the polishing tool and the common materials include pitch, leather, cloth, polyurethane or other polymeric materials with a hardness ranging from 10 to 50 Shore D (Sousa, 2014). These polishing tools impose the pressure and relative motion with respect to the target surface and affect slurry and swarf transport through the contact. Beaucamp et al. (2015; 2014b) proposed an innovatively shaped adaptive grinding (SAG) tool composed of several layers to finish freeform surfaces made of various difficult-to-machine materials with high efficiency. Enomoto et al. (2011) also proposed a double-layered polishing pad which attempted to achieve a high finishing efficiency by improving the surface flatness of the polishing tool. As a result, how to control the pad modulus and pad topography without deterioration to maintain the contact mechanics and fluid films may be functionally important in the contact polishing process.

In non-contact polishing processes, such as fluid jet polishing, the polishing tool shape and size can affect the expansion of the jetting slurry, and hence results in different fluid dynamic conditions or material removal rate. The inclination angle of the polishing tool also affects the shape of influence function, or corresponding surface characteristics (Shiou and Asmare, 2015).

2.3.2 Material Removal Mechanisms involving Brittle Fracture

When a high force is used to press hard angular particles against the surface of a brittle material, material of the target surface is primarily removed by brittle fracture, while material removal by means of plastic deformation is negligible. An appreciation of material removal mechanisms involving brittle fracture can be obtained by studying the indentation-sliding analysis conducted by Lawn et al. (1980, 1977).

Figure 2.12 shows the various stages of indention (loading and unloading) of a brittle material (Lawn and Wilshaw, 1975). The material under the tip of the sharp indenter is initially subjected to high stresses, which includes shear and hydrostatic compression, released by local plastic flow or densification around the tip, and so a small inelastic deformation zone is presented. When the loading on the indenter increases to a critical value, a deformation-induced flaw suddenly develops into a median vent crack. Further increase in loading causes the progressive extension of the median crack. On reducing the load of the median vent crack, it closes but does not heal. Further unloading causes the formation and growth of lateral vent cracks. This is the consequence of the residual elastic stresses due to the relaxation of the deformed

material close to the region of contact. As unloading is finished, the lateral cracks continue their extension towards the specimen surface, eventually, it may lead to the removal of material by chipping.

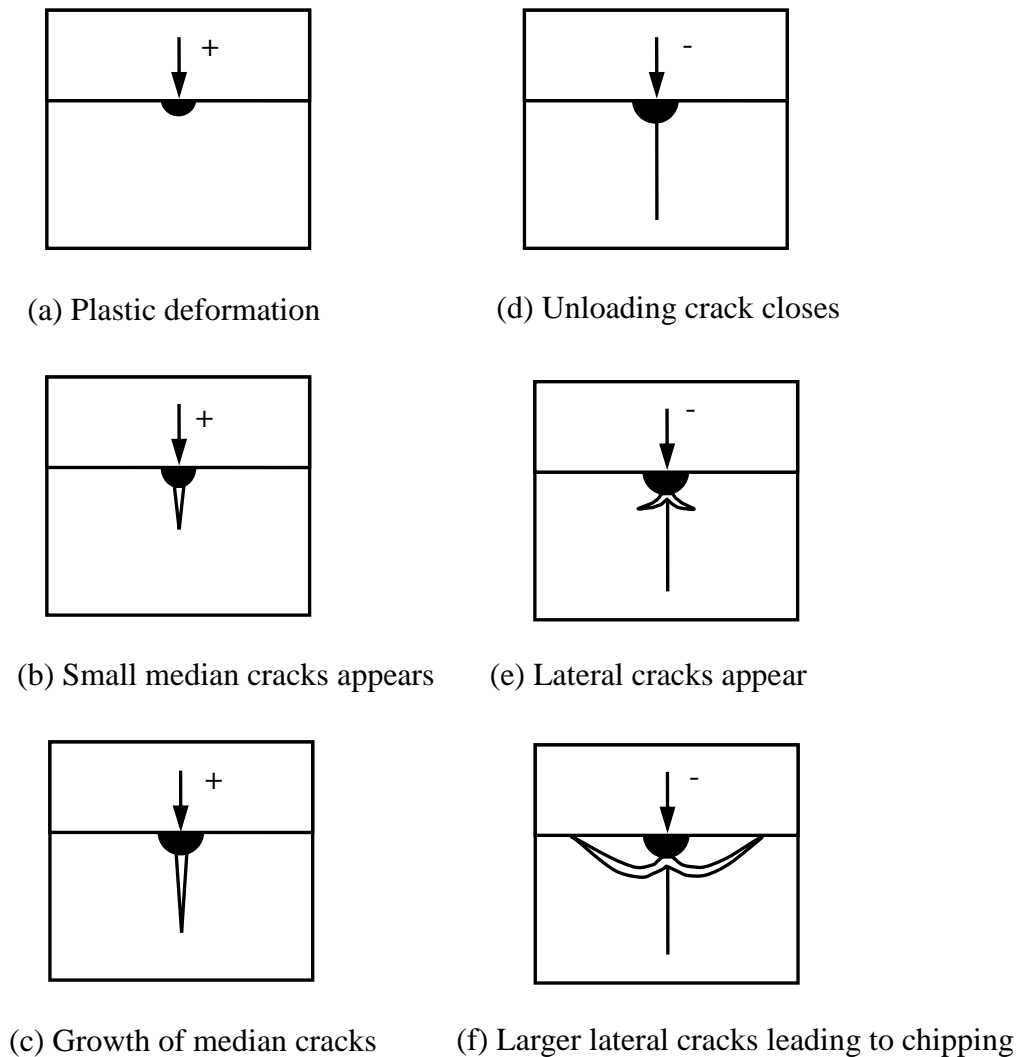


Figure 2.12 A schematic diagram of vent crack formation under point indentation, showing plastic deformation and median vent form during loading (+) half-cycle, lateral vents during unloading (-) half-cycle (Lawn and Wilshaw, 1975).

2.3.2.1 Models for Abrasion by Brittle Fracture

The amount of material removal by the abrasive wear of brittle materials is determined by the extent of the lateral fracture. As shown in Figure 2.13, a plastic groove is formed as a sharp particle slides over the target surface, while lateral cracks extend towards the target surface from the base of the subsurface deformed region due to the residual stresses released by the deformed material (Marshall et al., 1982). Marshall et al. (1982) assumed that the region bounded by the lateral cracks and the target surface enables material removal as chips and the volume of this region is estimated to be the volumetric material removal rate. Evans (2011) presented another analysis of the same model. But they used alternative methods of estimating the sideways spread of the cracks and the depth of the lateral cracks and hence obtained slightly different results.

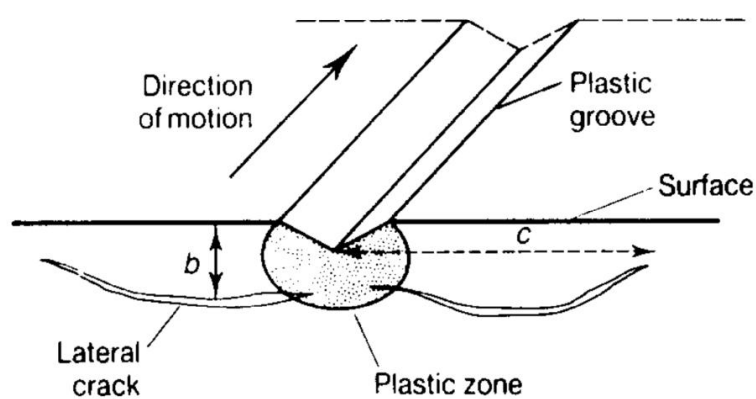


Figure 2.13 Schematic illustration of material removal in a brittle material by the extension of lateral cracks from beneath a plastic groove (Evans, 2011).

The models for abrasion by brittle fracture described have several important

features in common. Their predicted material removal rates are significantly higher than those associated with plastic deformation. This suggests that the material removal rates due to brittle fracture should increase more promptly than linearly with the applied load. The predicted results of the models show an inverse correlation between material removal rate and some power of the fracture toughness of the work material. The models also suggest that brittle fracture will take place only under the condition that applied load on abrasive particles exceeds the critical load.

2.3.2.2 Models for Erosion by Brittle Fracture

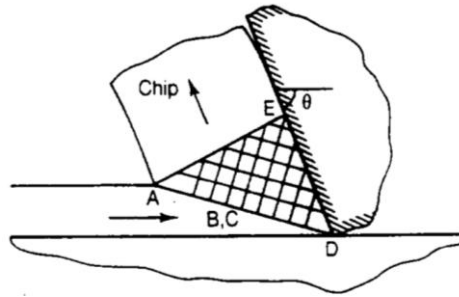
The high-speed impact of an erosive particle can cause brittle fracture and the material removal occurs due to the formation and intersection of cracks. Hutchings (1993) stated that the normal impact of particles causes the most serious cracking and hence the most rapid erosion. Models for erosion by brittle fracture have been developed mainly for normal impact, with some assumptions that the intersection of lateral cracks is the only agent for material removal. In these models, the contact force during the impact of a particle is generally calculated in two ways: (i) the quasi-static hardness of the surface is assumed as the pressure resisting penetration; (ii) a dynamic wave-propagation model is used to determine the impact pressure (Ruff and Wiederhorn, 1979). The calculated contact force is then used in semi-empirical analysis to predict the extent and depth of the lateral cracks formed, and hence obtain the volumetric material removal rate. The two different methods of calculating the contact force result in slight differences of predicted results.

The models discussed so far assume that the material being eroded is homogeneous and isotropic. So far, there is still a lack of satisfactory predictive models for the erosion of heterogeneous material. Moreover, the understanding of the mechanisms of material removal reported in many studies is unclear and the models based on lateral cracking do not provide accurate predicted results.

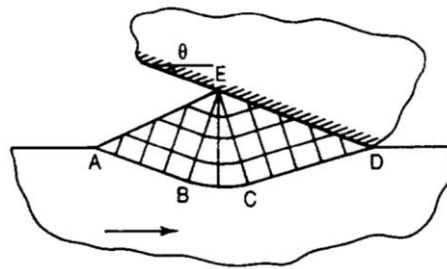
2.3.3 Material Removal Mechanisms without Brittle Fracture

Bridgman and Šimon (1953) proved that a lot of brittle materials can be machined in a ductile regime under high hydrostatic pressures. In the abrasive machining processes, the fine abrasive particles are very small and numerous particles are embedded in the contact region. The load exerted on each particle may be below the critical value causing brittle fracture. Below this critical value, a hard abrasive particle causes only plastic deformation, with a negligible contribution associated with the brittle mechanism.

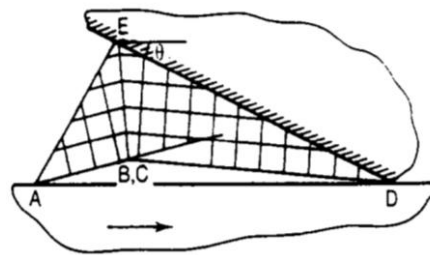
Figure 2.14 shows slip-line fields for the deformation of a perfectly plastic deformation caused by the sliding of a rigid two-dimensional wedge from right to left (Challen and Oxley, 1979). Figure 2.14(a) shows the cutting mode, in which all material is removed by the formation of the chip. Figure 2.14(b) depicts the ploughing mode, in which a ridge of deformed material is pushed along ahead of the particle and no material is removed from the surface. A mode of deformation by wedge formation is illustrated in Figure 2.14(c).



(a) Cutting



(b) Ploughing



(c) Wedge formation

Figure 2.14 Slip line fields for the deformation of a perfectly plastic deformation caused by the sliding of a rigid two-dimensional wedge from right to left (Challen and Oxley, 1979).

Both cutting and wedge formation can remove material from the surface. An analysis of the forces involved in each of the three modes of deformation allows the operative mode to be identified for any sliding conditions. The attack angle of the particle, θ , and the shear strength of the interface between the surface and the particle are the controlling factors. When the attack angle is smaller than the critical

angle, the solid material is primarily removed by the mode of elastic-plastic deformation and this will cause no material removal. With the increase of the attack angle, the material removal would be transited from microploughing to microcutting, and hence material is removed from the worn surface in the form of a chip.

2.3.3.1 Models for Abrasion by Plastic Deformation

In the polishing process, the abrasive wear of the solid surface is caused by hard particles, or particles embedded in the polishing pad in relative motion, or by the presence of hard protuberances on a polishing pad sliding with the velocity relatively along the surface. According to an early abrasion model (Archard, 1953; Rabinowicz, 1965), wear volume depends on the applied load, the tool geometry and the sliding distance, the attack angle, and the hardness of the material, and the material removal can be estimated by the volume of the generated groove. However, not all the volume of the generated groove cause material removal as wear debris and a portion of it come up with plastic deformation (Stroud and Wilman, 1962; Zum Gahr, 1981).

Hence, a more general model was developed by addition of the ratio of material removal as wear debris to the volume of the generated groove to distinguishably consider the four modes of interactions between the abrasive particles and the wearing material which include: microploughing, microcutting, microfatigue and microcracking (Zum Gahr, 1988), respectively. In the polishing process, lubrication can lead to more cutting by particles, and hence to a higher wear rate by lowering the friction between the particles and the surface. Angular particles tend to present larger

attack angles, resulting in a greater proportion of particles involved in cutting, thus leading to a higher material removal rate than more rounded particles (Hutchings, 1992).

2.3.3.2 Models for Erosion by Plastic Deformation

Finnie (1960) was the first to derive a single-particle erosive cutting model based on Newton's laws and set the basic pattern and tone for all single-particle erosion models. In his model, a particle is assumed to be an irregularly shaped object that removes the material in a ductile regime. The model assumes that the velocity and the attack angle of the particle have no effect on the material resistance, the ratio of the horizontal and vertical force components is constant, the length over which the abrasive grain contacts the surface is considerably greater than the depth of cut, and any elastic deformation is ignored. In this model, Finnie (1960) considered the erosive effect of translation in the vertical and horizontal directions, regardless of the rotation of the particle. The predicted amount of material removal has a quadratic relationship with the impact velocity of particles. Since subsequent experiments had shown that the exponent of the impact velocity is greater than 2 (Finnie, 1995; Finnie and McFadden, 1978; Finnie, 1995). Finnie and McFadden (1978) modified their erosion model by adding a rotation term based on some more realistic assumptions. The modified version turns out that the material removal appears to be not simply quadratic with the impact velocity of particles. Finnie's model shows a reasonable agreement with the experimental data for ductile samples at shallow angles of attack.

However, it considerably underestimates the weight loss at large angles of attack and predicts that no material is removed by vertical attack on such materials.

Bitter (1963a and 1963b) assumed that erosion phenomena could be simultaneously caused by deformation wear and cutting action. He developed an erosion model, based on Hertzian contact theory and the energy balance equation, as a function of mass, impact velocity, and angle of the particles, and the material properties of the particles and the eroded element. In his model, the total amount of material removal is a summation of one part due to repeated deformation and the other part due to cutting wear. Bitter's model can be used for both brittle and ductile materials.

However, the deformation wear factor and the cutting wear factor have to be determined experimentally in Bitter's model, making it impossible to apply in most practical situations. Neilson and Gilchrist (1968) developed an experimental study on the erosion by a stream of solid particles based on the analyses of Finnie and Bitter and delivered the simplified form of Bitter's model. However, the simplified form could not reduce the experimental work required to determine the erosion constants.

Huang et al. (2008) developed a mechanical erosion model considering the factors of the impact velocity, the impact angle, the particle size and the material properties of the workpiece. Two force components named tangential force and normal force were separately described as having different roles in the material removal mechanisms. The predicted results of the simplified model showed reasonable agreement with Finnie's experimental data. However, all the exponents of

the coefficients in this model must be determined experimentally. Sheldon and Kanhere (1972) investigated the erosive action of relatively large single particles on both annealed and work-hardened aluminium surfaces. They developed a single particle erosion model based on indentation hardness theory and made a conclusion that a velocity exponent of 3, particle size exponent of 3 and surface hardness exponent of $(-3/2)$ seems to match more closely the experimental data.

From the literature review, a number of single-particle models have been proposed based on Finnie's and Bitter's models. However, all these single erosion models are delivered under dry conditions without considering the effects of fluid dynamics. In the polishing process, the material removal mechanisms depend not only on the material properties of the workpiece and the nature of the particles, but also on the conditions under which the particles impact the workpiece. As a result, these erosion models should be modified and improved with the consideration of hydrodynamics conditions to better understand the complicated machining mechanisms of the polishing process.

2.4 Surface Measurement and Characterization Methods

The performance of the polishing processes can be assessed based on their achievable surface finish, geometry accuracy and surface integrity while the requirements tend to be different with respond to different applications. One of the examples is that for metal optics, the requirement of geometry accuracy and surface finish is stringent instead of the subsurface damage. In contrast, for semiconductors,

the flatness or subsurface damage is more important than the surface finish (Komanduri et al., 1997).

2.4.1 Surface Topography

At present, there is a large number of instruments for surface texture measurement, which include stylus instruments, optical instruments, scanning probe microscopes (SPM) and scanning electron microscopes (SEM).

The operating principle of the stylus measurement instruments is relatively simple and the path of the ball-ended stylus over the measurand surface can be calculated with a comparatively easy method. However, the measurand surface may be contaminated by the stylus and it is a time consuming process to measure areal surface topography. The optical instruments can overcome the shortages for the stylus instruments since the most of the optical methods are non-contact and areal based. Although optical instruments have some advantages over stylus instruments from the above descriptions, more attention should be paid when performing data processing for an optical instrument as compared to that from a stylus instrument. For a stylus instrument, it is relatively easy to estimate the measurement result by modelling it as a ball over the measurand surface. While it is not the same with optical instrument since it has to model the phenomenon of an electromagnetic field for the interaction of the surface. The measureable spatial wavelength for the scanning probe and electron microscopes are 500nm and smaller, while the spatial wavelength for stylus and far-field optical instruments are 500nm and larger (Leach, 2014).

There are many kind of SPM instruments and the atomic force microscope (AFM) is one of the most common one (Binnig et al., 1986). For the measurement setup for a typical AFM system, the sample is placed on a piezoelectric scanner which is moveable in three dimensions relative to a sharp tip which is very close to the sample. The measurement range and the lateral and vertical resolution of some of the surface topography measurement instruments is summarized in Table 2.4 (Lonardo et al., 1996; Whitehouse, 1994). In fact, many factors including surface materials, geometries, measure area and time, could determine the method for measuring surface texture. Since polishing is a multi-scale and multi-physics machining process, instruments with different resolution and range may be needed to comprehensively analyze the polished surface.

Table 2.4 Resolution and range of some surface measurement instruments (Lonardo et al., 1996; Whitehouse, 1994)

Instrument	Resolution (nm)		Range (mm)	
	Lateral	Vertical	Lateral	Vertical
Stylus	100-250	0.3	>100	1
Interferometric microscope	500	0.1	7	0.1
AFM	2	<0.1	0.1	0.005
STM	2.5	0.2	0.1	0.0001
Nomarski microscope	>500	-	-	-
SEM	10	2	-	0.002
TEM	2	2000	-	0.0001

2.4.2 Surface Integrity

Both the surface and the subsurface layers quality including the metallurgical and mechanical state affect the functional performance of components in the polishing process. Besides the topological (geometric) aspects of surfaces, surface integrity also considers the integration of metallurgical, mechanical, physical, chemical, and biological characteristics and properties. The objective of surface integrity is to ensure the surfaces for parts and products meet the requirement of the service properties in the manufacturing operations. It is well-known that polishing has a great potential to be applied in manufacturing super finished surfaces without the formation of subsurface damage, even for brittle materials. However, improper polishing conditions may lead to subsurface damage of the material, such as subsurface cracks, microhardness, dislocations and residual stress. To avoid failures in machined surfaces, there is a need for the detection of the subsurface damage to optimize the polishing process.

Nowadays, the surface integrity and characterization methods such as measurement of residual stresses (Brinksmeier et al., 1982), determination of microhardness using experimental methods and non-destructive methods including X-rays, Raman spectroscopy, photothermal microscopy and scanning acoustic microscopy for characterizing surface integrity and subsurface damage (Brinksmeier, 1989) have been studied intensely. Griffiths (2001) reviewed and analyzed the surface integrity parameters comprehensively. Figure 2.15 shows the recent advances in

measurement methods of residual stress for structural integrity assessment by Withers et al. (2008). Jawahir et al. (2011) presented a review of quantitative analysis of residual stress rate, characterization methods, and deformation characteristics and microstructure alteration of surface and subsurface machined layers. In particular, Diffraction-based methods (x-ray diffraction (XRD) and Electron Backscatter Diffraction (EBSD)), Micromagnetic methods (Barkhausen noise (BN) and Magnetic Barkhausen emission (MBE)), Raman spectroscopy, Acoustic methods (acoustic emission, scanning acoustic microscopy and laser ultrasonics) and methods for evaluation of plastic strain in machined layers (recrystallization technique, mirogrids methods and particle image velocity (PIV)).

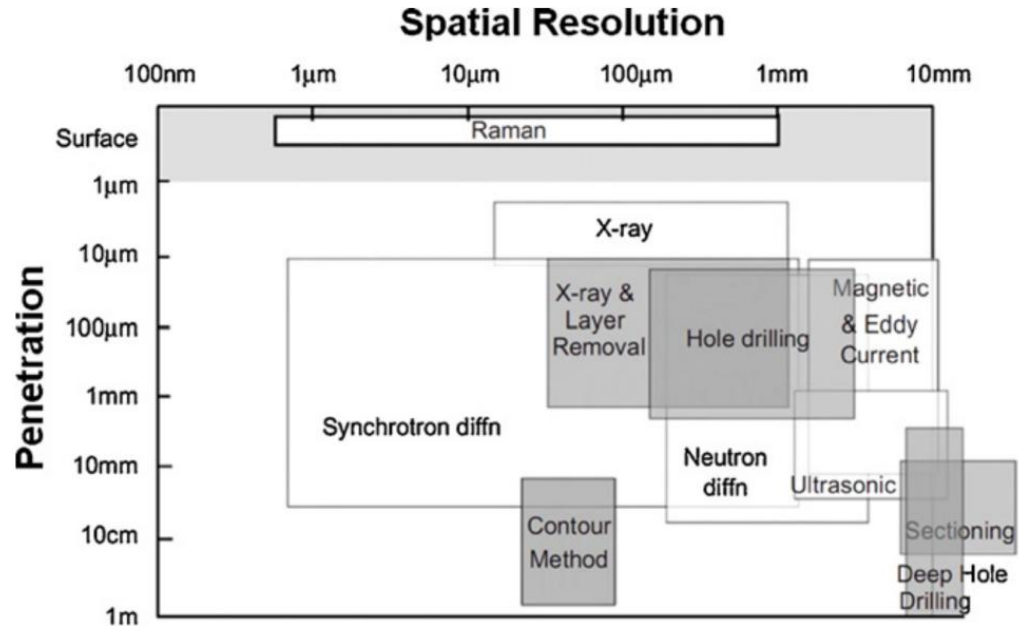


Figure 2.15 Approximate current capabilities of various residual stress measurement techniques-the destructive tech are shaded grey (Withers et al., 2008).

2.5 Modelling and Simulation of Polishing Processes

2.5.1 Computational Fluid Dynamics

Computational Fluid Dynamics (CFD) has been widely used to predict fluid flow fields and erosion phenomena in the production and transportation of slurries. Keating and Nesic (2001) predicted hydrodynamic flow fields using CFD coupled with a Lagrangian particle tracking method in bends. Wall impact information was used in Finnie's model to predict the erosion rate for sand particles. However, these predicted results were not supported by experimental data. Edwards et al. (2001) developed an erosion prediction procedure based on a CFD code, for the surface of pipe fittings in elbows and plugged tees. This erosion prediction procedure included three main parts: modelling of the flow field, computation of particle trajectories and the application of erosion model equations. Edwards et al. (2001) proved the feasibility of using this CFD-based erosion prediction procedure for various complex geometries by delivering three test cases.

To further understand the erosion phenomenon in transportation facilities, Wang et al. (2009b) used CFD combined with phenomenological local erosion models to predict the total erosion rates and the erosion patterns on surfaces. The predicted results showed a reasonable agreement with the experimental data. Gnanavelu et al. (2009, 2011) developed a methodology using a combination of computational fluid dynamic simulations and experimental research to build a material-specific wear map. The predicted wear profile agreed with the test results for the combination of 316L steel-AFS50 and 70 sand appropriately. Due to significant differences in the particle

size between sand and abrasives, the material removal mechanism of solid particle erosion in fluid transport systems should be different from that occurring in the FJP system.

Liu et al. (2004) established CFD models to simulate the jet dynamic characteristics of the flow downstream of the exit from a long thin nozzle. The jet velocity was ultra-high with peak velocities of 600 m/s, 700 m/s, 800 m/s, and 900 m/s, and garnet particles were used with four different diameters of 0.08 mm, 0.12 mm, 0.16 mm, and 0.20 mm. Although these parameters are not available in FJP, his study supports an in-depth understanding of the jet characteristics in ultrahigh velocity abrasive water jet machining. Matsumura et al. (2011) used the stagnation effect of abrasive water jet machining to manufacture micro grooves of glass and then finished them with crack-free surfaces. In his study, CFD analysis with a $k - \varepsilon$ model and a free boundary was developed by the commercial code PHOENICS, and the fluid flow field of the stagnation area was simulated with no mention of the particle tracking and erosion phenomenon.

Li et al. (2010) used a mixture model and the standard $k - \varepsilon$ turbulence model to compute the velocity field and pressure field for analyzing the material removal mechanism in FJP. However, a larger number of studies (e.g. Beaucamp et al., 2012; Yu et al., 2010; Zhang and Kleinstreuer, 2003) stated that the $k - \omega$ model tends to be better suited to simulating transitional flow through constrictions in FJP. The success of the CFD-based erosion modelling depends on the accuracy of the hydrodynamics established from the CFD simulation, the correctness of the particle

tracking algorithm applied in the simulation and the relevance of the erosion models used in the simulation (Wang et al., 2009b). As a result, CFD study should be conducted in depth so as to predict the material removal rate in FJP accurately while the uncertainties are required to be evaluated by conducting experiments so as to validate the CFD-based erosion modelling.

2.5.2 Finite Element Methods

Generally, finite element methods (FEM) for simulating the polishing processes can be divided into macroscopic and microscopic concepts. In most instances, the macroscopic simulation is used in calculating the influence of heat and mechanical surface pressure on the workpiece in the light of temperature distribution or form deviation (Des Ruisseaux and Zerkle, 1970; Enomoto et al., 2011; Li et al., 2013; Wang et al., 2012). The calculations are mainly based on thermo-mechanical and elasto-mechanical material characteristics without considering the plastic material behaviour and chip formation. On the contrary, microscopic simulation is restricted to analyzing the working zone (Klocke, 2003).

Microscopic simulation is based on the single grain scratch test and it allows for the determination of stress, phase transformation, and temperature analysis during chip formation in the polishing process. However, a few problems with finite element models for the polishing processes have to be solved such as the effect of fluid lubrication for macroscopic simulation and the quantitative description of the material behaviour at high strain rates for the microscopic simulation (Brinksmeier et al.,

2006).

2.5.3 Discrete Element Method

Discrete Element Method (DEM) proposed by Cundall and Strack (1979) is widely used in addressing engineering problems in the field of granular media. In a DEM simulation, all particles of the system are modelled with the consideration of the initial state, physical laws and contact models. The success of contact models significantly depend on the relation between the normal contact force and the relative displacement of each particles. Particle dynamics method was presented by resolving Newton's second law to study the effect of particle characteristics on flowability of powder assemblies (Lian and Shima, 1994; Thornton and Antony, 1998). This method is successful in solving non-linear elastic problems and treating the variation in coordination number in a simple way. Quasi-static schemes was presented to model the compaction of granular media (Heyliger and McMeeking, 2001; Redanz and Fleck, 2001). However, Quasi-static schemes tend to be only used in relative density of granular media. It is interesting to note that dynamics methods have already been implemented in quasi-static situations for particulate media successfully (Cambou et al., 2000; Thornton and Antony, 1998). The DEM is also well adapted to simulate media that have a large number of interfaces, such as tribological problems like wear phenomena (Fillot et al., 2007; Iordanoff et al., 2005). Iordanoff et al. (2008) and Andre et al. (2012) used the DEM to simulate the polishing process and analyze the impact on sub-surface damage creation. The disadvantage of the DEM is the using of

dashpots and springs systems, which may cause it to be unsuitable for truly predictive calculations.

2.5.4 Kinematic Models

In the contact polishing processes such as chemical mechanical polishing, kinematic models are always described by a combination of the polishing pad, the work materials and the process kinematics, when focusing on the study of the mechanical effect. Since the surfaces of polishing pads are rough and porous, the micro-contacts between the pad and workpiece could affect the pressure distribution and spatial distribution of active abrasive particles, commonly modelled using the Greenwood and Williamson elastic model (Greenwood and Williamson, 1966). Using this model, the real contact area and active number of abrasive particles contributing to material removal can be calculated with some assumptions (Jeng and Huang, 2005; Luo and Dornfeld, 2001; Zhao and Chang, 2002). Preston (1927) firstly proposed the mechanical model, in which the material removal rate is linearly related to the contact pressure and the relative velocity. Since then, a large number of models have been proposed based on a modified Preston equation (Song et al., 2008; Zeng and Blunt, 2014). However, the material removal rate in the contact polishing processes is affected by various parameters, while the predictive model based on Preston's equation is only concerned with the velocity of polishing tool relative to the workpiece and the contact pressure between the polishing tool and the workpiece.

The theory of fluid dynamics was used to study the lubrication condition and

material removal rate of the polishing process with the consideration of slurry erosion rather than mechanical abrasion by particles (Runnels, 1994; Runnels and Eyman, 1994; Sundararajan, 1991). However, experimental study conducted by Larsen-Basse and Liang (1999) presents that abrasion by abrasive particles tend to be the major wear mechanism in the polishing process. Hence, modelling based on the combination of contact mechanics and computational fluid hydrodynamics appears to be a promising approach to understand comprehensively the polishing processes (Tichy et al., 1999). Although many kinematic models have been developed to predict the material removal rate in the polishing process, most of these kinematics models are only concerned with the polishing process. There is a need for developing a comprehensive model with the consideration of the polishing slurry, the material properties of polishing pad and polished materials.

2.5.5 Molecular Dynamic Models

Molecular-dynamic simulations (MD) provides a important means to better understand the nature of interatomic interactions for various materials. Commonly, the Newtonian equations of motion are used to numerically solve the trajectories of atoms in the phase space of systems. These simulations can enable a better understanding of energetic, mechanical, structural and dynamical properties of the system at nano levels and femtosecond timescales, and sometimes show good correlations with the predictions of theories constructed on the basis of macroscopic considerations (Luedtke and Landman, 1992). As a result, these simulated results help to illuminate

the microscopic origin of the macroscopic behaviour and can be of great value for the establishment of nano- and microfabricated devices and the atomic-scale manipulation of materials (Luedtke and Landman, 1994).

Ikawa et al. (1991) firstly published a molecular model to gain a better understanding of nanometric machining of ductile materials, in which the Morse potential is used to calculate the atomic forces of the system. Since the Morse potential cannot be used to describe the structure of brittle materials, Tersoff potential was later used by Rentsch and Inasaki (1994, 1995) to embody the material properties for various brittle materials. To simulate the abrasive machining processes, a sliding micro-hardness indenter tip was adopted by Shimada et al. (1995), and the simulation used Tersoff potentials and the results indicated that the assumed conditions can obtain quite super smooth surfaces without subsurface damage. Since then, a large number of three-dimensional (3D) (e.g. Inasaki et al., 1993; Rentsch and Inasaki, 1994; Rüdiger Rentsch and Inasaki, 1995) and two-dimensional (2D) (e.g. Chen et al., 2011; Han, 2007; Han and Gan, 2011; Maekawa and Itoh, 1995) MD simulations have been developed.

However, the existing models and analyses of many MD simulations tend to have some of their faults, such as the material description, the model size, the simulated time and the numerical setting (Brinksmeier et al., 2006). This may be caused by the problems of establishing acceptable models in the light of micro topography, potential functions and the very large CPU-power needed. Moreover, most present MD simulations do not consider fluids. There is a need to extend the MD

machining process simulation by molecular fluid dynamics (Hoover, 2012; Rapaport, 2004) to better understand the polishing process.

2.6 Summary

Computer Controlled Ultra-precision Polishing (CCUP) based on fluid jet polishing and bonnet polishing with multi-axis machining is an enabling ultra-precision machining technology which is capable of fabricating ultra-precision freeform surfaces with sub-micrometre form accuracy and surface roughness in the nanometre range. This is particularly useful for machining difficult-to-machine and ferrous materials, which are not amenable for other ultra-precision machining technologies such as single-point diamond turning and ultra-precision raster milling. However, most previous research on the polishing process was based on surface roughness processing without regarding and focusing on shape or form accuracy, and our present understanding of the material removal mechanisms is still far from complete. This is particularly true for ultra-precision, multi-axis, freeform polishing, which is a kind of non-conventional polishing method that has been widely used for machining ultra-precision freeform components that require precise control and accuracy across the polishing surface so as to maintain the form and achieve nanometre surface finishes, which improve the functionality of the components.

With the increasing demands for functional enhancement, it is of paramount importance to understand how various polishing process parameters affect the ability to accurately produce a complete smooth mirror surface with geometrically

dimensional shapes in the nanometre order. Material removal analysis is clearly a fundamental element in achieving the corrective polishing and optimization of the polishing process. Nowadays, the acquisition of tool influence functions still depends largely on the experience and skill of the machine operator through an expensive trial-and-error approach when new materials, new surface designs or new machine tools are used. It is found that studies on polishing mechanisms, especially nano-mechanics, are still sparse because it is nearly impossible to observe the interface between the workpiece surface and the polishing pad during the process.

In the aspect of mechanical behaviour, the wear of materials in the polishing process is mainly caused by the abrasion wear due to the abrasive-workpiece and abrasive-pad contact and/or erosion caused by hard particles striking the surface. Since the material removal is extremely small, in the order of sub-micrometres or less, the mechanisms of abrasive wear or erosion in the polishing process can involve both plastic flow and brittle fracture owing to the polishing process parameters, even for brittle materials. As a result, experimental study of the material removal analysis for the CCUP process is much needed to further understand and optimize the polishing process. As the optimal cutting conditions and polishing strategy for ensuring good surface quality and form accuracy depend largely on the machining environment, work materials, and the geometry of surfaces being polished, there is a need for the research of modelling and simulation methods and tools which can simulate and predict the effect of polishing process parameters on the material removal characteristics and surface generation in CCUP.

Although many researchers have carried out scientific research in an attempt to improve the surface finish of polished surface and gain fundamental understanding of the polishing process involved in CCUP, research work on the polishing mechanism is still far from complete, and relatively little attention has been found on the theoretical modelling of the material removal characteristic for CCUP. Since the material removal mechanism of the CCUP process usually exhibits multidisciplinary and multi-scale complexity, it is still difficult to model the material removal characteristics and simulate the surface generation. As a result, the research in the present study focuses on modelling and analysis of the material removal characteristics in CCUP.

CHAPTER 3 EXPERIMENTAL INVESTIGATION OF FACTORS AFFECTING MATERIAL REMOVAL IN COMPUTER CONTROLLED ULTRA-PRECISION POLISHING

3.1 Introduction

As an ultra-precision machining process, Computer Controlled Ultra-precision Polishing (CCUP) is commonly used to remove tool marks to obtain super finished mirror surfaces. However, recent studies tend to apply CCUP for form correction so as to achieve corrective polishing. It is interesting to note that the material removal rate is an important criterion for CCUP considering time efficiency and the improvement of surface quality, and the material removal analysis is also critical for the deterministic polishing process of CCUP. Hence, the Taguchi method was used to design the experiments so as to investigate the effect of the factors on the material removal rate in fluid jet polishing and bonnet polishing, and a series of experiments was also performed to investigate the effect of the polishing parameters on the material removal characteristics in fluid jet polishing, as well as the material removal mechanism in bonnet polishing.

3.2 Taguchi Approach for Material Removal Analysis in Fluid Jet Polishing

3.2.1 Experimental Design

The material removal characteristics are commonly described as a tool influence function and assessed in terms of the width, maximum depth and volumetric material removal rate. In the present Taguchi design experiment, the material removal rate is quantified in terms of the volumetric material removal rate (VMMR) and the parameters are selected based on the work range of typical parameters in the FJP system due to the operational range for safety and the stability of the polishing machine. Experiments were conducted on a Zeeko IRP200 ultra-precision freeform polishing machine using the five fixed process parameters and the five control factors (each with four levels), as shown in Table 3.1 and Table 3.2, respectively. Accordingly, the Taguchi design method was configured using a Double Orthogonal Array, in which the five control factors were arranged in an L16(4⁵) Orthogonal Array. The polished specimens were measured by a Zygo Nexview 3D Optical Surface Profiler.

Table 3.1 The fixed process parameters in Taguchi design of experiments

Fixed factors	Levels
Diameter of nozzle	1.1 mm
Additives	water
Machining time	5 minutes
Workpiece material	BK7 (Knoop hardness: 610)
Particle material of the slurry	Al ₂ O ₃ (Specific gravity: 3.95)

Table 3.2 The control factors and levels in the Taguchi design of experiments

No.	Control factors	Levels			
		1	2	3	4
A	Pressure (bar)	5	8	12	15
B	Impact angle (°)	30	45	60	90
C	Standoff distance (mm)	5	10	15	20
D	slurry concentration	1:3	1:6	1:9	1:12
E	Particle diameter (µm)	3.22	6.69	9.41	13.12

3.2.2 Results and Discussion

3.2.2.1 Optimal Process Parameters

The Taguchi method provides an effective tool for optimizing the operational parameters with a minimum number of experimental trials. Furthermore, the optimal process parameters determined by the Taguchi trials tend to be robust to unavoidable variations in the environmental conditions, or other forms of external noise. In the Taguchi methodology, the experimental results based on the special design of orthogonal array (OA) are then transformed into a signal-to-noise (S/N) to evaluate the performance characteristics. The calculation of S/N ratio depends on the experimental objectives: higher-the-better, lower-the-better and nominal-is-best. In these experiments, a higher-the-better signal-to-noise (S/N) ratio was used and a larger S/N ratio infers that the corresponding factor level setting provides a larger material removal rate in FJP. Table 3.3 summarizes the Taguchi experimental results and the

determination of the mean value and the S/N ratio. The signal-to-noise ratio data of each of the five experimental variable factors at every level are presented in Table 3.4. As shown in Table 3.4, it is interesting to note that the pressure has the largest effect on the material removal rate and that standoff distance has the smallest effect.

Table 3.3 Experimental results for the volumetric material removal rate

Exp. No.	Control factors					Volumetric material removal rate ($\mu\text{m}^3/\text{min}$)				S/N ratio
	A	B	C	D	E	T i,1	T i,2	T i,3	Mean	
1	1	1	1	1	1	1690330	1454650	1520220	1555067	123.784
2	1	2	2	2	2	1759670	1567120	1467750	1598180	124.000
3	1	3	3	3	3	2453860	2477790	2249170	2393607	127.556
4	1	4	4	4	4	4885750	4203210	3983650	4357537	132.689
5	2	1	2	3	4	12358300	10857800	11323500	11513200	141.186
6	2	2	1	4	3	5571330	4989430	4669980	5076913	134.044
7	2	3	4	1	2	21691400	22090100	19865000	21215500	146.505
8	2	4	3	2	1	4747210	4008520	4063820	4273183	132.540
9	3	1	3	4	2	18459200	19784000	18968900	19070700	145.597
10	3	2	4	3	1	11916600	10721400	9709280	10782427	140.564
11	3	3	1	2	4	91697900	81704700	76699700	83367433	158.349
12	3	4	2	1	3	147701000	137057000	131425000	138727667	162.813
13	4	1	4	2	3	97490700	85646300	90015400	91050800	159.149
14	4	2	3	1	4	249900000	207371000	185291000	214187333	166.421
15	4	3	2	4	1	12465200	11335100	13042300	12280867	141.740
16	4	4	1	3	2	46390800	40314700	38591500	41765667	152.337

Table 3.4 S/N ratio factor response data for material removal rate

No.	Control factors	Average η by levels (dB)				Δ	Rank
		1	2	3	4		
A	Pressure	127.0	138.6	151.8	154.9	27.9	1
B	Impact angle	142.4	141.3	143.5	145.1	3.8	4
C	Standoff distance	142.1	142.4	143.0	144.7	2.6	5
D	Concentration	149.9	143.5	140.4	138.5	11.4	3
E	Particle diameter	134.7	142.1	145.9	149.7	15.0	2

Remark: η represents the signal-to-noise (S/N) ratio; Δ denotes the difference between the maximum and minimum mean response across levels of a factor.

Figure 3.1 and Figure 3.2 show the plots of the S/N ratios and means for the material removal rate in graphical form, respectively. The main effects plot for the S/N ratios indicates that the factor level combination which ensures the optimal material removal rate is under the combination of the experimental conditions of A4B4C4D1E4. However, the main effects plot for the means shows that the combination of the optimal factor level for the material removal rate is A4B2C3D1E4. As shown in Figure 3.1, the impact angle (factor B) and standoff distance (factor C) have very little influence on the S/N ratio. Since they have an insignificant effect on S/N, it is the perfect choice for the mean adjustment factor. The main effects plot for the means indicates that shifting impact angle and standoff distance to a higher level increases the material removal rate but does not affect S/N distinctively. As a result, the combination of the optimal factor level for the material removal rate should be A4B2C3D1E4.

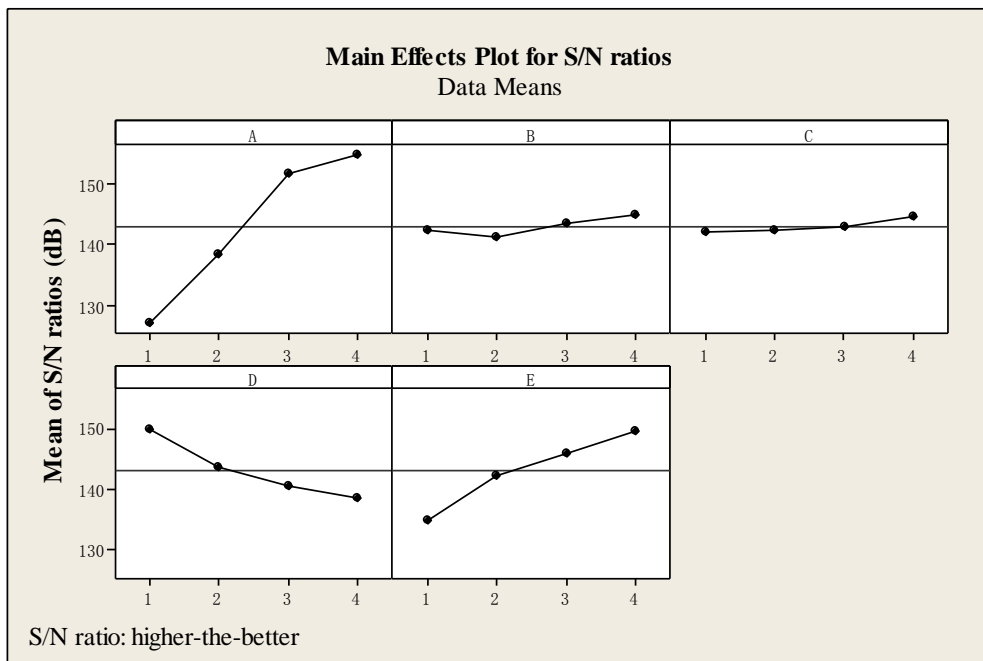


Figure 3.1 S/N ratio factor response graphs for the volumetric material removal rate

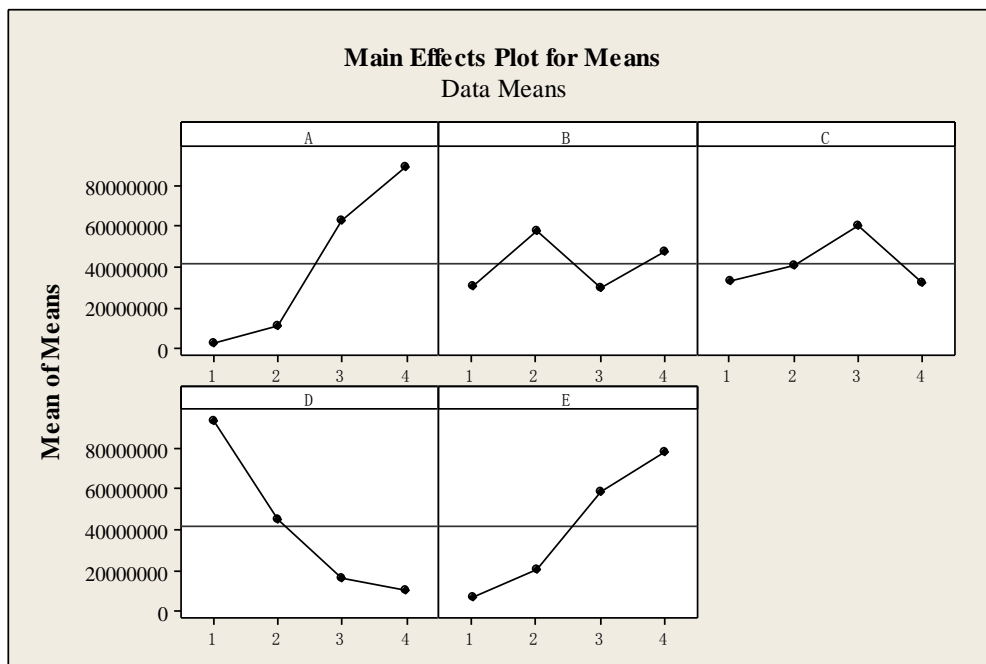


Figure 3.2 Mean factor response graphs for the volumetric material removal rate

3.2.2.2 Confirmatory Experiments

To confirm the reliability of the Taguchi experiments, two polishing experiments were performed under the optimal operational parameters obtained from the Taguchi

designed experiments. The results of the confirmatory experiments are presented in Table 3.5. It is interesting to note that a very slight discrepancy is observed between the predicted material removal rate and the experimental data. However, the overall results of the confirmation trials indicate that the optimal factor level combination of A4B2C3D1E4 provides a consistent material removal rate in FJP. In other words, the optimal process parameters are given as pressure of 15 bar, impact angle of 45 °, standoff distance of 15 mm, slurry concentration of 1:3 and particle size of 13.12 µm, when the BK7 workpiece material was polished using a 1.1 mm diameter nozzle, pure water additives, together with Al₂O₃ abrasive particles.

Table 3.5 Results of confirmation trials

Trial no.	VMMR (µm ³ /min)	Predicted mean value
1	207371200	214187333
2	215192000	214187333

3.3 Effect of Polishing Parameters on Material Removal Rate in Fluid Jet Polishing

3.3.1 Experimental Design

In this study, a series of experiments was conducted to study the effect of polishing time, slurry pressure, standoff distance, impingement angle, slurry concentration, particle size and the radius of curvature on material removal in fluid jet polishing (FJP). All polishing experiments were performed on optical glass (BK7 with

the Knoop hardness value of 610) using Aluminium oxide (Al_2O_3) abrasive particles. As shown in Table 3.6, they were conducted by changing one process factor and keeping the other process factors constant. The polishing machine used was a Zeeko IRP 200 ultra-precision freeform polishing machine which is equipped with three linear axes and three rotational axes. The polished surface made of BK7 which is a glass material was measured by a Zygo Nexview 3D Optical Surface Profiler.

Table 3.6 The parameter settings for studying the effect of individual parameter on the material removal in fluid jet polishing

Polishing time (s)	Pressure (bar)	Distance (mm)	Angle (°)	Concentration	Particle Size (μm)
(i)*	12	10	90	1:12	3.22
180	(ii)*	10	90	1:12	3.22
180	12	(iii)*	90	1:12	3.22
180	12	10	(iv)*	1:12	3.22
180	12	10	90	(v)*	3.22
180	12	10	90	1:12	(vi)*
180	12	10	90	1:12	3.22

Remark: (i)* The polishing time : 60 s, 120 s, 240 s, 300 s; (ii)* The slurry pressure: 5 bar, 8 bar, 10 bar, 12 bar, 15 bar; (iii)* The standoff distance: 5 mm, 8 mm, 10 mm, 15 mm, 20 mm; (iv)* The impingement angle: 30°, 45°, 60°, 75°, 90°; (v)* The slurry concentration: 1:3, 1:6, 1:9, 1:12; (vi)* The particle size: 3.22 μm , 6.69 μm , 9.41 μm , 13.12 μm .

3.3.2 Results and Discussion

3.3.2.1 Effect of Polishing Time

Figure 3.3 shows that the width of the polished spots are approximately the same and the maximum depth and the volumetric removal of the polished spots increase linearly with increasing polishing time. This implies that the material removal rate is constant for different polishing time and hence the form error can be corrected by the compensatory 'dwell time map' of the polishing tool.

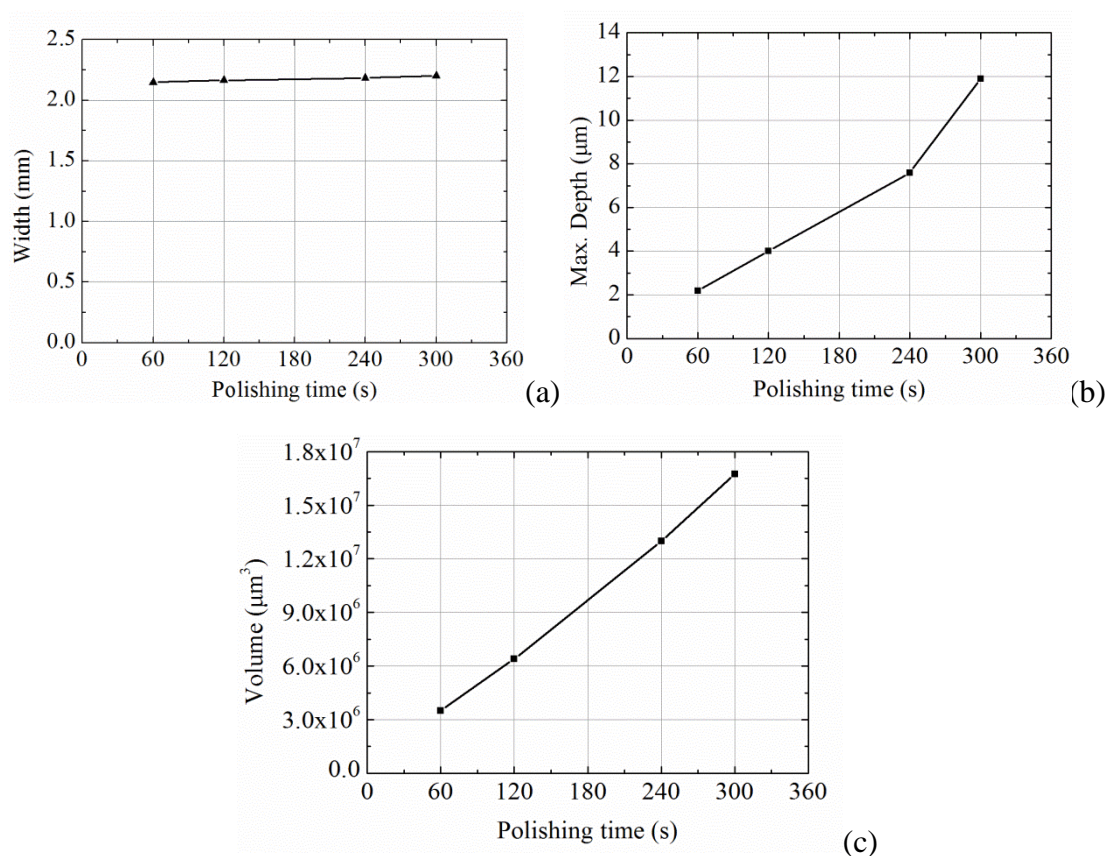


Figure 3.3 The effect of the polishing time on: (a) the width; (b) the maximum depth and (c) the volumetric removal of the polished spot

The experimental data are found to linearly fit Eq. (3.1) with the residual sum of squares of 1.83×10^{11} .

$$Q_i = 55104.275 \times t \quad (3.1)$$

where Q_i is the volume of the polished spot in μm^3 and t is the machining time in s. The slope of the linear curve could be affected by different polishing conditions, such as the pressure, concentration, particle size, material properties, etc.

3.3.2.2 Effect of Slurry Pressure

Figure 3.4(a) shows that the width of the influence function increases slightly with increasing pressure. Figure 3.4(b) and Figure 3.4(c) show that the maximum depth and volumetric material removal rate also increase with increasing pressure. This may be due to the fact that the larger pressure presents a higher kinetic energy to the impact particles, and hence a higher material removal rate is obtained. Furthermore, the relationship between the volumetric material removal rate and the pressure can be fitted well by Eq. (3.2) using the polynomial fit in the OriginPro software.

$$Q_p = 6863.19P^3 - 81517.62P^2 + 694084.23P - 1.98 \times 10^6 \quad (3.2)$$

where Q_p is the volumetric material removal rate in $\mu\text{m}^3/\text{min}$ and P is the pressure in bar. Since the impact velocity of the slurry depends linearly on the pressure, it turns out that the exponent of velocity corresponding to the material removal rate tends to be between 2 and 3.

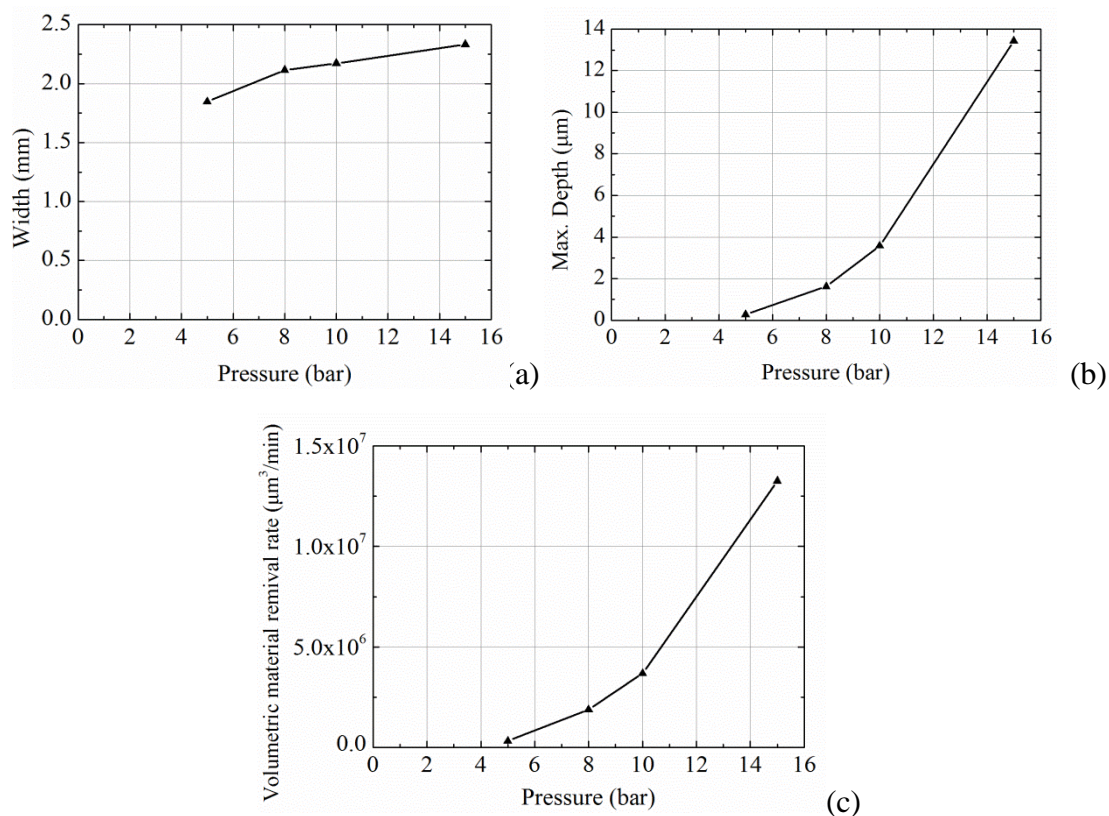


Figure 3.4 The effect of the slurry pressure on: (a) the width; (b) the maximum depth and (c) the volumetric material removal rate of the tool influence function

3.3.2.3 Effect of Standoff Distance

Figure 3.5 shows that the maximum depth and the volumetric material removal rate increase as the standoff distance is increased, while the width of the influence function fluctuates slightly. This result contradicts the experimental data of previous research (Booij et al., 2001). In theory, the change of standoff distance could result in different kinetic energies of the particles and different hydrodynamic conditions for the jet slurry, and hence a different material removal rate is obtained in FJP. The material property of the polished surface is also a factor that should be considered when the effect of the standoff distance on the material removal characteristics is

studied. How the standoff distance affects the material removal rate and the relation between the standoff distance and material removal rate under different polishing conditions still need to be investigated further using the computational fluid dynamic (CFD) theory and erosion mechanisms.

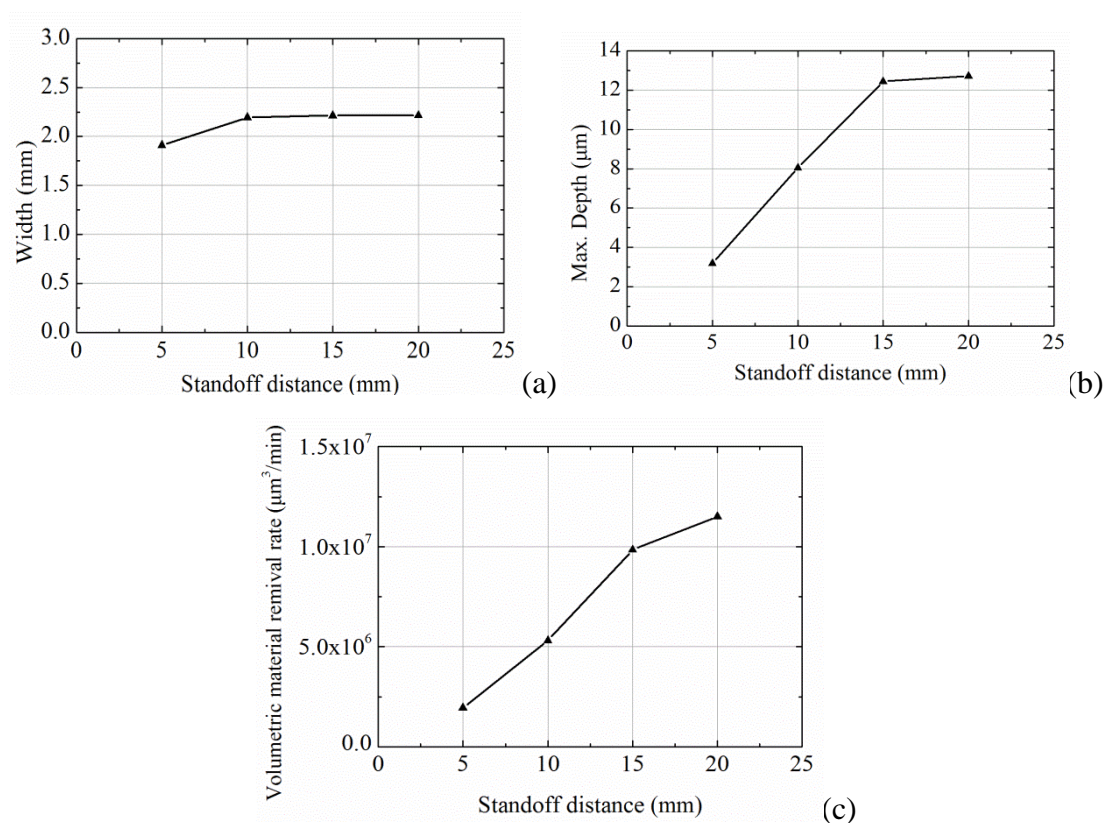


Figure 3.5 The effect of the standoff distance on: (a) the width; (b) the maximum depth and (c) the volumetric material removal rate of the tool influence function

3.3.2.4 Effect of Impingement Angle

As shown in Figure 3.6, the shape and area of the influence function is varied corresponding to different impingement angles. This means that the optimal impingement angle can be selected for polishing super finished mirror surface with

consideration of the designed polishing path in order to improve the polishing efficiency.

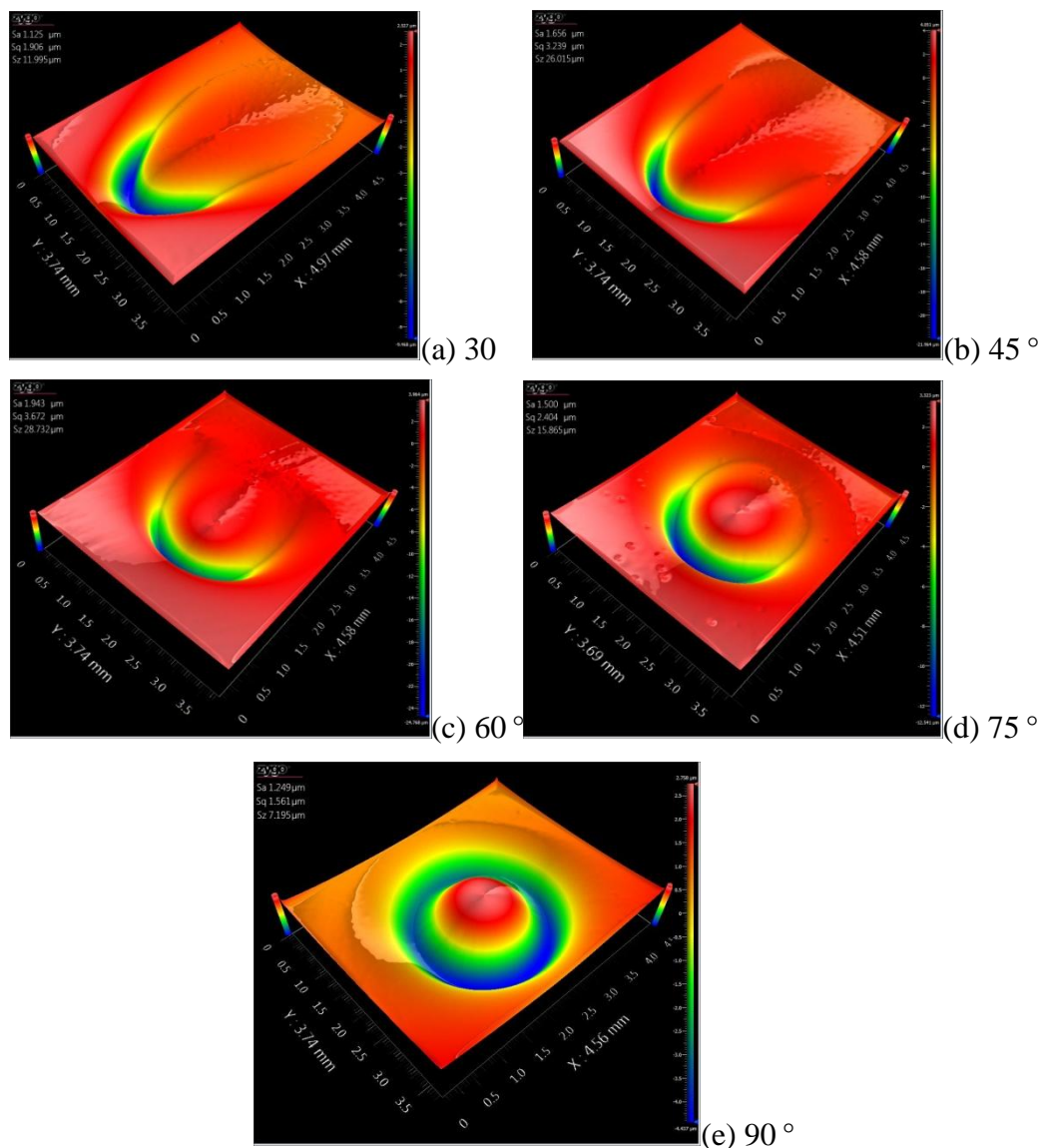


Figure 3.6 The 3D surface topography of the influence function for the different impingement angle

Figure 3.7 shows that the relationship between the material removal rate and the impact angle is nonlinear. The maximum depth and the volumetric material removal rate increase as the impact angle increases between 0° and 45° and both of them

decrease as the impact angle increases between 60° and 90° . According to the polynomial fitting of the experimental data, the maximum depth and volumetric material removal rate are maximum between 45° and 60° . This can be due to the reason that the different impact angles result in different hydrodynamic conditions of jet slurry and hence different particle trajectories in the polishing process.

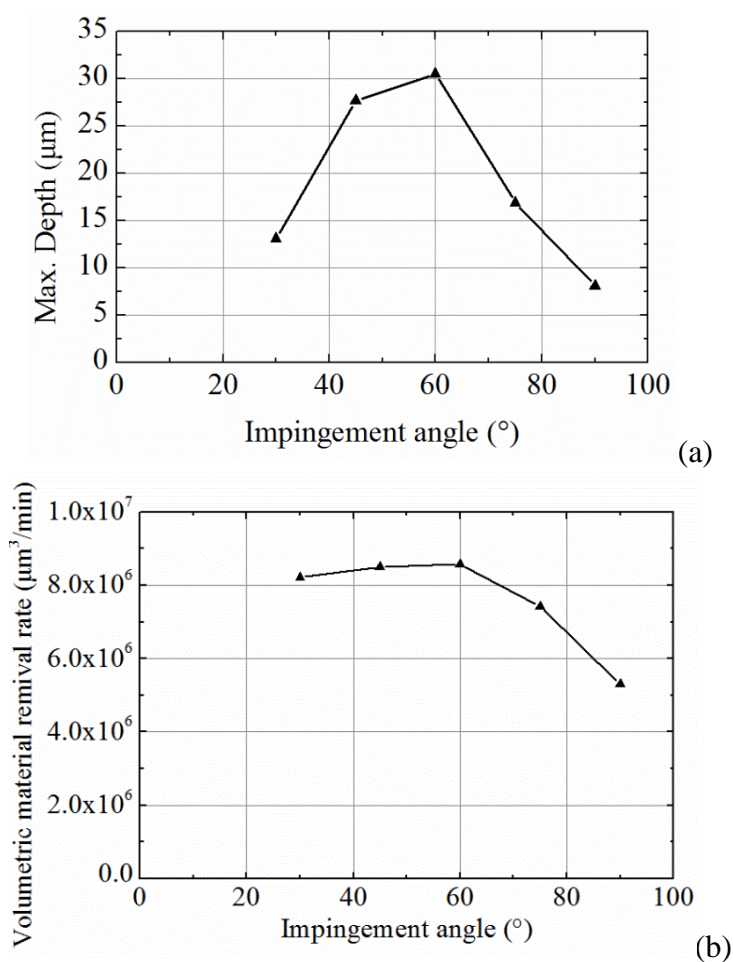


Figure 3.7 The effect of the impingement angle on: (a) the maximum depth and (b) the volumetric material removal rate of the tool influence function

3.3.2.5 Effect of Slurry Concentration

Figure 3.8 shows that the maximum depth and volumetric material removal rate

increases linearly with increasing slurry concentration and the width of the influence function appears to be constant. The result may be due to the fact that the number of impact particles increases as slurry concentration is increased, and this results in increasing material removal rate.

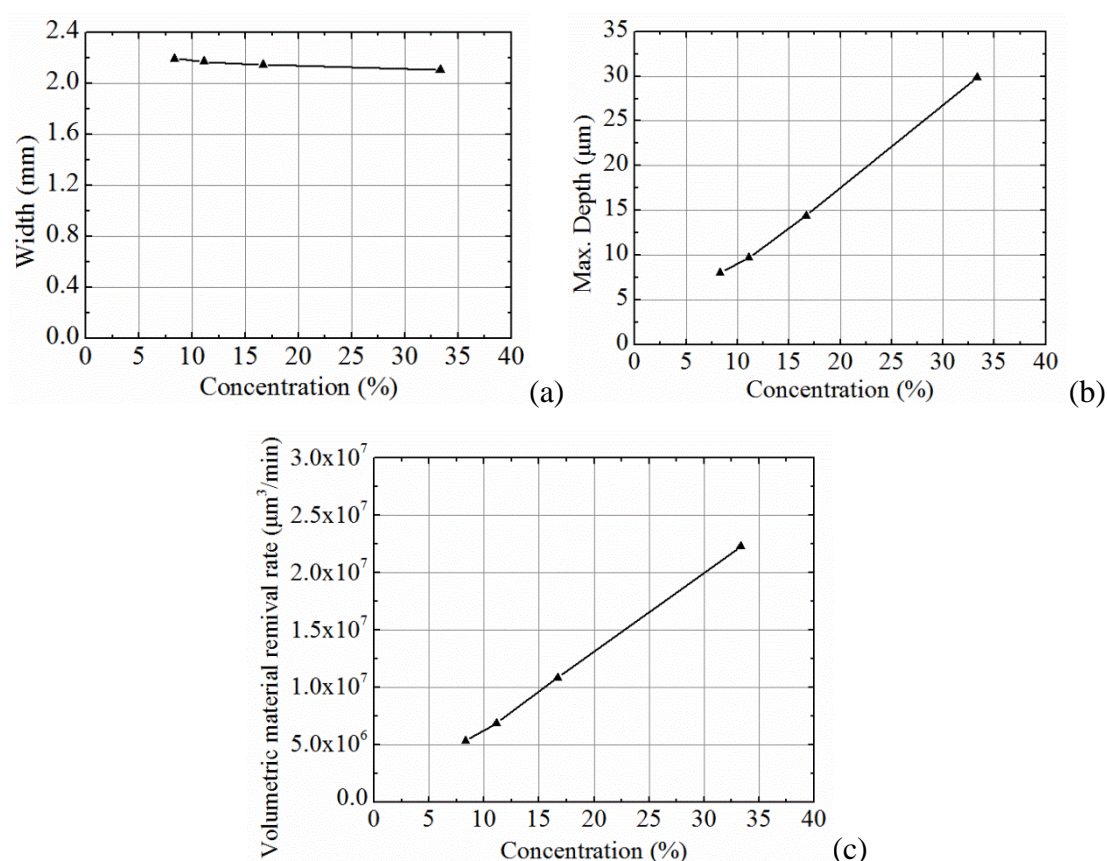


Figure 3.8 The effect of the slurry concentration on: (a) the width; (b) the maximum depth and (c) the volumetric material removal rate of the tool influence function

3.3.2.6 Effect of Particle Size

Figure 3.9 presents the relationship between the material removal rate and the particle size. As shown in Figure 3.9, #500 Al_2O_3 abrasive particles have the largest diameter of the current abrasives and they tend to provide the largest material removal

rate. Conversely, #1200 A_2O_3 abrasive particles have the smallest diameters of the current abrasives, and hence their cutting capability is found to be the lowest among the four particle types used in the experiment. Furthermore, it can be seen that the material removal rate increases as the diameter of the abrasive particles increases.

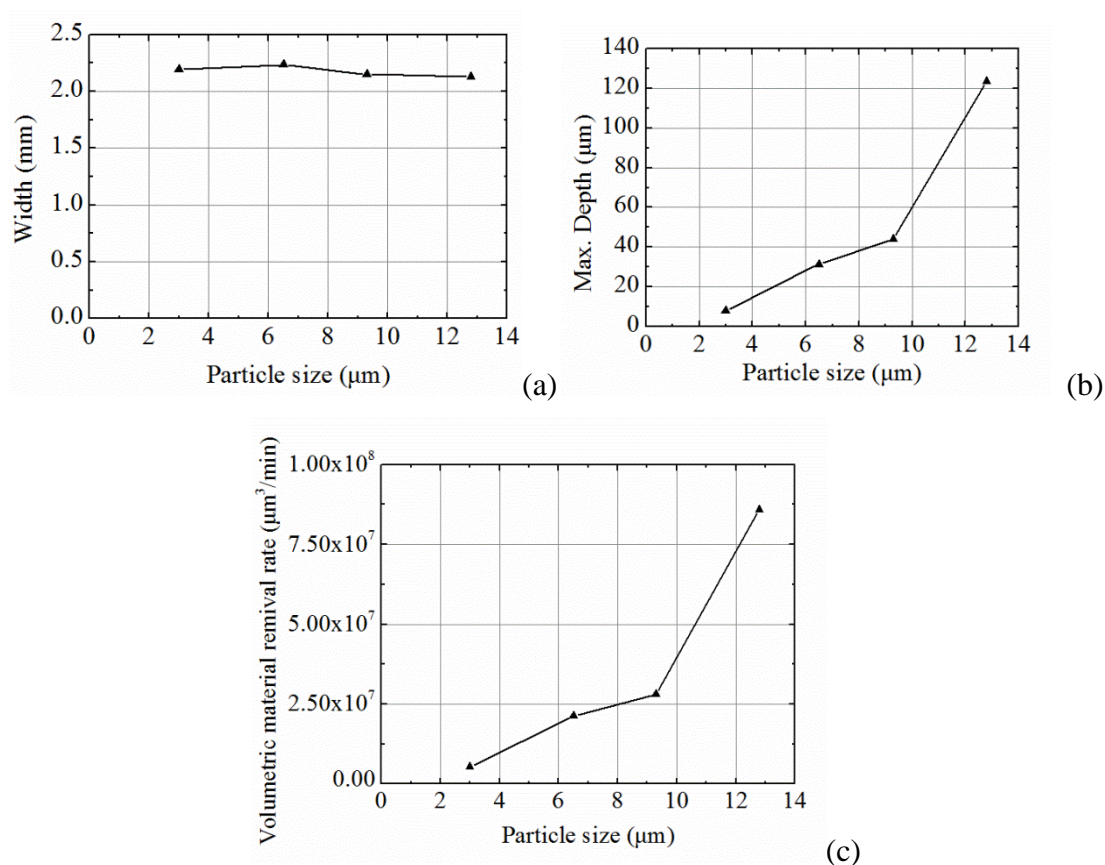


Figure 3.9 The effect of the particle size on: (a) the width; (b) the maximum depth and (c) the volumetric material removal rate of the tool influence function (TIF)

The effects of particle size on the material removal rate can be summarized as follows:

- (i) The particle size may affect the hydrodynamic conditions in Fluid Jet Polishing.

Hence, different particle sizes determine different particle trajectories and they

finally lead to different impact velocities and angles between the particles and target surface.

- (ii) Different particle sizes donate different masses of particles, and hence they present different kinetic energies of the impact particles. This is regarded as the main reason behind material removal in fluid jet polishing.
- (iii) When a particle impacts the target surface, different contact areas due to the differences in particle size may cause different erosion characteristics. Besides this, the particle shape and particle size distribution also need to be considered.

3.4 Taguchi Approach for Material Removal Analysis in Bonnet Polishing

3.4.1 Experimental Design

In the present study, the material removal rate is quantified in terms of the volumetric material removal rate (VMMR) in bonnet polishing. Experiments were conducted on a Zeeko IRP200 ultra-precision freeform polishing machine using five fixed process parameters and six control factors (each with three levels), as shown in Table 3.7 and Table 3.8, respectively. Accordingly, the Taguchi design method was configured using a Double Orthogonal Array, in which the six control factors were arranged in an L18(3^6) Orthogonal Array. The polished specimens were measured by a Zygo Nexview 3D Optical Surface Profiler.

Table 3.7 The fixed process parameters in Taguchi design of experiments

Fixed factors	Levels
Tool radius	20 mm
Polishing cloth	LP-66
Machining time	4 min
Workpiece material	S136 (Rockwell C Hardness: 55)
Particle material	Al ₂ O ₃ (Specific gravity: 3.95)

Table 3.8 The control factors and levels in Taguchi design of experiments

No.	Control factors	Levels		
		1	2	3
A	Head speed (rpm)	500	1000	1500
B	<i>Precess</i> angle (°)	5	15	25
C	Tool pressure (bar)	0.5	1	1.5
D	Tool offset (mm)	0.12	0.24	0.36
E	slurry concentration	1:9	1:6	1:3
F	Particle diameter (µm)	3.22	6.69	9.41

3.4.2 Results and Discussion

3.4.2.1 Optimal Process Parameters

In these experiments, a higher-the-better signal-to-noise (S/N) ratio was used and a larger S/N ratio implies that the corresponding factor level setting provides a larger material removal rate in bonnet polishing. Table 3.9 summarizes the Taguchi experimental results and the determination of the mean value and the S/N ratio. The signal-to-noise ratio data of each of the six experimental variable factors at every level are presented in Table 3.10. As shown in Table 3.10, it is interesting to note that the *precess* angle, head speed, particle diameter, tool offset, slurry concentration and tool pressure are the significant factors in descending order which affect the material removal rate.

Figure 3.10 and Figure 3.11 show the plots of the S/N ratios and means for the material removal rate in graphical form, respectively. The main effects plot for the S/N ratios indicates that the factor level combination which ensures the optimal material removal rate is under the combination of the experimental conditions of A3B3C2D3E3F3. However, the main effects plot for the means shows that the combination of the optimal factor level for the material removal rate is A3B3C1D3E3F3. As shown in Figure 3.11, the tool pressure (factor C) has very little influence on the S/N ratio. Since they have an insignificant effect on S/N, it is the perfect choice for the mean adjustment factor. The main effects plot for the means indicates that tool pressure to a lower level increases the material removal rate but does not affect S/N distinctively. As a result, the combination of the optimal factor level for

the material removal rate should be A3B3C1D3E3F3.

Table 3.9 Experimental results for the volumetric material removal rate

Exp. No.	Control factors						Average volumetric material removal rate ($\mu\text{m}^3/\text{min}$)	S/N ratio
	A	B	C	D	E	F		
1	1	1	1	1	1	1	8853280	138.942
2	2	2	2	2	2	2	377774000	171.545
3	3	3	3	3	3	3	1231196000	181.807
4	1	1	2	2	3	3	69903000	156.890
5	2	2	3	3	1	1	162440000	164.214
6	3	3	1	1	2	2	1084890000	180.708
7	1	2	1	3	2	3	294444000	169.380
8	2	3	2	1	3	1	476821000	173.567
9	3	1	3	2	1	2	206424000	166.295
10	1	3	3	2	2	1	136504000	162.703
11	2	1	1	3	3	2	195629000	165.829
12	3	2	2	1	1	3	461385000	173.281
13	1	2	3	1	3	2	151661000	163.617
14	2	3	1	2	1	3	976641000	179.795
15	3	1	2	3	2	1	115307000	161.237
16	1	3	2	3	1	2	389497000	171.810
17	2	1	3	1	2	3	121815000	161.714
18	3	2	1	2	3	1	413533000	172.330

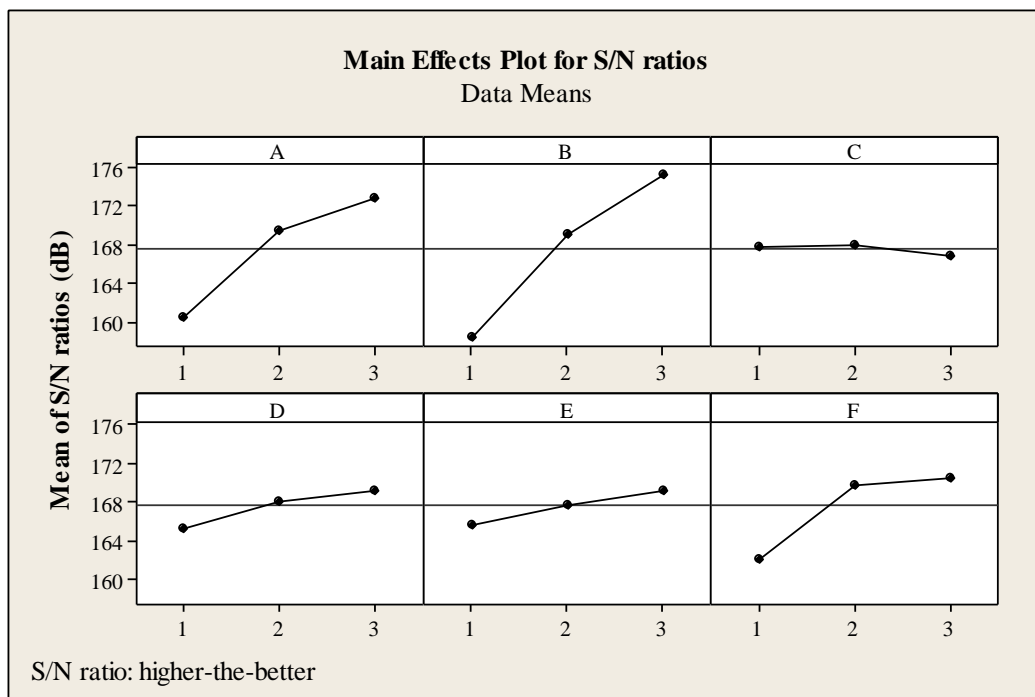


Figure 3.10 S/N ratio factor response graphs for the volumetric material removal rate

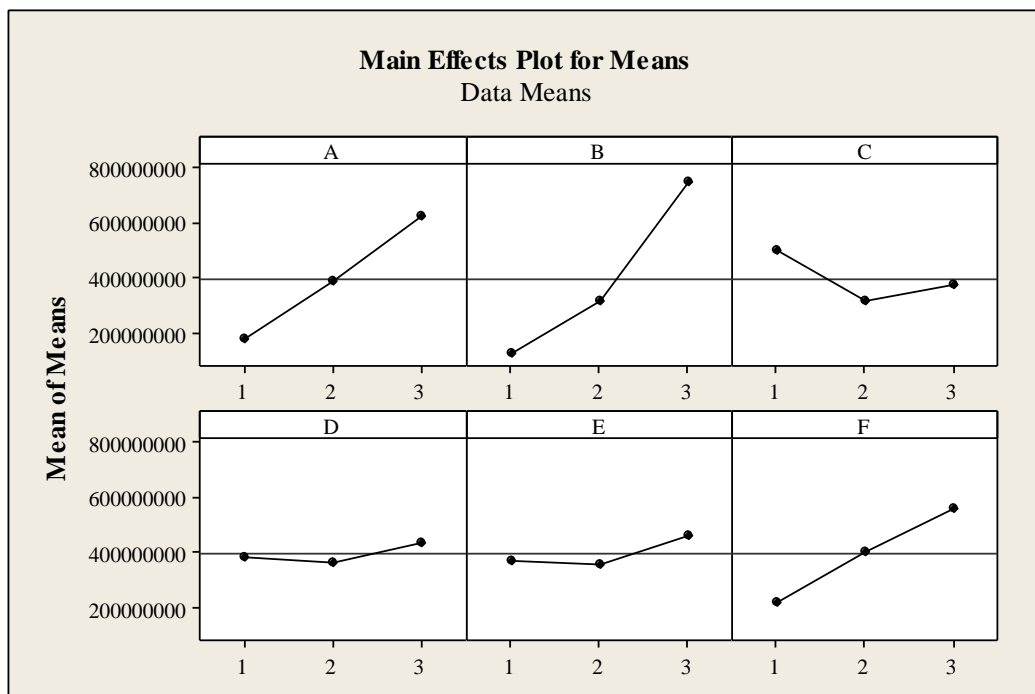


Figure 3.11 Mean factor response graphs for the volumetric material removal rate

Table 3.10 S/N ratio factor response data for material removal rate

No.	Control factors	Average η by levels (dB)			Δ	Rank
		1	2	3		
A	Head speed	160.6	169.4	172.8	12.3	2
B	<i>Precess</i> angle	158.5	169.1	175.3	16.8	1
C	Tool pressure	167.8	168.1	167.0	1.1	6
D	Tool offset	165.3	168.3	169.3	4.0	4
E	concentration	165.7	167.9	169.2	3.5	5
F	Particle diameter	162.2	170.0	170.7	8.5	3

3.4.2.2 Confirmatory Experiments

To confirm the reliability of the Taguchi experiments, two polishing experiments were performed under the optimal operational parameters obtained from the Taguchi designed experiments. The results of the confirmatory experiments are presented in Table 3.11. It is interesting to note that a very slight discrepancy is observed between the predicted material removal rate and the experimental data. However, the overall results of the confirmation trials indicate that the optimal factor level combination of A3B3C1D3E3F3 provides a consistent material removal rate in bonnet polishing. In other words, the optimal process parameters are indicated as a head speed of 1500 rpm, *precess* angle of 25 °, tool pressure of 0.5 bar, tool offset of 0.36 mm, concentration of 1:3, and particle diameter of 9.41 μm , when the S136 workpiece material was polished

using a bonnet with a radius of 20 mm and LP-66 polishing cloth, pure water additives, and Al₂O₃ abrasive particles.

Table 3.11 Results of confirmation trials

Trial no.	VMMR ($\mu\text{m}^3/\text{min}$)	Predicted mean value
1	1355544247	1234508691
2	1449060000	1234508691

3.5 A Study of Material Removal Mechanisms in Bonnet Polishing

3.5.1 Experimental Design

The bonnet polishing process involves forcing a spinning, inflated bonnet, covered with the polishing pad, against the polished surfaces flooded with a liquid slurry of abrasive particles. The slurry is dragged by the porous polishing pad into the interface between the pad and the workpiece. The material removal in bonnet polishing is accomplished by the interactions between the polishing pad, workpiece and abrasive particles as shown in Figure 3.12. The mechanism of material removal is a complex process, which is affected by various factors such as tool radius, *precess* angle, polishing depth, head speed, tool pressure, polishing time, polishing cloth, slurry concentration, particle size, material properties of the particles and workpiece, etc. To have a better understanding of the pad-abrasive-workpiece contact mechanics

and material removal mechanisms in the bonnet polishing process, a series of experiments was conducted as follows:

- (i) To investigate the interactions among the polishing pad, workpiece and abrasive particles, three samples made of NiCu (Hardness HV: 110) were prepared by the Moore Nanotech 350FG using single-point diamond tooling which were then polished by a Zeeko IRP 200 ultra-precision freeform polishing machine. Sample N1 was polished without water and abrasive particles, sample N2 was polished using pure water without abrasive particles and sample N3 was polished using a slurry comprising 2.066 vol. % of Al_2O_3 abrasives with an average size of 3.22 μm . All these samples were polished under the identical polishing parameters as shown in Table 3.12 and measured by a Zygo Nexview 3D Optical Surface Profiler and HITACHI TM3000 Tabletop Scanning Electron Microscope.
- (ii) To study the hydrodynamics conditions in the contact area for bonnet polishing, three samples made of S136 HRC 55 steel were prepared by deterministic micro-grinding of Moore Nanotech® 450UPL and then polished by a Zeeko IRP 200 ultra-precision freeform polishing machine using a slurry comprising 2.066 vol. % of Al_2O_3 abrasives with an average size of 13.12 μm . Experiments were conducted using different polishing depths of 0.1 mm, 0.3 mm and 0.5 mm, while other parameters are shown in Table 3.12.
- (iii) With consideration of the importance of the dwell time map for the surface generation by bonnet polishing, three samples made of different materials

including steel, BK7 and Nicu were polished using a slurry comprising 2.066 vol. % of Al_2O_3 abrasives with an average size of $13.12 \mu m$ to study the effect of polishing time on the surface generation for various materials. All these experiments were conducted on a Zeeko IRP 200 ultra-precision freeform polishing machine using different polishing times of 60 s, 120 s, and 180 s and the other parameters are shown in Table 3.12.

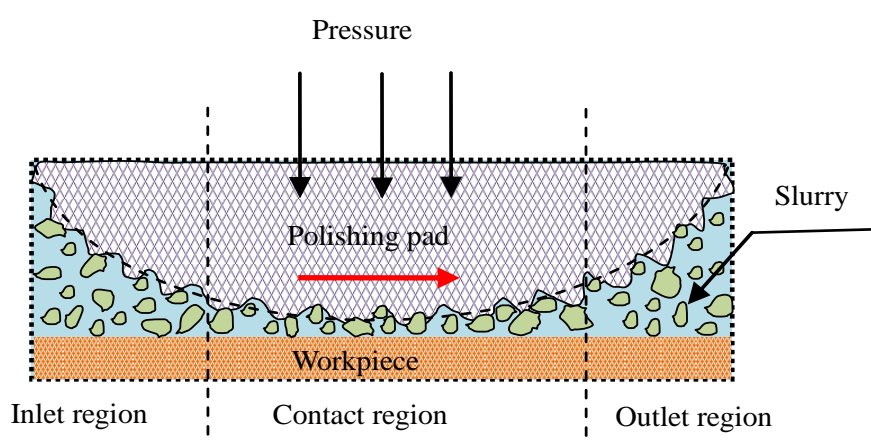


Figure 3.12 Schematic diagram of bonnet polishing and workpiece-pad interactions

Table 3.12 Polishing parameters used in the experimental studies

Polishing pad	LP-66 (Cerium oxide D'27)
<i>Precess</i> angle	15°
Tool size	20 mm radius bonnet
Tool pressure	1.2 bar
Polishing depth	0.2 mm
Head speed	1200 rpm
Polishing time	60s

3.5.2 Results and Discussion

3.5.2.1 *Pad-abrasive-workpiece Interactions*

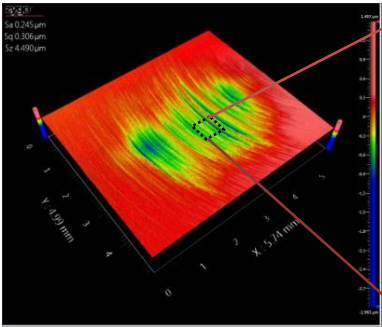
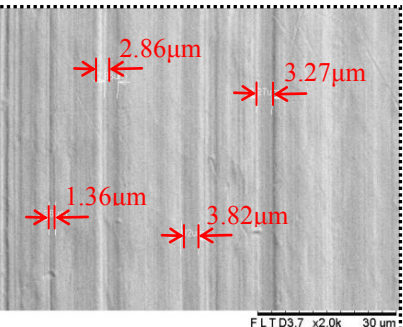
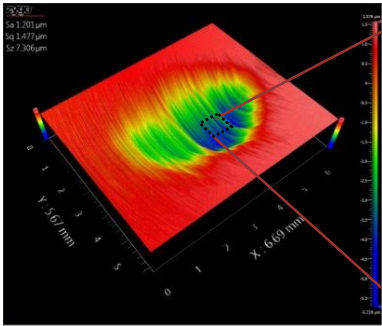
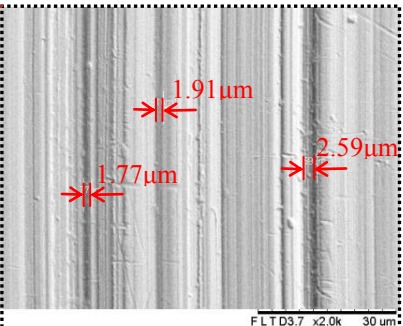
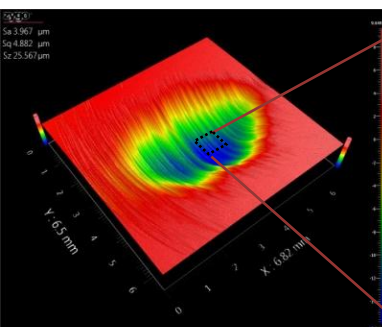
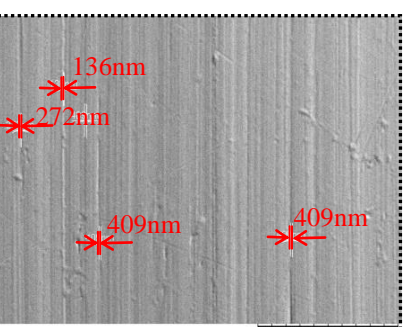
Table 3.13 shows that sample N3 had the highest material removal rate while the amount of material removal of sample N2 was smaller than that of sample N3, and sample N1 had the lowest material removal. It was also found that the polishing pad not only contributes to the material removal but also generates micro-scale scratches on the polished surface as shown in the scanning electronic microscopy (SEM) photographs in Table 3.13. The outcomes of these experiments can be summarized as follows:

- (i) The interaction between the pad and the polished surface decreases the material removal rate for the dry bonnet polishing process;
- (ii) The functions of the abrasive slurry in bonnet polishing include the conversion of an abrasive to a loose abrasive process, flushing or the transport of the debris away from the abrasive process, culling in the contact area, mechanical lubrication of the abrasive contacts, etc.
- (iii) The material removal in bonnet polishing is shared by the polishing pad and the abrasives trapped in the pad-workpiece interface, and the amount of material removal by the polishing pad is much smaller than that by the abrasive particles. More importantly, the material removal produced by the polishing pad is mainly caused by the abrasion associated with plastic deformation of the polishing pad which produces the scratches and hence damages the surfaces being polished.

To obtain super mirror finished surfaces without pad scratches, the abrasive wear that

occurs in bonnet polishing which is dominated by the plastic removal mode of abrasive particles, while the material removal is caused by the polishing pad should be mitigated through flattening the asperities (Hutchings, 1993; Kim et al., 2013; Saka et al., 2010), controlling reasonably the polishing depth and/or appropriately adopting a polishing pad with low pad hardness.

Table 3.13 Experimental results for studying interactions between the pad, workpiece and particles

Sample No.	Zygo photographs	SEM photographs (Center area)
A1.1 (No water and no abrasive particles)		
A1.2 (with water but no abrasive particles)		
A1.3 (with water and abrasive particles)		

3.5.2.2 Hydrodynamic Lubrication

It is well-known that abrasive slurry is vital to facilitate the material removal at nano level and the polishing mechanisms of bonnet polishing usually exhibit multidisciplinary and multi-scale complexity, possibly accomplishing contact mechanics, lubrication mechanics, erosion, and wear mechanisms. Hence, the material removal mechanisms tend to vary under different polishing conditions. Similar to the lubrication theory, the polishing conditions can be divided into three parts: boundary lubricant, mixed lubricant and hydrodynamic lubricant polishing.

Table 3.14 shows that the amount of material removal is increased with increasing polishing depth while the pad scratching is presented in the centre area with the highest pressure when using a polishing depth of 0.5 mm. The results can be explained as follows:

- (i) A larger polishing depth means a larger contact area and a higher pressure distribution in the contact area and hence obtains a higher material removal rate;
- (ii) when using a large polishing depth, the pressure of the centre area of a polished spot is the highest and the slurry is hard to be entrapped in the gap between the pad and the polished surface and hence the polishing pad may contact the surface directly with little water and no abrasive particles. This plastic-contact mode between the workpiece and polishing pad in the centre area is named boundary lubricant polishing condition and causes the minimal material removal rate and results in high surface quality. Hence, there exists a critical polishing

depth which if exceeded leads to the breaking of the hydrodynamic lubrication condition in the high pressure area of the polished spot which causes the pad scratching.

Table 3.14 Experimental results used to study hydrodynamic conditions in the contact

area

Sample No.	Zygo photographs	SEM photographs (Center area)
D1 (Polishing depth: 0.1 mm)		
D2 (Polishing depth: 0.3 mm)		
D3 (Polishing depth: 0.5 mm)		

In other words, the tool offset in bonnet polishing should be smaller than the critical polishing depth in order to ensure high surface quality without pad scratching. The

critical polishing depth may be affected by tool pressure, pad topography, particle size, and the material of polishing pad and polished surface in bonnet polishing. Conversely, when using a small polishing depth, the contact mode of bonnet polishing is dominated by the hydro-dynamical contact mode and the material removal rate under hydrodynamic lubricant polishing conditions is significantly small. As a result, the polishing depth should be selected properly to ensure that the contact mode of bonnet polishing is a mixed lubricant polishing condition including the hydrodynamic contact model and the solid-solid contact mode. The mixed lubricant polishing condition is greatly valued due to the fact that it can obtain high surface quality with high polishing efficiency. The results discussed are helpful for a better understanding of the polishing process and process optimization.

3.5.2.3 Effect of Polishing Time

Since the surface generation by bonnet polishing is dominated by the polishing tool influence function instead of the actual geometry of the cutting tool, the surface generation mechanism of bonnet polishing is quite different from that of other ultra-precision machining processes such as single-point diamond turning and raster milling (Cheung et al., 2011). The influence function (TIF) is affected by various factors which is commonly regarded as a tool that is used in calibration, prediction or form correction. With the data of the tool influence function, the polishing tool can be told where it should stay longer or shorter for removing more or less materials from the surface.

Figure 3.13 shows that the removal volume increases linearly with increasing polishing time and this infers that the material removal rate is constant when using only one variable factor of polishing time while keeping other parameters constant. This implies that bonnet polishing is a relative and cumulative process for various materials and the surface generation of bonnet polishing is a linearly cumulative effect of dwell time together with constant material removal rate under identical polishing conditions.

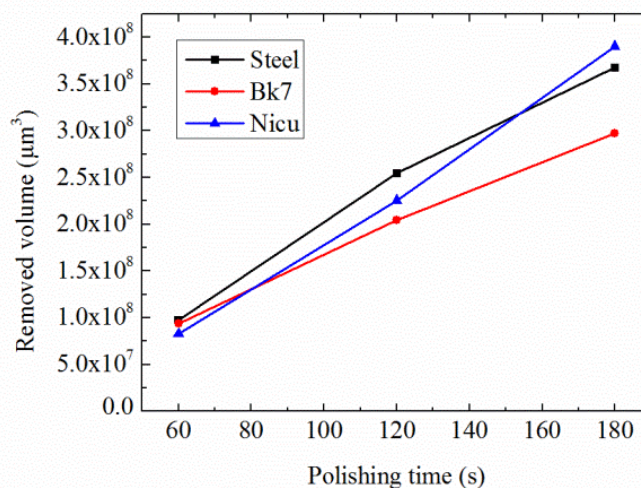


Figure 3.13 The effect of polishing time and on the surface generation

3.6 Summary

In this chapter, the Taguchi design of experiments is described to identify the optimal operational parameters and the significance of the important parameters for the volumetric material rate in fluid jet polishing. The Taguchi trials show that pressure has the largest effect on the material removal rate and that standoff distance has the smallest effect. The results of the Taguchi design process indicate that the optimal

process parameters are given as follows: pressure of 15 bar, impact angle of 45 °, standoff distance of 15 mm, slurry concentration of 1:3, and particle size of 13.12 μm, when polishing BK7 using a 1.1 mm diameter nozzle, pure water additives, and Al₂O₃ abrasive particles.

A series of experiments was performed to study the effects of important process parameters on the material removal characteristics in fluid jet polishing. The results can be summarized as follows:

(i) the width of the influence function increases slightly with increasing pressure and standoff distance.

(ii) the maximum depth as well as volumetric removal increase linearly with increasing polishing time and slurry concentration, while they increase non-linearly with slurry pressure, slurry distance, and particle size. It is interesting to note that the maximum depth as well as the volumetric removal increase first then decrease with increasing impingement angle.

The Taguchi design experiments were also used to identify the optimal operational parameters and the significance of the important parameters for the volumetric material rate in bonnet polishing. The Taguchi trials show that the *process* angle, head speed, particle diameter, tool offset, slurry concentration and tool pressure are the significant factors in descending order of significance which affect the material removal rate. The results of the Taguchi design process indicate that the optimal process parameters in the present experiments are a head speed of 1500 rpm, *process* angle of 25 °, tool pressure of 0.5 bar, tool offset of 0.36 mm, concentration of 1:3, and

particle diameter of 9.41 μm , when the S136 workpiece material was polished using a bonnet with a radius of 20 mm and LP-66 polishing cloth, pure water additives, and Al_2O_3 abrasive particles.

The material removal mechanism was studied through a series of polishing experiments. The main findings are summarized as follows:

- (i) Experimental results reveal that the functions of the abrasive slurry in bonnet polishing include conversion of an abrasive to loose abrasive process, flushing or the transport of the debris away from the abrasive process, culling in the contact area to avoid some interactions, mechanical lubrication of the abrasive contacts, etc. Although the material removal is shared by the abrasive particles and the pad asperities in the designed experiments, the abrasive wear that occurs in bonnet polishing is dominated significantly by the plastic removal mode of abrasive particles, while the material removal caused by the polishing pad should be mitigated in order to obtain super mirror finished surfaces without pad scratches.
- (ii) Experimental results suggest that there exists a critical polishing depth which if exceeded leads to the breaking of the hydrodynamic lubrication condition in the high pressure area of polished spot which causes pad scratching. As a result, the polishing depth should be selected properly to ensure that the contact mode of bonnet polishing is mixed lubricant polishing condition including the hydrodynamic contact model and the solid-solid contact mode. The mixed lubricant polishing condition is greatly valued due to the fact that it can obtain better surface quality with higher polishing efficiency.

- (iii) The experimental results show that the removed volume increases linearly with increasing polishing time when polishing steel, optical glass (BK7) and nickel copper (NiCu). This implies that the surface generation of bonnet polishing is a linearly cumulative effect of dwell time together with the constant material removal rate when polishing is undertaken under the identical polishing conditions.

CHAPTER 4 CFD-BASED MODELLING OF MATERIAL REMOVAL CHARACTERISTICS AND SURFACE GENERATION IN FLUID JET POLISHING

4.1 Introduction

Fluid Jet Polishing (FJP) has the advantages of localized force and cooling of the debris, and of a stable and controllable material removal function with very little tool wear. Due to the complex machining mechanism, it is still difficult to model the material removal characteristics and simulate the surface generation for FJP. In the present study, an attempt was made to better understand the material removal characteristics and surface generation mechanisms in the FJP process.

Hence, a theoretical model was built to predict and characterize the material removal characteristics and surface generation in FJP based on computational fluid dynamics modelling. A series of spot and pattern polishing tests, as well as simulation experiments by the theoretical model, were conducted. The results show that the theoretical model satisfactorily predicts the surface generation under different polishing conditions and enables a better understanding of the polishing process in FJP.

4.2 Polishing Mechanisms

4.2.1 Material Removal Mechanism

In the FJP system, abrasive particles are accelerated by the drag force of water to impact on the workpiece and then initiate material removal at the nano scale. The mechanism of material removal is a complex process, which is affected by various parameters such as abrasive particle concentration, particle size, particle type, slurry pressure, machining time, impingement angle, standoff distance, etc.

While the FJP process bears some similarities to abrasive water jet machining, it operates at much lower slurry pressure and with smaller particle size (Beaucamp et al., 2012). As a result, the particle energy is insufficient to immediately perform a cut, but rather erodes the material at a small rate (Wang et al., 2009a). More generally, target surfaces are machined mechanically by the repeated impact of the small abrasive particles in the ductile mode. The amount of material removed by the fluid jet depends on the flow conditions of the jet slurry and on the abrasive particles' erosion mechanism, as shown in Figure 4.1.

It seems clear that an understanding of the material removal in FJP can be divided into two major parts. The first part involves the determination of the relative motion between the workpiece and the particles, which can be solved by multiphase fluid theory. With the availability of such information, the second part is related to the modelling of the erosion rate caused by abrasive particles. In the FJP process, the material removal characteristics represent the distribution of the material removal rate across the surface of the polishing tool (Markus Schinhaerl et al., 2007; Walker et al.,

2002b). They are referred to as the Tool Influence Function (TIF) which is assessed in terms of width, maximum depth and volumetric material removal rate.

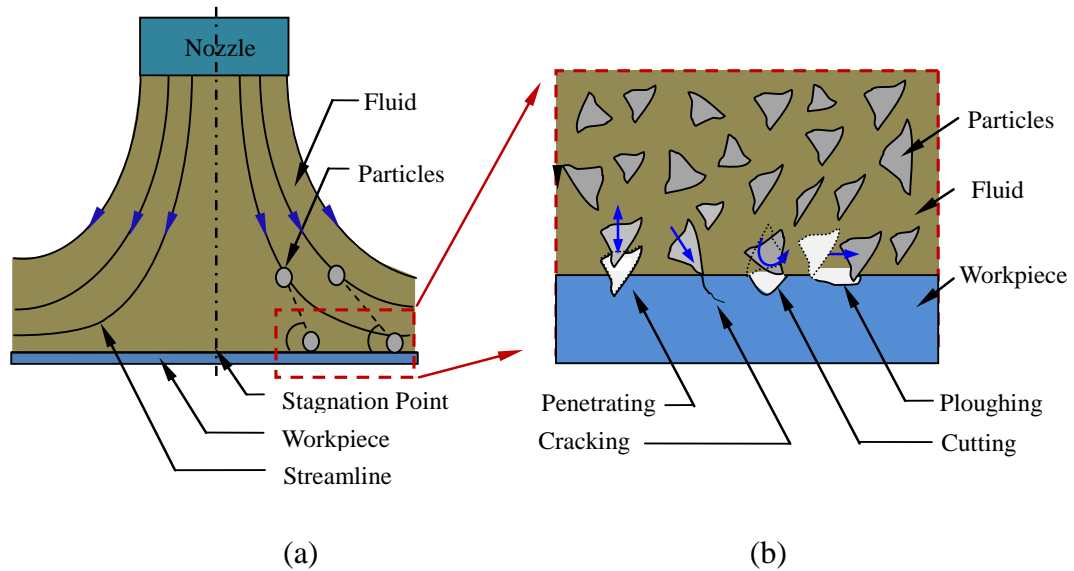


Figure 4.1 Material removal mechanism in the FJP process: (a) fluid conditions in the case of perpendicular impact and (b) abrasive particles' erosion conditions

4.2.2 Surface Generation Mechanism

Fluid Jet Polishing (FJP) is a type of computer controlled ultra-precision polishing (CCUP) technology. In the present study, it is operated on an ultra-precision polishing machining system with three linear axes (X, Y and Z axis), and three rotational axes (A, B and C axis). The slurry nozzle is mounted on the B axis and the fluid jet is released from the slurry nozzle. The workpiece is mounted on the C axis. The machining process of FJP is quite different from that of other diamond machining technologies, such as single point diamond turning and ultra-precision raster milling.

The surface generation in FJP is dominated by the polishing Tool Influence Function (TIF) rather than the geometry of the cutting tool (Cheung et al., 2011). It

turns out that the material removal distribution on the polished surface in FJP can be viewed as the convolution of the tool influence function and polishing tool path planning. Hence, there are two ways to control the surface generation: (a) controlling the tool influence function through changing the polishing process conditions and (b) controlling the polishing path generator with a constant tool influence function.

The former method can achieve non-uniform material removal and shows high polishing efficiency, while it tends to introduce waviness, texture or other non-negligible form error (Schinhaerl et al., 2008a; Tam and Cheng, 2010). The latter method is commonly used by computing the 'dwell time map' for a constant tool influence function during the polishing process (Dunn and Walker, 2008). The slower the velocity of the polishing tool, the more material is removed. Due to the technical restrictions, this method is limited by the velocity of the polishing tool and turns out to have low polishing efficiency.

4.3 Theoretical Modelling of Material Removal in FJP

Figure 4.2 shows a flowchart of theoretical modelling of material removal characteristics and surface generation by FJP. In the first step, the material removal characteristics are obtained using the integrated computational fluid dynamic-based erosion model, which is established by a combination of Computational Fluid Dynamics (CFD) simulation, erosion model and experimental study. Hence, the polishing path planning is determined based on the desired surface integrity of the optical surface to be generated using the data of the material removal characteristics.

Finally, a theoretical model is built for predicting and simulating the surface generation in FJP.

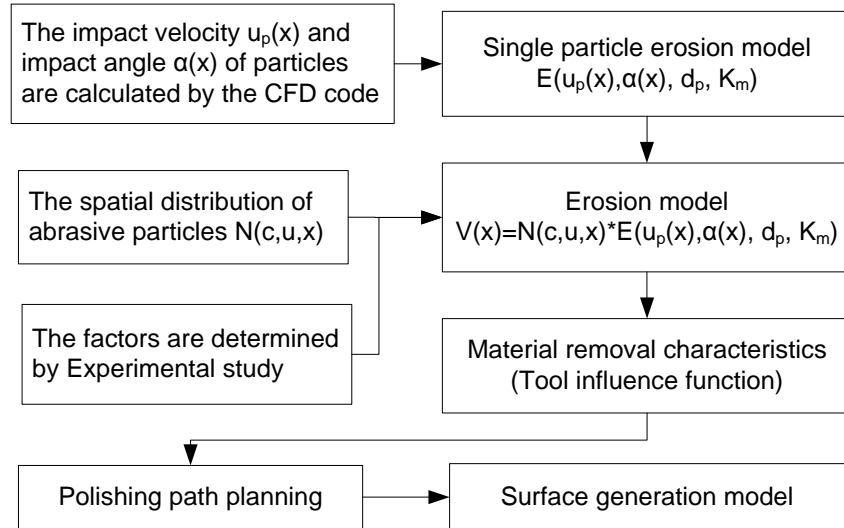


Figure 4.2 Flowchart of theoretical modelling of the material removal characteristics and surface generation by FJP

4.3.1 Computational Fluid Dynamics Modelling

Since direct measurement of particle velocities and visualization of particle trajectories are very difficult in FJP, Computational Fluid Dynamics (CFD) modelling tends to be an effective tool, which is widely used to study the polishing process mechanism and predict the material removal rate due to the impact of abrasive particles (Fang et al., 2006b; Liu et al., 2004; Obikawa and Yamaguchi, 2015). CFD modelling can provide insights into the forces acting on the abrasive particles which affect particle motion and hence determines the conditions of abrasive particles impacting on the target surface. In this study, an Eulerian-Eulerian-Lagrangian

method, which treats the water and air as Eulerian phases and the abrasive particles as Lagrangian particles, is used in the Computational Fluid Dynamics (CFD) software package named FLUENT. The coupled discrete phase model (DPM) and volume of fluid (VOF) model are used to describe the multiphases, and the transport equation for the shear stress transport (SST) $k-\omega$ model together with level set method are used to describe the slurry/air interface in FJP. After solving the flow field, the particulate phase is tracked separately through the flow field based on a force balance around individual particles and particle impact information (velocity, angle and position) is gathered as particles strike the target surface. In the entire CFD process, some assumptions are made as follows:

- (i) In reality, the shape of the particles can affect the particle drag (which couples the particle motion to the fluid motion) to some extent, and the more irregular the particle, the greater the drag. The value of scruple for polishing particles may be 2.08 and a typical particle Reynolds number in this case is around 500. Consequently, the drag of the irregular particles is estimated to be within 5% of the drag of a sphere (Loth, 2008; Thompson and Clark, 1991). Hence, the shape of particles is considered to be spherical in the CFD modelling.
- (ii) The abrasive particles used in FJP commonly come in a specified size distribution, including small and large particles. The abrasive particles supplied by Panadyne Inc., USA are of very small particle size, with a narrow size distribution, so the particle size is assumed to be constant, equal to the average size of the particle distribution used for testing.

- (iii) Due to the low abrasive particle concentration, particle-particle interactions are considered negligible and the particulate phase does not affect the prevailing flow field.
- (iv) The abrasive particle spatial distribution at the inlet is uniform and the initial particle velocity at the inlet is the same as the velocity of its surrounding water.
- (v) Since direct impact can be the dominant type when the impact velocity of the jet slurry is small in the FJP process, only the first impact of the abrasive particles against the surface is considered.

4.3.1.1 Dynamic Flow Description

The impacted slurry in the vertical FJP process is assumed to be a two-dimensional, incompressible, steady axisymmetric turbulent flow with constant properties and temperature conditions (Beaucamp et al., 2012). This turbulence flow field can be established by solving the Reynolds averaged Navier-Stokes (RANS) equations:

$$\frac{\partial \rho}{\partial t} + \frac{\partial}{\partial x_i}(\rho u_i) = 0 \quad (4.1)$$

$$\frac{\partial}{\partial t}(\rho u_i) + \frac{\partial}{\partial x_j}(\rho u_i u_j) = -\frac{\partial p}{\partial x_i} + \frac{\partial}{\partial x_j} \left[\mu \left(\frac{\partial u_i}{\partial x_j} + \frac{\partial u_j}{\partial x_i} - \frac{2}{3} \delta_{ij} \frac{\partial u_i}{\partial x_i} \right) \right] + \frac{\partial}{\partial x_j} \left(-\rho \overline{u'_i u'_j} \right) \quad (4.2)$$

where u_i and u'_i are the mean and fluctuating velocity components ($i=1, 2, 3$); p is the fluid pressure; ρ is the fluid density; μ is the fluid viscosity; δ_{ij} is the Kronecker-Delta function and $-\rho \overline{u'_i u'_j}$ is the Reynolds stresses.

4.3.1.2 Turbulence Flow Description

In the Reynolds averaged Navier-Stokes (RANS) equations, the turbulent correlation for Reynolds stresses should be modelled in order to close the RANS equations. In this study, the shear stress transport (SST) $k-\omega$ model, which was developed by Menter (1994), is applied to describe the turbulent regime in FJP. The SST $k-\omega$ model combines the robust and accurate formulation of the $k-\omega$ model in the near-wall region and the free-stream independence of the $k-\varepsilon$ model in the far field. This makes the SST $k-\omega$ model more accurate and reliable to simulate the laminar to turbulent flow transition of the jetting slurry in the FJP process. The transport equation for the (SST) $k-\omega$ model is described in detail in the Fluent 13.0 Theory Guide (Ansys., 2010a).

4.3.1.3 Multiphase Flow Description

The volume of fluids (VOF) model and the level-set method are popular interface-tracking techniques used to simulate the evolution of the interfaces between the slurry and air. The level-set method can exactly assess the interface curvature and surface tension force (Olsson et al., 2007). However, it is not adequate in accurately maintaining the volume conservation of the immiscible phases. On the contrary, the VOF model is effective in preserving the volume conservation (Annoni et al., 2014). The limitation of the VOF model is that the computation of the interface curvature and surface tension is inaccurate because of the discontinuity of the VOF function

across the interface. To avoid the limitations of both methods, the Coupled Level-Set and VOF Model are used to describe the multiphase systems and the interface according to the Fluent 13.0 Theory Guide (Ansys., 2010a).

4.3.1.4 Lagrangian Particle Phase

To determine the detailed information of the interaction of the particles and workpiece, the particulate phase is modelled using the Lagrangian description rather than the Eulerian method. In this study, particle-particle interactions are considered negligible and the particulate phase does not affect the prevailing flow field which has been shown to be a valid assumption by Chen et al. (2004). A Lagrangian description of the particulate phase is based on a force balance around individual particles accounting for particle drag, gravitational force and additional forces (virtual mass force, Saffman's lift force and pressure gradient), as shown in Eq. (4.3). The effect of the fluid turbulence on the particle motion is taken into account by using a discrete random walk model as referred to by Wallace et al. (2004).

$$\frac{du_p}{dt} = F_D(u - u_p) + \frac{g_x(\rho_p - \rho)}{\rho_p} + F_x \quad (4.3)$$

where F_D is given by:

$$F_D = \frac{18u}{\rho_p d_p^2} \frac{C_D R_e}{24} \quad (4.4)$$

where u is the fluid phase velocity, u_p is the particle velocity, ρ is the fluid density, ρ_p is the density of the particle, d_p is the particle diameter, R_e is the relative Reynolds number, $F_D(u - u_p)$ is the drag force per unit particle mass and

F_x is an additional acceleration (force per unit particle mass) term. In the simulation model, each particle is tracked separately through the flow field and particle impact information (velocity and location) is gathered as particles strike the wall.

4.3.1.5 Boundary Conditions and Other Numerical Settings

The geometry of the computational domain with boundary conditions is shown in Figure 4.3. The CFD simulation starts where the slurry enters the computational domain through the boundary of the INLET and ends after the jet exits the fluid domain from the boundary of the OUTLET. The established CFD model was run with higher-order discretization schemes and a Pressure-Implicit with Splitting of Operators (PISO) scheme for pressure-velocity coupling. The interface sharpening routine applied for the VOF model is Geo-reconstruct. The solution initialization was computed from all zones with the default turbulence kinetic energy and specific dissipation rate and the water volume fraction was set to zero. The rest of the numerical settings were selected to obtain the best results in terms of simulation convergence and accuracy, as suggested in the Fluent 13.0 User's Guide (Ansys., 2010b).

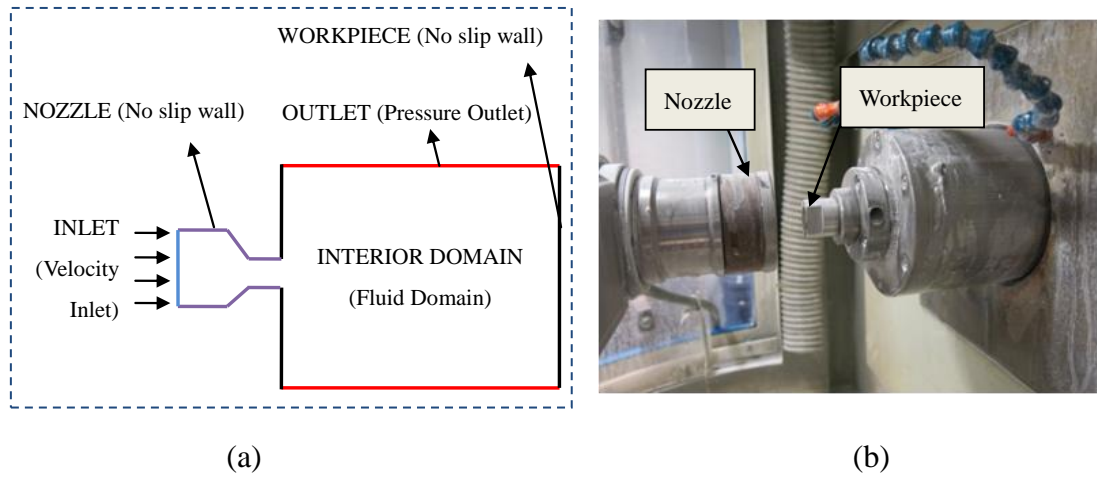


Figure 4.3 (a) Boundary conditions of the CFD model and (b) experimental setup of fluid jet polishing

4.3.2 Spatial Distribution of Abrasive Particles

Due to the axisymmetric characteristics in the vertical FJP, the equation of erosion model can be expressed as:

$$V(x) = N(c, u, x) \cdot E(u_p(x), \alpha(x), d_p, k_m) \quad (4.5)$$

where $V(x)$ is material removal amount at position x , term $N(c, u, x)$ is the abrasive particle spatial distribution that represents the effect of the slurry concentration c , the slurry velocity u , and the impact position x , and the term $E(u_p(x), \alpha(x), d_p)$ is the volume removed by a single particle that describes the effect of the impact velocity $u_p(x)$, the impact angle $\alpha(x)$, the particle size d_p and material property k_m . Generally, CFD-based erosion modelling does not require a detailed knowledge of instantaneous particle distribution, but only the information of time-averaged particle distribution, which reflects the state of the fluid jet as a whole, rather than individual particles. Similar to Abrasive Water Jet technology, the

spatial distribution of the abrasive particles tends to be a Gaussian radial distribution (Balz et al., 2013). A Gaussian Function is given by:

$$f(x) = A \exp\left(-\frac{1}{2} \left| \frac{x-C}{B} \right|^2\right) \quad (4.6)$$

In fact, the spatial distribution of the abrasive particles can also be affected by the nozzle diameter, nozzle shape, standoff distance, etc. Considering the influence of these factors, the modified Gaussian Function is used to describe the abrasive particle spatial distribution (Cheung et al., 2011) and it can be expressed as:

$$f(x) = A \exp\left(-\frac{1}{2} \left| \frac{x-C}{B} \right|^\lambda\right) \quad (4.7)$$

where A controls the height of the curve's peak; C controls the position of the curve's peak; B controls the width of the curve and this can be derived as the half width at the point with the curve height of $A \exp(-0.5)$. The parameter λ can be derived as:

$$\lambda = \frac{\ln(\ln(k_1') / \ln(k_2'))}{\ln(w_1 / w_2)} \quad (4.8)$$

where k_1' is a positive value near 0, w_1 is the width of the curve at the height of $k_1' A$; k_2' is a positive value close to 1, w_2 is the width of the curve at the height of $k_2' A$. As a result, the spatial distribution of particles can be expressed as:

$$N(c, u, x) = k_\eta k_n \cdot cut \pi \left(\frac{d_n}{2}\right)^2 \cdot \frac{6}{\rho_p \pi d_p^3} \cdot \exp\left(-\frac{1}{2} \left| \frac{x-C}{B} \right|^\lambda\right) = \frac{3k_\eta k_n cut d_n^2}{2\rho_p d_p^3} \exp\left(-\frac{1}{2} \left| \frac{x}{B} \right|^\lambda\right) \quad (4.9)$$

where k_η is the efficiency factor to allow for the fact that not all particles are involved in the erosion process and some particles do not have sufficient energy to cut the material, k_n is the scale factor, C controls the position of the curve's peak and

is assigned to be zero in the FJP process, t is the machining time, ρ_p is the density of particles, d_p is the diameter of particles and d_n is the nozzle diameter.

4.3.3. Erosion Model for a Single Particle

Since the particle size and work pressure in the FJP system are relatively small, the abrasive particles are dragged by the water at lower velocities and then impact the surface with much lower kinetic energies as compared with Abrasive water jet machining (Beaucamp et al., 2012). The resulting impact most probably erodes surfaces made of hard and brittle materials in a ductile regime, and produce minimal damage to abrasive particles. In the present study, it is assumed that only the first impact of the abrasive particles against the surface is considered and all particles in the jetting slurry arrive at the surface in the same orientation as shown in Figure 4.4. In reality, the material removal amount and profile due to the impact of a hard particle depend on the impact velocity, shape and orientation of the particle as well as the impact angle as illustrated by Hutchings (1977) and Papini and Spelt (2000a and 2000b). Hutchings (1977) observed that forward rotating particles resulted in target material being pushed to the edge of deep and short triangular craters, and backward rotating particles resulted in the actual machining and removal of a chip of target material. Papini and Spelt (2000b) further found that the maximum material removal occurs at the transition between forward and backward rotation where the particle rotation through the impact is minimized. Despite the evidence that the material removal caused by an angular particle depends on the orientation of the particle as it

strikes the surface, and on whether the particle rolls forwards or backwards during contact, the erosion model can be established regardless of the material removal caused by the rotation energy due to the relatively small impact velocity in the FJP process. The particle velocity can be resolved into two components which include the normal component and the tangential component. The normal component is responsible for the particle penetration in the target surface (deformation wear) while the tangential component gives the particle cutting action as shown in Figure 4.4.

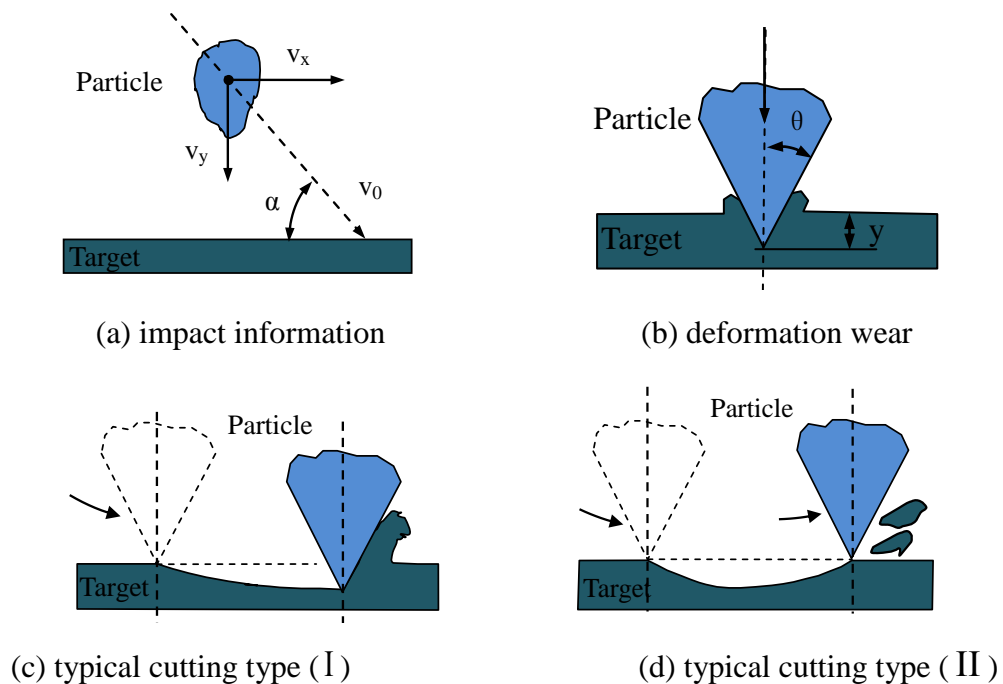


Figure 4.4 Schematic illustration of erosion behaviour of impacting particle

To establish an erosion model for the ductile-mode machining of hard and brittle materials, the following assumptions are made:

- (i) Abrasive particles are assumed to be cones of semiangle θ and have the same diameter.

- (ii) Particle deformation can be neglected and the deformation of the surface is perfectly plastic with a constant plastic flow pressure P_n (normal direction) and P_t (tangential direction) during the impact process.

4.3.3.1. The Normal Component of Kinetic Energy

At time t after initial contact, the particle of mass m_p has indented the surface to the depth of y ; the cross-sectional area of the indentation at the surface is A_y , where A_y is determined by the shape of the particle. The normal force acting on the particle is due to the plastic flow pressure acting over the area A_y :

$$A_y = \pi y^2 \tan^2 \theta \quad (4.10)$$

where θ is the semiangle of the particle. The equation of motion of the particle can be written as:

$$du_y = \frac{F_y}{m_p} dt = -\frac{P_n A_y}{m_p} dt = -\frac{P_n A_y}{m_p} \cdot \frac{dy}{u_y} \quad (4.11)$$

Eq. (4.11) can be solved under the initial conditions $u_y = u_{y0}$: when $y=0$ and $u_y = 0$ when $y = y_{\max}$, where u_{y0} is the initial normal component of a particle's impacting velocity and y_{\max} is the maximum depth of the indentation, one has:

$$\int_0^{y_{\max}} A_y dy = \frac{m_p u_{y0}^2}{2P_n} \quad (4.12)$$

As a result, the final volume of the indentation V_{ey} is given by:

$$V_{ey} = \int_0^{y_{\max}} A_y dy = \frac{m_p u_{y0}^2}{2P_n} = \frac{m_p u_0^2 \sin^2 \alpha}{2P_n} \quad (4.13)$$

where u_0 is the initial velocity of the particle and α is the impact angle of the particle. Some researchers (Hutchings, 1976, 1993; Hutchings et al., 1981; Hutchings

and O'Brien, 1981) presented that the material displaced from the indentation can be accommodated in several ways which include: elastic deformation, plastic deformation or removed as wear debris. Due to a number of different energy dissipations, only part of the work of indentation can contribute to the erosion process since the elastic work of indentation is returned to the particle during rebound (Bull, 2006; Papini and Dhar, 2006). As a function of the particle's kinetic energy only, Slikkerveer et al. (1998) concluded that the erosion efficiency, ε , is the parameter best suited to characterize the erosion process, where:

$$\varepsilon = k_1 \left(\frac{m_p u_0^2 \sin^2 \alpha}{2} \right)^n \quad (4.14)$$

where k_1 and n are coefficients, determined by experiments. As a result, the volume removed by the normal component of a particle's impacting velocity can be expressed as:

$$V_y = \varepsilon V_{ey} = k_2 \frac{m_p^{1+n} u_0^{2(1+n)} \sin^{2(1+n)} \alpha}{p_n} \quad (4.15)$$

where $k_2 = k_1 / 2^{n+1}$.

4.3.3.2. The Tangential Component of Kinetic Energy

As a result of the normal component of kinetic energy, the particle can penetrate into the surface, while the tangential component of kinetic energy can produce the cutting action. The cutting volume caused by the tangential component of kinetic energy is expressed as:

$$V_{ex} \approx \int_0^L A_x dx \quad (4.16)$$

where A_x is the cross-cutting area; L is the cutting length and x is the cutting position. Huang et al. (2008) simplified the cutting profile and expressed the cross-cutting area A_x by using Eq. (4.17):

$$A_x = \frac{2y_{\max} D_{\max}}{L^2} x^2 \quad (4.17)$$

The tangential component force acting on the particle is expressed as:

$$F_x = c_1 p_t A_x^b \quad (4.18)$$

where c_1 is a coefficient and b is the exponent of the cross-section area ($0.5 \leq b \leq 1$). By substituting Eq. (4.10) into Eq. (4.12), the maximum depth of the indentation can be expressed as:

$$y_{\max} = \left(\frac{3m_p u_{y0}^2}{2\pi p_n \tan^2 \theta} \right)^{1/3} \quad (4.19)$$

The maximum width of the indentation of the surface is given by Eq. (4.20):

$$D_{\max} = 2y_{\max} \tan \theta = 2 \tan \theta \left(\frac{3m_p u_{y0}^2}{2\pi p_n \tan^2 \theta} \right)^{1/3} \quad (4.20)$$

In the cutting process, there are two cases:

Case (1): the tangential velocity component becomes zero during the collision which is shown as typical cutting type (I) in Figure 4.4(c);

Case (2): the particle has a tangential velocity component when it leaves the surface and this is shown as typical cutting type (II) in Figure 4.4(d).

To describe these cases, the energy equation of the particle can be expressed approximately by using Eq. (4.21):

$$c_2 \int_0^{L/2} F_x dx = \frac{1}{2} m_p (u_{x0}^2 - u_{xout}^2) \quad (4.21)$$

where c_2 is a coefficient and about 1 for the Case (1) (see Figure 4.4(c) typical cutting type(I)), 2 for the Case (2) (see Figure 4.4(d) typical cutting type(II)); u_{xout} , the tangential velocity when the particle leaves the surface, can be expressed as $u_{xout} = cu_{x0}$, where $c \leq 1$ is a coefficient. Substituting Eqs. (4.17) and (4.18) into Eq. (4.21) and integrating it, we have:

$$L = \frac{c_3 m_p u_{x0}^2}{y_{max}^b D_{max}^b P_t} \quad (4.22)$$

where $c_3 = (1 - c^2)(2b + 1) / (c_1 c_2)$. By substituting Eqs. (4.17), (4.19), (4.20) and (4.22) into Eq. (4.16), and integrating it, the cutting volume (V_{ex}) caused by the tangential component of kinetic energy can be expressed as:

$$V_{ex} = \frac{c_4 m_p^{1+2(1-b)/3} u_0^{2+4(1-b)/3} (\cos \alpha)^2 (\sin \alpha)^{4(1-b)/3}}{P_t P_n^{2(1-b)/3} (\tan \theta)^{(1-b)/3}} \quad (4.23)$$

where $c_4 = (2^{1+(1-b)/3} \cdot 3^{2(1-b)/3-1} c_3) / (\pi^{2(1-b)/3})$. The actual material removal by cutting action of a particle is proportional to the cutting volume (V_x):

$$V_x = c_5 \frac{c_4 m_p^{1+2(1-b)/3} u_0^{2+4(1-b)/3} (\cos \alpha)^2 (\sin \alpha)^{4(1-b)/3}}{P_t P_n^{2(1-b)/3} (\tan \theta)^{(1-b)/3}} = k_3 \frac{m_p^{1+2(1-b)/3} u_0^{2+4(1-b)/3} (\cos \alpha)^2 (\sin \alpha)^{4(1-b)/3}}{P_t P_n^{2(1-b)/3} (\tan \theta)^{(1-b)/3}} \quad (4.24)$$

where $k_3 = c_4 c_5$. The volume of material removal caused by the impacting particle can be obtained by the sum of volume losses produced by the normal and tangential component of kinetic energy approximately and expressed as:

$$E(x) = V_x + V_y = k_3 \frac{m_p^{1+2(1-b)/3} u_0^{2+4(1-b)/3} (\cos \alpha)^2 (\sin \alpha)^{4(1-b)/3}}{P_t P_n^{2(1-b)/3} (\tan \theta)^{(1-b)/3}} + k_2 \frac{m_p^{1+n} u_0^{2(1+n)} (\sin \alpha)^{2(1+n)}}{P_n} \quad (4.25)$$

4.3.3 Polishing Tool Path Planning

In practice, polishing is a multi-stage process conducted by repeatedly running particular designed polishing cycles until the expected surface finish and form error are obtained. Within each cycle, the polishing tool sweeps through the polished surface under the adopted polishing tool path and desired polishing parameters. Hence, an important part of freeform surface polishing is the tool-path generation (Tam et al., 1999) in considering time efficiency and surface quality improvement. It is interesting to note that the amount of material removal can be considered as the convolution of the influence function and the dwell time map along the pre-specified tool path. Hence, the dwell time map, processed by the variations of the feed velocity of the polishing tool, is computed through a complicated deconvolution process. This implies that the programmed dwell time map can correct the form error while uneven polishing can lead to undesirable surface waviness (Tsai et al., 2009).

As shown in Figure 4.5, there are various polishing paths that can be planned based on the desired surface integrity of the optical surface to be generated. For example, the polishing path can be the raster path, cross path, spiral path, Hilbert path, Peano path (Tam et al., 2013), Lissajous path or Pseudo-random path (Dunn and Walker, 2008), etc.

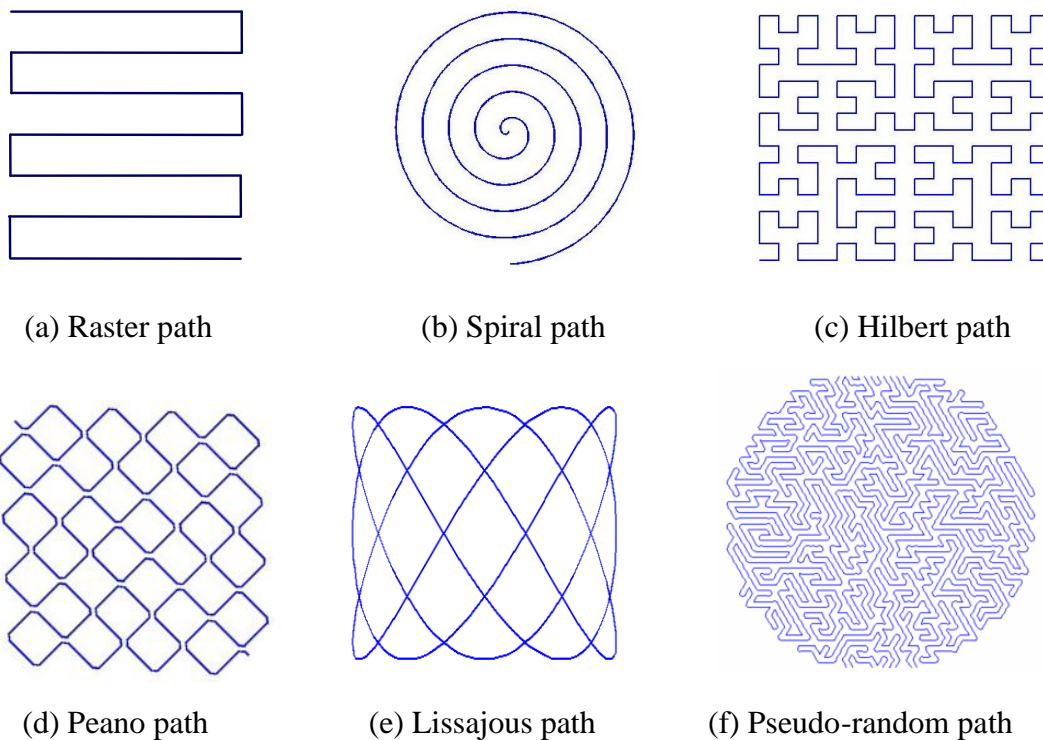


Figure 4.5 Tool path planning for Fluid Jet Polishing

As shown in Figure 4.6, a surface generation model was built and developed by using the MATLAB software package so as to verify the predictability of the surface generation model and to compare the measured and the predicted results by using the feature parameters in this study. The polishing conditions in the polishing paths are assumed to be constant and hence the tool influence function is stable and constant, and the polishing paths are also assumed to be evenly spaced straight lines on a flat surface. As the sample was polished with an impingement angle of 90° , it is interesting to note that the influence function has axial symmetry and a W-shaped spot, as shown on the left side of Figure 4.6.

When this influence function follows a raster tool path with a constant surface feed rate, the removal profile is constant along all path lines. For raster polishing, the

material removal distribution is constant along the path line direction, and waves in the orthogonal direction arise from the overlapping of the removal profiles affiliated with adjacent polishing path lines. In this case, the surface generation is simplified to a 2D problem which can be solved numerically for a given polishing path spacing and path number. The spacing of the polishing path represents the translational distance of the removal profile along the orthogonal direction and the feed rate determines the dwell time of each polished spot, and hence the surface height of the removal profile along the path line direction.

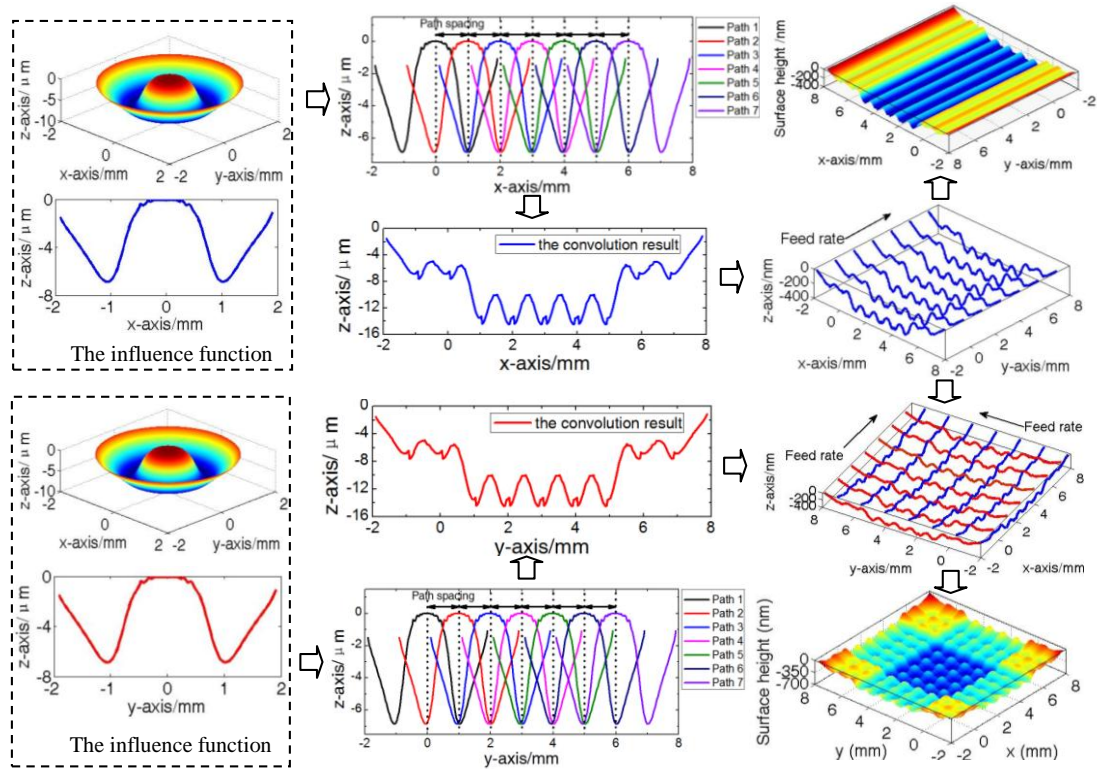


Figure 4.6 Schematic diagram of the theoretical modelling of the surface generation in the raster and cross polishing

Most importantly, the surface generation of FJP is assumed to be a linearly

cumulative effect of the dwell time together with the constant material removal rate for the identical polishing condition. For cross polishing, the surface generation can be considered as the superposition of two orthogonal raster polishing results. The influence function and the polished surface area are expressed as meshes of the same size. The surface generation by cross polishing is computed by summing up the removal amount at all the mesh points.

4.4 Experimental and Simulated Results

The experimental study was divided into two parts, i.e. spot polishing tests and pattern tests. Spot polishing tests were conducted to verify the feasibility of the theoretical modelling under various polishing conditions; while pattern tests focused on the experimental evaluation of the surface generation model for various materials. Experiments were conducted on a Zeeko IRP 200 ultra-precision freeform polishing machine. All specimens were polished by using Al_2O_3 slurry and measured by a non-contact 3D optical system, Wyko NT 8000 from Veeco Inc., USA.

4.4.1 Experimental Verification of the Material Removal Model using Various Polishing Conditions

Table 4.1 tabulates the experimental parameters used for the validation of the theoretical modelling under various polishing conditions. Three groups of experiments (i.e. group A1-A3, group B1-B3 and group C1-C4) were conducted under

different polishing times, abrasive particle concentrations and work pressures. All experiments in Part A were conducted using the Al_2O_3 slurry with a particle size of $3.22 \mu m$ for polishing of the optical glass BK7 and they were performed by changing one process factor and keeping the other process factors constant for each of the groups. A series of CFD simulations was constructed under the same conditions that were adopted for polishing experiments as shown in Table 4.1.

Table 4.1 The experimental parameters used for validation of theoretical modelling

Condition No.	Impingement angle (°)	Slurry concentration	Pressure (Bar)	Nozzle diameter(mm)	Standoff distance(mm)	Machining time (s)
A1	90	1:12	12	1.1	10	60
A2	90	1:12	12	1.1	10	120
A3	90	1:12	12	1.1	10	240
B1	90	1:6	12	1.1	10	180
B2	90	1:9	12	1.1	10	180
B3	90	1:12	12	1.1	10	180
C1	90	1:12	5	1.1	10	180
C2	90	1:12	8	1.1	10	180
C3	90	1:12	10	1.1	10	180
C4	90	1:12	12	1.1	10	180

The results of the simulation (in the case of 10 bar) are shown in Figure 4.7. As

shown in Figure 4.7(a), the blue area with deep colour represents the Al_2O_3 slurry and red area with light colour represents the surrounding air in FJP. Figure 4.7(b) shows the distribution of pressure in the FJP process. It shows that high pressure focuses on the shrinkage aperture of the nozzle and the impact area between the slurry and the workpiece. Figure 4.7(c) shows the distribution of the velocity in the FJP process, which indicates that the velocity is increased in the shrinkage area of the nozzle and arrives at a maximum when the slurry jets out of the nozzle. A relatively small velocity occurs at the centre of the impact area. Figure 4.7(d) shows the concentration distribution of the CFD simulation in a given moment. Due to the dynamic characteristics of particles being random in the slurry, it is interesting to note that the concentration distribution tends to be different at any given time.

Figure 4.8 shows a comparison between the measured results and simulated results for the maximum depth of the influence function. Figure 4.8(a) reveals that the amount of material removal increases linearly with increasing polishing time. This proves that the form error can be corrected by the compensatory 'dwell time map' of the polishing tool. It is shown that the predicted value is slightly larger than the measured data when the initial design concentration (1:12) is used. However, the predicted results agree well with the measured data when the concentration is changed to 1:14. This implies that the real abrasive particle concentration is varied in the polishing process. The variation of the abrasive particle concentration affects the slope of the fitted curve between the polishing time and the maximum depth of the influence function, and this phenomenon can be predicted reasonably well by the

established theoretical model.

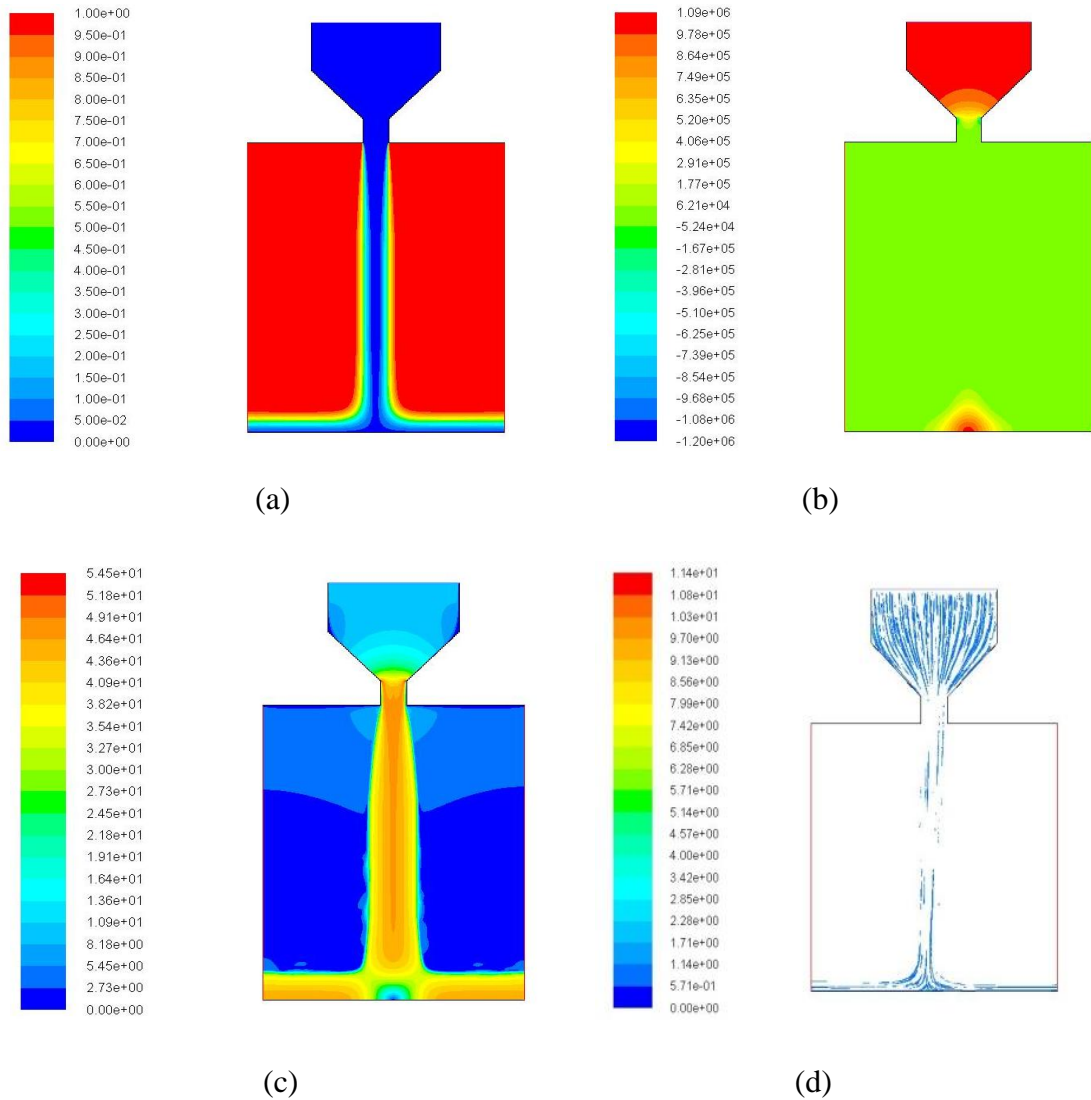
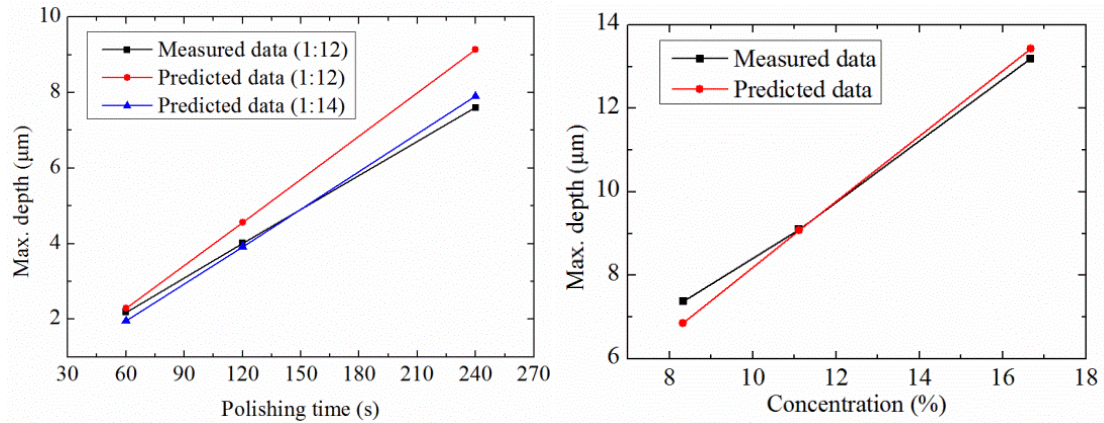


Figure 4.7 (Colour online) Distribution of normal impact fluid field (for 10 bar): (a) phase field, (b) pressure field (Pa), (c) velocity field (m/s) and (d) concentration field (kg/m³)

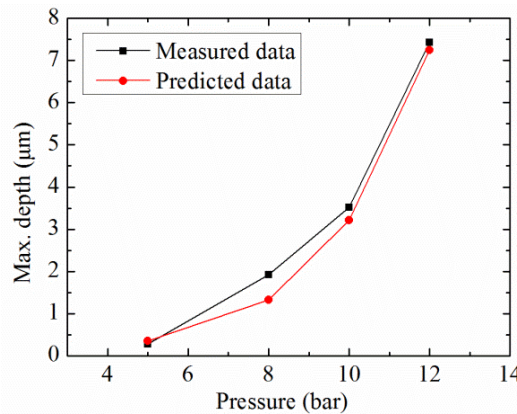
Figure 4.8(b) shows that the maximum depth of the influence function depends linearly on the abrasive particle concentration and can be well predicted by the theoretical model. Figure 4.8(c) suggests that the exponent of pressure corresponding

to the material removal rate tends to be between 2 and 3, according to the polynomial fitting of the experimental data, and this is adequately explained by the theoretical model. Since various polishing parameters are difficult to detect in real time, and to control them accurately, the theoretical model provides an important means for explaining the experimental phenomena and better understanding of the polishing process.



(a) Polishing time

(b) Slurry concentration



(c) Pressure

Figure 4.8 Comparison between the measured and simulated results for the maximum depth of the influence function

To further verify the effectiveness of the developed prediction model, a least-squares-based surface matching method was used to evaluate the deviation of the measured surface from the corresponding simulated surface (Ren et al., 2012a, 2012b). Figure 4.9 shows the surface matching and error evaluation process for case C3. It is clearly seen from Figure 4.9(a) that some misalignment exists between the coordinate frames of the measured surface and the simulated surface. Hence, surface matching is required to eliminate the misalignment of the coordinate frame.

The surface matching method is an optimization process to search for an optimal Euclidean motion for the measured surface so that it is aligned with the theoretical surface as closely as possible. Figure 4.9(b) shows two surfaces after the surface matching. Hence, the deviation of the measured data from the design surface is considered to be the prediction error of the proposed model as shown in Figure 4.9(c). It is interesting to note that the topography of the 3D error map is not rotationally symmetrical, and relatively large deviations may occur at some positions. This may be due to the asymmetry of experimental results and may be affected by some experimental conditions, including the instability of the pumping system, the surface inclination of the samples and/or the abrasion of the nozzle, etc. (Cao and Cheung, 2014). When vertical FJP is used to polish the target surface, the asymmetry of the influence function could lead to undesirable surface waviness and hence affect the final surface generation. As a result, the experimental conditions should be critically controlled to obtain a stable and controllable influence function, especially for the achievement of corrective polishing and deterministic machining using FJP

technology.

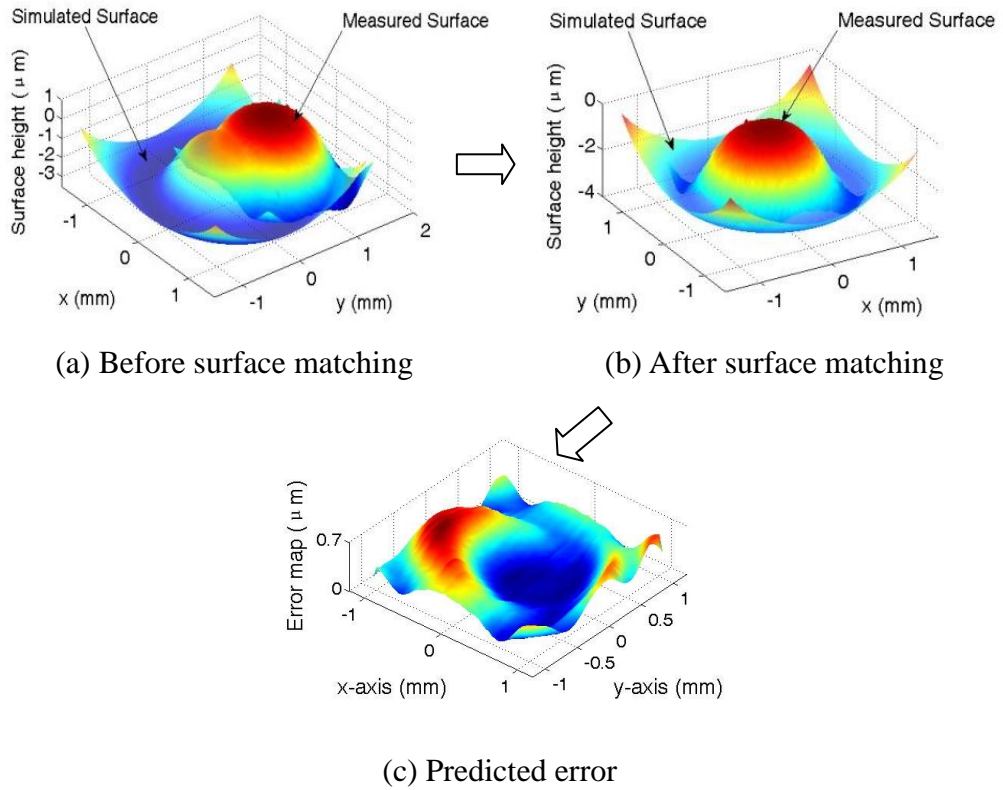


Figure 4.9 Surface matching and error evaluation process for case C3

Table 4.2 shows the quantitative analysis for spot polishing tests under different polishing conditions. In this table, PV and RMS represent the peak-to-valley value and root-mean-squared value of the prediction error, respectively. S_t represents the maximum peak to valley height of the measured surface of the tool influence function, while $P_a = PV / S_t$ is used to evaluate quantitatively the deviation of the modelled and the measured surface of the tool influence function. Although the polishing parameters are hard to control accurately in the FJP process, the predicted results show an average of 76.54 percent agreement with the measured data under the

various polishing conditions. This validates the technical feasibility and effectiveness of the theoretical modelling for understanding and predicting the effect of some important process parameters on the influence function in Fluid Jet Polishing.

Table 4.2 Evaluated results of polished spots under different polishing conditions

Condition No.	PV	RMS	S_t	P_a
A1	0.5261 μm	0.1704 μm	2.21 μm	23.8%
A2	0.7862 μm	0.1580 μm	4.01 μm	19.6%
A3	1.8914 μm	0.3998 μm	7.7 μm	24.6%
B1	3.1625 μm	0.6718 μm	13.21 μm	23.9%
B2	2.0406 μm	0.4600 μm	9.1 μm	22.4%
B3	2.0387 μm	0.4486 μm	7.42 μm	27.5%
C1	0.1388 μm	0.0405 μm	0.48 μm	28.9%
C2	0.4467 μm	0.1108 μm	1.92 μm	23.3%
C3	0.6771 μm	0.3170 μm	3.52 μm	19.2%
C4	1.5769 μm	0.4024 μm	7.37 μm	21.4%

4.4.2 Experimental Verification of the Surface Generation Model for the Various Materials

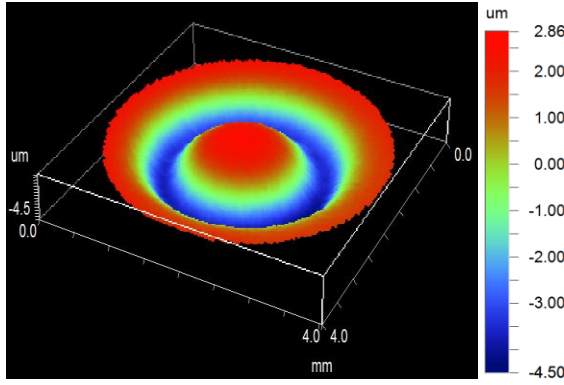
A series of practical polishing experiments was designed to validate the surface generation model developed in this study. Three groups of experiments were conducted using the Al_2O_3 slurry for polishing different materials under identical polishing conditions. One of the experiments was designed for polishing a workpiece

made of Nickel Copper (NiCu), which is a ductile material while another experiment was designed for polishing steel, which is a hard and difficult-to-machine material and is not amenable for diamond machining technologies due to significant tool wear problems. And the third experiment was designed for polishing optical glass material (BK7), which is a brittle material commonly used in advanced optics applications. Table 4.3 shows the polishing parameters used for testing the tool influence function and the generation of different surface patterns. In the tool influence function tests, all samples were polished at a constant polishing time of 180 s, while the raster polishing mode with two polishing steps was used for generating different surface patterns.

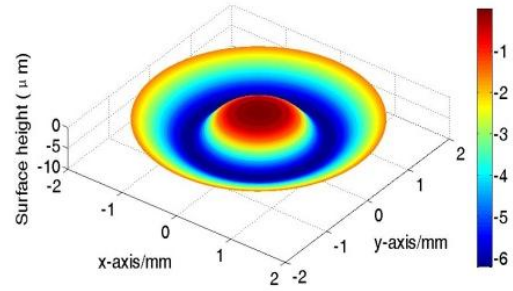
Table 4.3 Parameters for tool influence function tests and pattern tests of FJP

Parameters	Setting
Abrasive particle concentration	1:12
Particle size	3.22 μm
Standoff distance	10 mm
Work pressure	10 bar
Nozzle diameter	1.1 mm
Impingement angle	90°
Surface feed rate	5 mm/min
Polishing mode	Raster
Polishing direction	Horizontal \rightarrow Vertical
Polishing spacing	1 mm

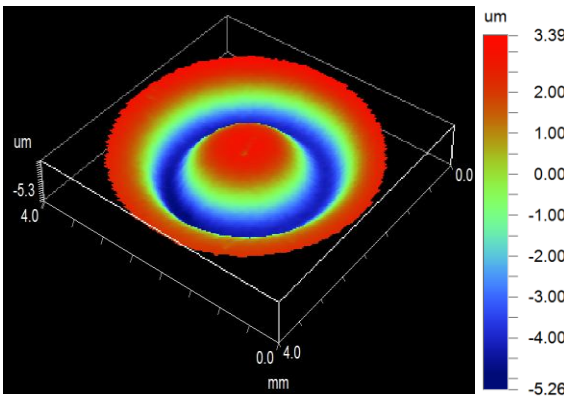
The measured results of the influence function tests and the simulated results of the theoretical modelling for different materials are given in Figure 4.10. It is shown that the width of the influence function only changes slightly and this can be considered to be constant for the various materials. Steel appears to possess the highest material removal rate while the amount of material removal for BK7 is smaller than that for polishing steel. NiCu is highly resistant to erosion by the jet slurry and thus has the lowest material removal rate. It is also found that the predicted polishing tool functions agree well with that for the experimental data. The central point of the polishing tool tends to be the stagnation point, where the pressure is the highest and the velocity is the smallest which can be approximated to be zero. Hence, the centre of the fluid jet has the minimum material removal rate due to the low kinetic energy of the jet slurry. This implies that the ductile-mode theoretical model can be used for better understanding of the polishing mechanisms and predicting the material removal characteristics for various materials in the FJP process.



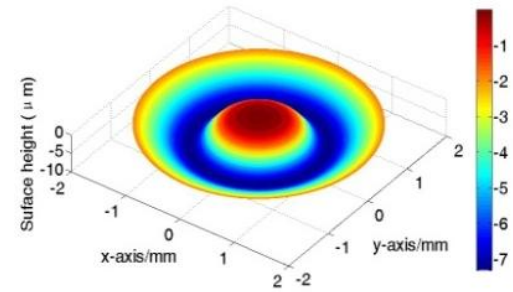
(a) Measured result of NiCu



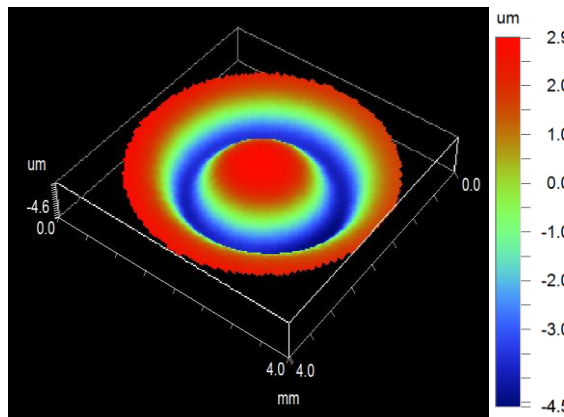
(b) Simulated result of NiCu



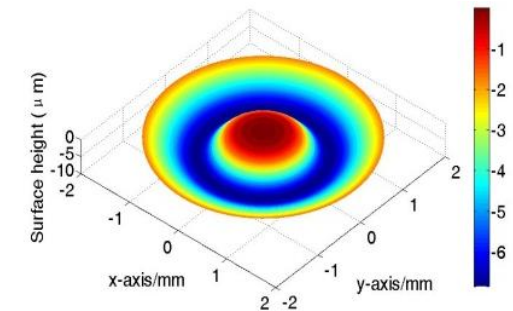
(c) Measured result of Steel



(d) Simulated result of Steel



(e) Measured result of BK7



(f) Simulated result of BK7

Figure 4.10 Comparison between the measured and simulated results of TIF for various materials

The experimental results obtained by the surface pattern tests show that more

material was removed in the central areas than that in the edge areas of the raster polishing and cross polishing tests. This is due to the overlapping of the polishing tool influence functions and this can be well predicted by the theoretical model. Figure 4.11 to Figure 4.13 show the experimental and the simulated results. It is found that the simulated surface patterns agree well with the measured patterns. This further validates the capability of the surface generation model presented in this study. For a constant material removal rate and under identical polishing conditions, it is found through the experimental study and the surface generation model that FJP is a cumulative process for various materials, depending linearly on the dwell time.

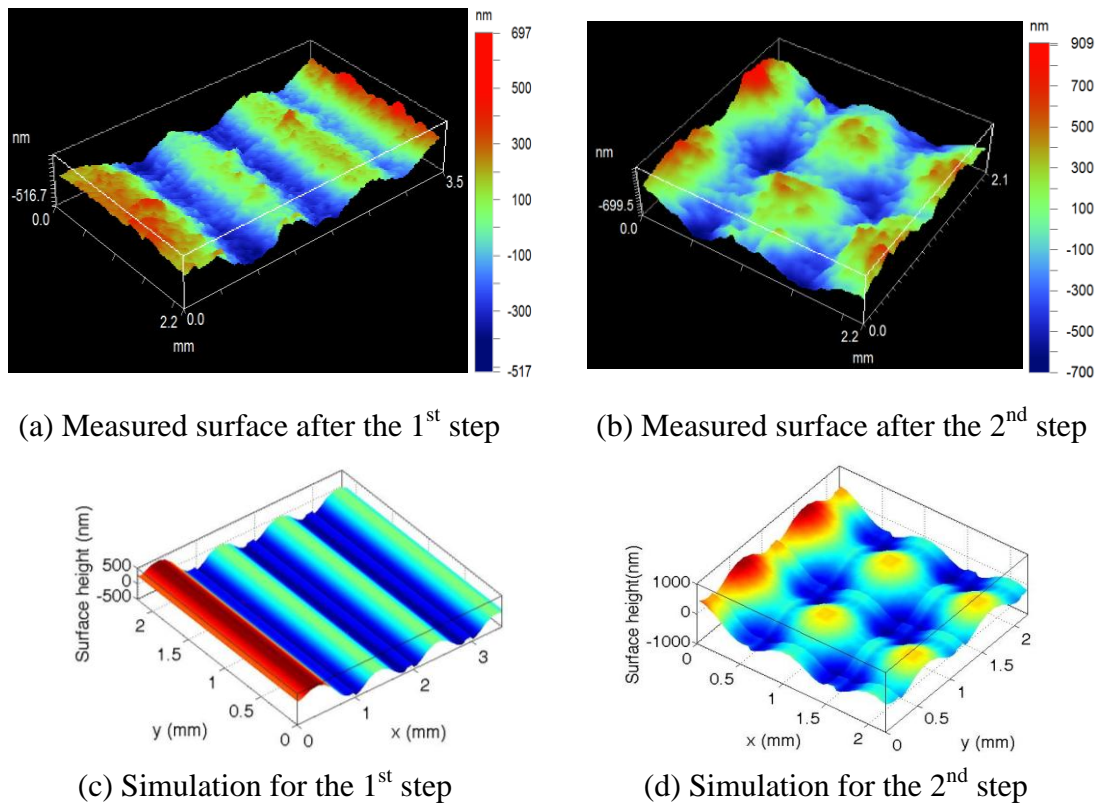


Figure 4.11 Comparison between the experimental and simulated results for NiCu

The comparison of the theoretical model and the pattern tests reveals that the model can be used for predicting and gaining a better understanding of the FJP process of various materials. It also implies that the surface generation in FJP is sensitive to the initial surface condition, the influence function, the dwell time map and the polishing path. Hence, the stability of the pressure system and the precision of the motion control are critical in regard to corrective polishing and deterministic machining. Any error of these parameters may cause undesired material removal and may produce unacceptable waviness when polishing optical surfaces.

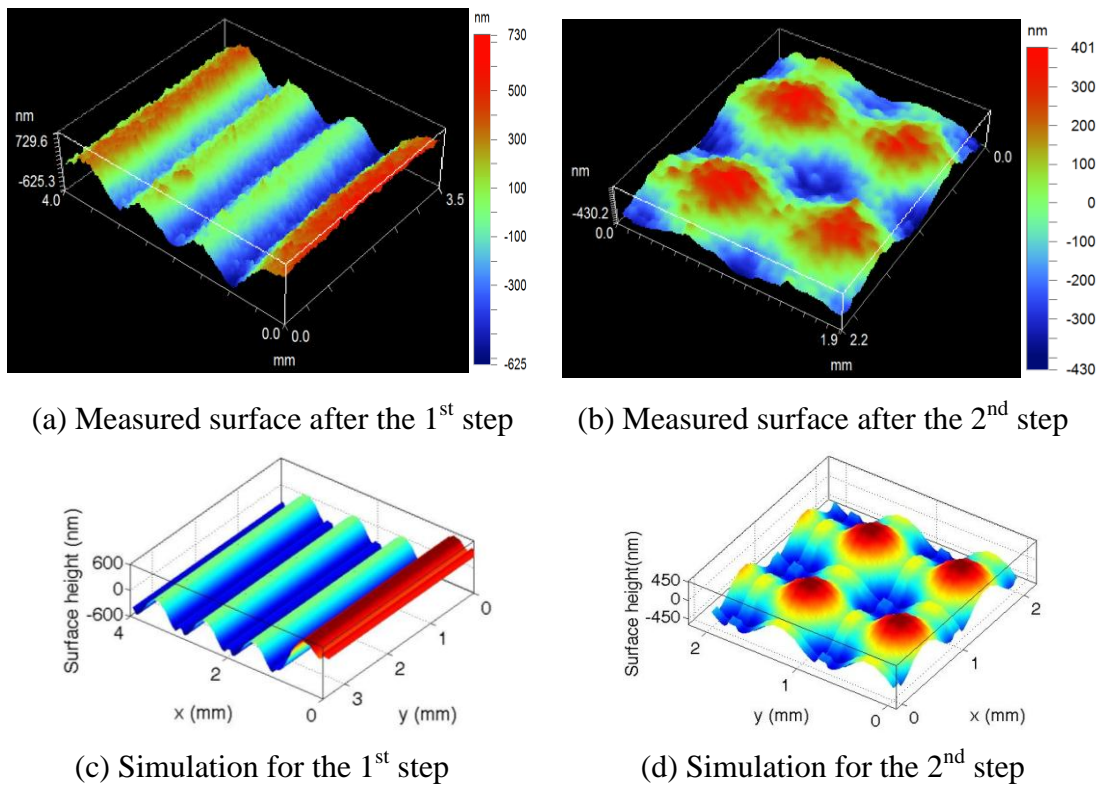
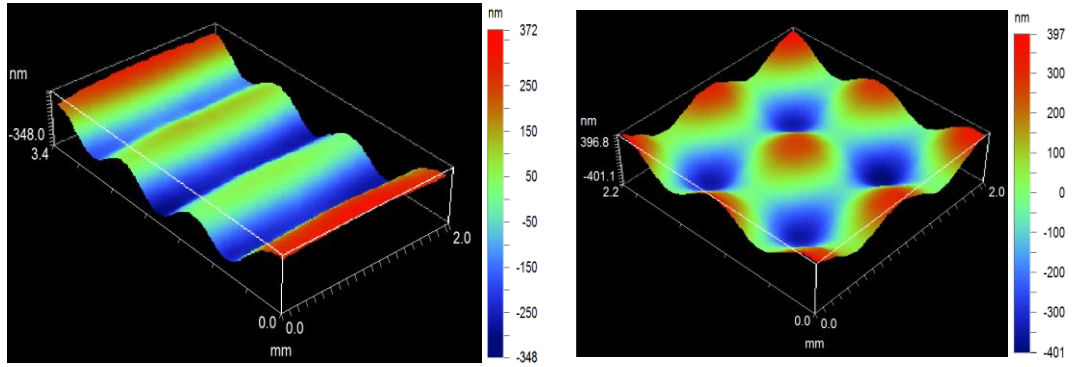
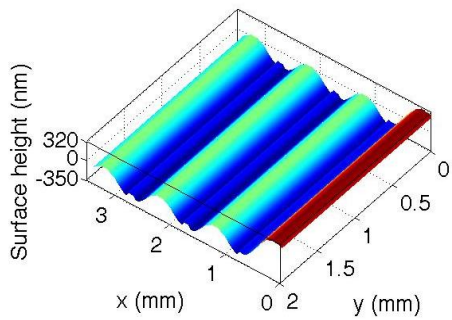


Figure 4.12 Comparison between the experimental and simulated results for steel

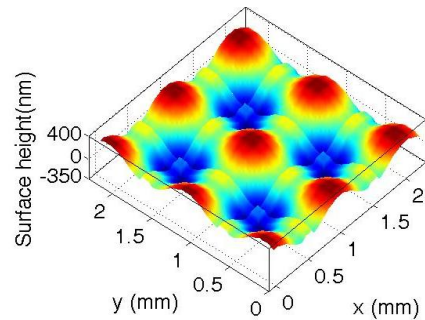


(a) Measured surface after the 1st step

(b) Measured surface after the 2nd step



(c) Simulation for the 1st step



(d) Simulation for the 2nd step

Figure 4.13 Comparison between the experimental and simulated results for BK7

To further verify the effectiveness of the surface generation model, the least-squares-based surface matching method (Ren et al., 2012a, 2012b) discussed in Section 4.4.1 was also used to evaluate the deviation of the measured surface from the corresponding simulated surface. Figure 4.14 shows the surface matching and error evaluation process for the pattern test (for the case of cross polishing of steel). The evaluated form errors of the pattern tests for different materials are shown in Figure 4.15. It is interesting to note that the simulation results agree reasonably well with the measured surfaces. As a result, the surface generation model provides a reliable prediction of the surface generation by Fluid Jet Polishing.

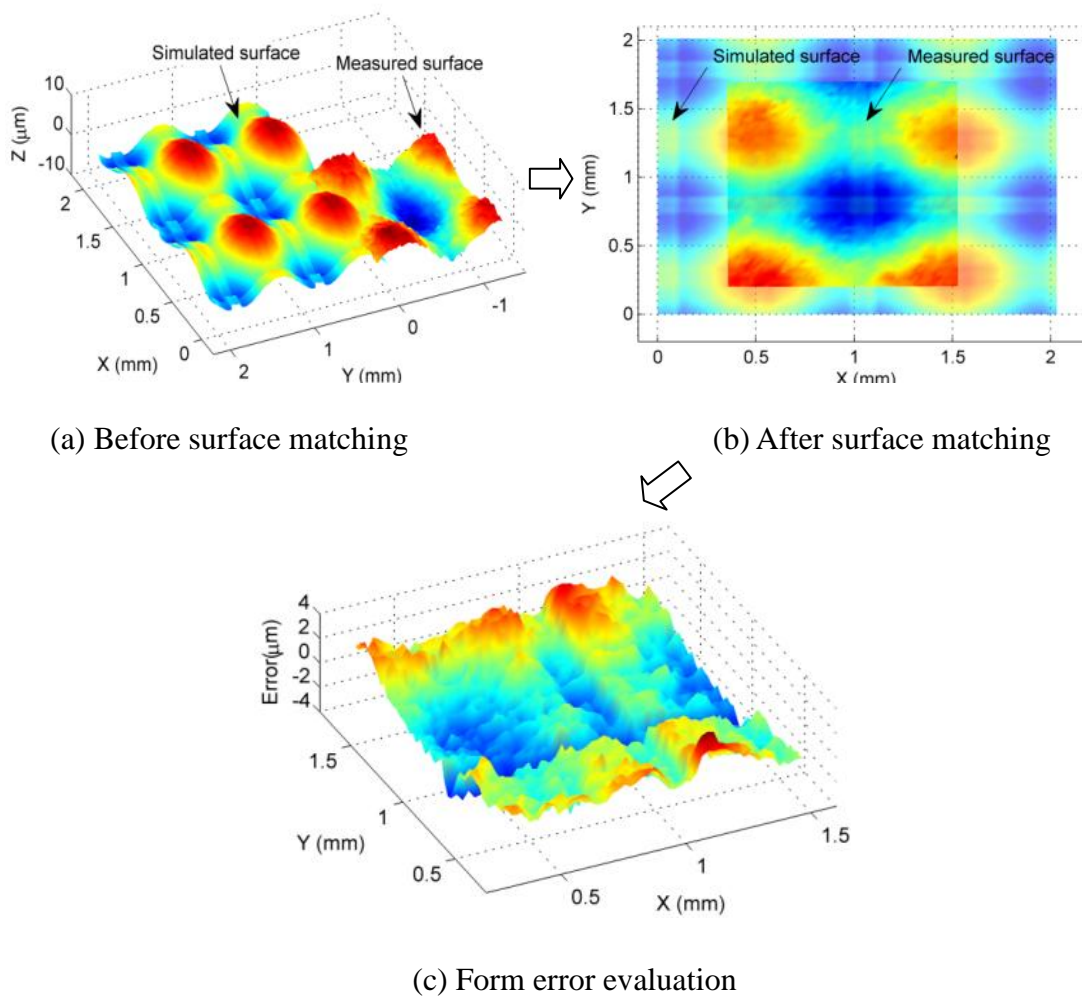
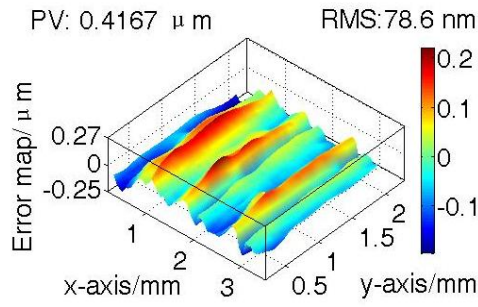
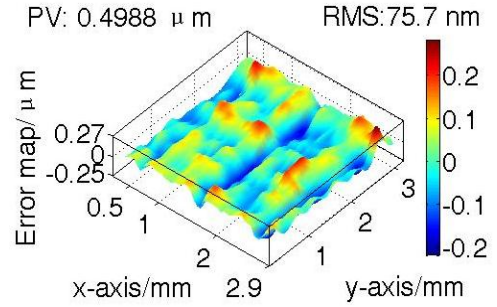


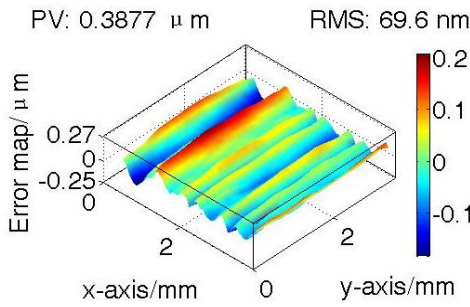
Figure 4.14 Schematic diagram of the error evaluation process for the pattern test



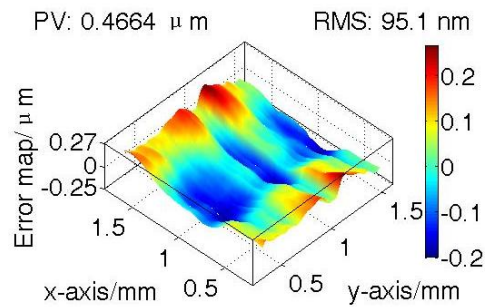
(a) Error map of NiCu for the 1st step



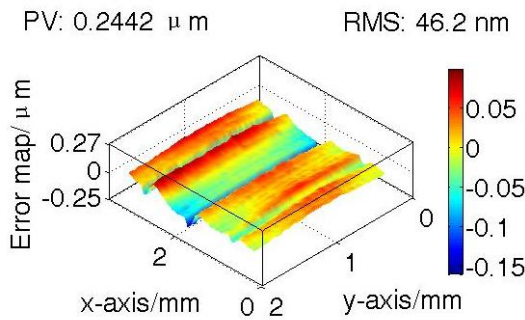
(b) Error map of NiCu for the 2nd step



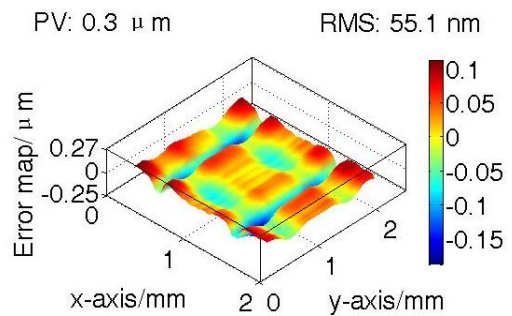
(c) Error map of Steel for the 1st step



(d) Error map of Steel for the 2nd step



(e) Error map of BK7 for the 1st step



(f) Error map of BK7 for the 2nd step

Figure 4.15 Evaluated form error of the testing patterns for different materials

4.5 Summary

This chapter presents a study of the modelling, simulation and testing of surface generation by using Fluid Jet Polishing (FJP) technology. Through a better understanding of the polishing process, a theoretical model is built for the prediction

and simulation of the surface generation in FJP. Computational Fluid Dynamics (CFD) theory and erosion mechanisms are used to establish the theoretical model, while the polishing strategy is determined by the desired surface integrity of the optical surface generated and using data on the material removal characteristics.

A series of spot polishing tests was conducted to verify the theoretical model under different polishing conditions. The results show that the theoretical model predicts well that the amount of material removal increases with increasing pressure, and depends linearly on the polishing time and abrasive particle concentration. Moreover, the theoretical model provides an important means for better understanding and predicting the effect of process parameters in the polishing process.

The deviation between the predicted and measured results of the spot polishing tests show that the influence function does not have rotational symmetry while the relatively large deviations may occur at some positions. The asymmetry of the influence function could lead to undesirable surface waviness and hence affect surface generation.

A comparison of the surface generation model and the pattern tests reveals that the model can be used for predicting the surface quality of the workpiece and acquiring a better understanding of the polishing process in FJP. Both experimental and theoretical results show that the surface generation in FJP is a linearly cumulative function of the dwell time, with a constant material removal rate under identical polishing conditions.

CHAPTER 5 MULTI-SCALE MODELLING OF MATERIAL REMOVAL CHARACTERISTICS AND SURFACE GENERATION IN BONNET POLISHING

5.1 Introduction

Bonnet Polishing (BP) is an enabling technology which is capable of fabricating ultra-precision freeform surfaces with sub-micrometre form accuracy and surface roughness in the nanometre range. This is particularly useful for machining difficult-to-machine and ferrous materials. However, the material removal mechanism of bonnet polishing usually exhibits multidisciplinary and multi-scale complexity and hence our understanding of the material removal characteristics and surface generation is still far from complete.

As a result, a multi-scale material removal model and a surface generation model were built based on the contact mechanics, kinematics theory, abrasive wear mechanism, as well as the relative and cumulative removal process of surface generation in bonnet polishing. The models were verified through a series of spot and pattern polishing experiments. Based on the results of spot polishing experiments, the multi-scale material removal model is found to predict the material removal characteristics well under various polishing conditions. The simulated patterns by the surface generation model are found to agree well with the measured patterns in the pattern polishing experiments which substantiate that the relative and cumulative

removal process is a key surface generation mechanism in bonnet polishing.

5.2 Multi-scale Material Removal Model

It is well-known that the surface generation of the polishing process can be regarded as the convolution of the influence function and the dwell time map along the pre-specified tool path. Hence, the determination of the material removal characteristics and an optimized tool path generator are of paramount importance for modelling and simulation of the surface generation in bonnet polishing. Figure 5.1 shows a flowchart of the theoretical modelling process of the material removal characteristics and surface generation by bonnet polishing.

In the first step, a multi-scale material removal model is developed by studying the contact mechanics, kinematics theory and abrasive wear mechanism. In the coming section, the material removal characteristics are modelled step by step with the following assumptions:

- (i) The polishing bonnet is assumed to be a perfect sphere and much softer than the polished flat surface. Hence, the polishing bonnet is elastically deformed while the polished surface remains flat in the contact area;
- (ii) The polishing bonnet with respect to the target flat surface is assumed to be a viscous sphere on a hard plane regardless of the contribution of slurry hydrodynamic pressure, pad asperities, contact-surface instability and pad-abrasive-workpiece contact;
- (iii) Material removal in bonnet polishing is assumed to be only related to the

removal of material by plastic deformation caused by abrasive particles. The polishing tool path is then planned based on the desired surface integrity of the optical surface to be generated using the predicted data of the material removal characteristics. Finally, the surface generation is simulated based on the developed multi-scale material removal model and polishing tool path planning.

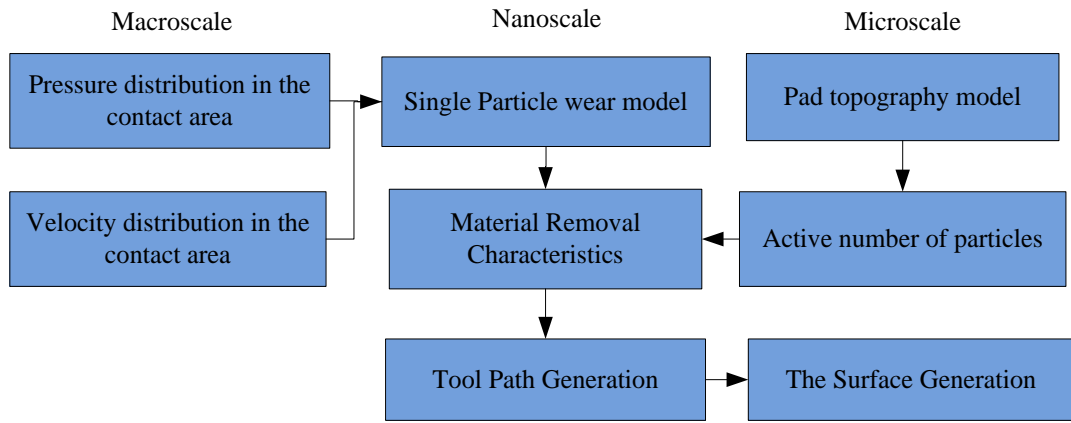


Figure 5.1 Flowchart of the theoretical modelling process of the material removal characteristics and surface generation for bonnet polishing

5.2.1. Modelling of Surface Velocity Distribution

Figure 5.2 shows the graphical illustration and detailed geometry in the polishing area by the bonnet on a flat surface, where ω is angular velocity in rad/min,

$$\vec{\omega} = \frac{\pi S}{30} \{0, -\sin(\varphi), \cos(\varphi)\}; \varphi \text{ is the inclination angle; } S \text{ is angular velocity in rpm; } O_b \text{ is the centre of the bonnet; } L \text{ is the axis of rotation of the bonnet; } O_w \text{ is the centre of polishing spot; } d \text{ is the polishing depth in mm; } R_b \text{ is the radius of the bonnet in mm; } O_r \text{ is the swing centre of point } P \text{ and can be expressed as } (0, y_0, -y_0 \cot \varphi); P \text{ is any point in the polishing contact area and can be expressed as}$$

$$\left((R_b - d) \tan \alpha \sin \theta, (R_b - d) \tan \alpha \cos \theta, -(R_b - d) \right), \quad 0 \leq \alpha \leq \arccos \left(\frac{(R_b - d)}{R_b} \right),$$

$0 \leq \theta \leq 2\pi$. Hence, the vector of $\overrightarrow{O_b O_r}$ and $\overrightarrow{O_r P}$ can be represented as follows:

$$\overrightarrow{O_b O_r} = \{0, y_0, -y_0 \cot \varphi\} \quad (5.1)$$

$$\overrightarrow{O_r P} = \{(R_b - d) \tan \alpha \sin \theta, (R_b - d) \tan \alpha \cos \theta - y_0, -(R_b - d) + y_0 \cot \varphi\} \quad (5.2)$$

Since $\overrightarrow{O_b O_r} \perp \overrightarrow{O_r P}$, the solution of y_0 can be expressed as:

$$y_0 = \frac{(R_b - d)(\tan \alpha \cos \theta + \cot \varphi)}{1 + (\cot \varphi)^2} \quad (5.3)$$

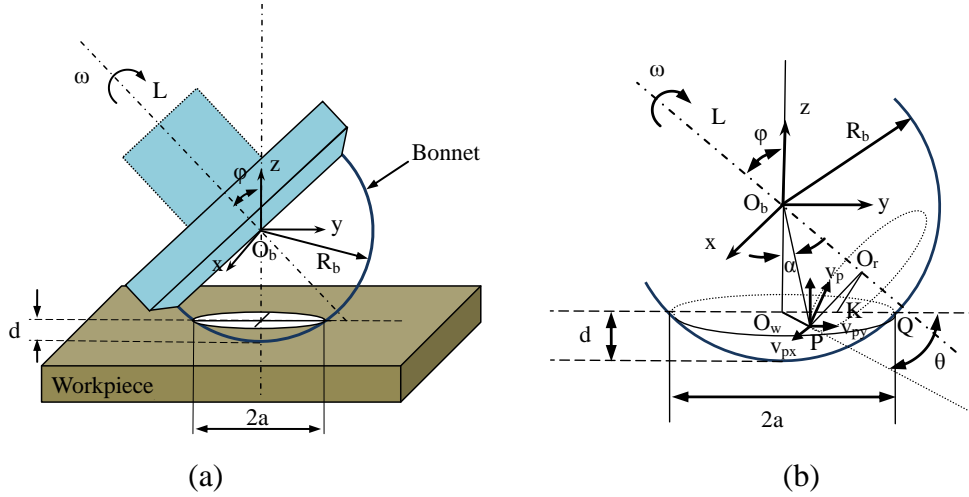


Figure 5.2 (a) Graphical illustration and (b) detailed geometry in the polishing area by the polishing bonnet on flat surface

Therefore, the vector of $\overrightarrow{O_r P}$ can be written as:

$$\overrightarrow{O_r P} = \{U, V, W\} \quad (5.4)$$

where,

$$U = (R_b - d) \tan \alpha \sin \theta; \quad V = (R_b - d) \tan \alpha \cos \theta - \frac{(R_b - d)(\tan \alpha \cos \theta + \cot \varphi)}{1 + (\cot \varphi)^2};$$

$$W = -(R_b - d) + \frac{(R_b - d)(\tan \alpha \cos \theta + \cot \varphi)}{1 + (\cot \varphi)^2} \cot \varphi.$$

The velocity vector $\overrightarrow{v_p}$ at point P can be obtained by using vector operation

(cross product):

$$\vec{v}_p = \vec{\omega} \times \vec{O_r P} = \frac{\pi S}{30} \left[-(V \cos \varphi + W \sin \varphi) \vec{i} + U \cos \varphi \vec{j} + U \sin \varphi \vec{k} \right] \quad (5.5)$$

As a result, the relative velocity V_r at the point P for polishing a flat surface is expressed as:

$$V_r = \frac{\pi S}{30} \sqrt{(V \cos \varphi + W \sin \varphi)^2 + U^2 (\cos \varphi)^2} \quad (5.6)$$

5.2.2. Modelling of Pressure Distribution

Since the plasticity index for a soft polymer has only about one tenth of the value for metal, the contact between a polymer and a metal is almost completely elastic, except against very rough surfaces (Hutchings, 1992). When an elastic sphere slides over a flat surface with abrasive slurry, the pressure distribution in the contact area between the polishing pad and workpiece and the surface deformations of the polishing bonnet cannot be determined independently by Hertz's theory.

Considering the strong time-dependence of mechanical properties of polymers, the polishing pad pressured on the target flat surface is assumed to be a viscous sphere on a hard plane regardless of the contribution of slurry hydrodynamic pressure, pad asperities, contact-surface instability and pad-abrasive-workpiece contact. As shown in Figure 5.3, the polishing surface is much harder than the polishing pad. Hence, the surface remains flat in the contact area while the polishing pad is deformed. According to Brilliantov and Poschel (1998), when the deformation of a sphere is rather small, $d/R_b \ll 1$, the rolling velocity is much lower than the sound speed in

the sphere's material and the characteristic time is much longer than the dissipative relaxation time of the material. The total stress σ_{ij} is a sum of the elastic part of the stress tensor σ_{ij}^{el} and the dissipative part of the stress tensor σ_{ij}^{dis} .

$$\sigma_{ij}^{el} = E_1(\varepsilon_{ij} - \frac{1}{3}\delta_{ij}\varepsilon_{kk}) + E_2\varepsilon_{kk}\delta_{ij} \quad (5.7)$$

$$\sigma_{ij}^{dis} = \eta_1(\dot{\varepsilon}_{ij} - \frac{1}{3}\delta_{ij}\dot{\varepsilon}_{kk}) + \eta_2\dot{\varepsilon}_{kk}\delta_{ij} \quad (5.8)$$

where ε_{ij} and $\dot{\varepsilon}_{ij}$ denote the strain and strain rates, respectively. $E_1 = Y/(1+\nu)$ and $E_2 = Y/3(1-2\nu)$ denote the elastic material constants with Y and ν being the Young's modulus and the Poisson ratio, respectively. η_1 and η_2 are the coefficients of viscosity, related to shear and bulk deformation respectively. δ_{ij} is the Kronecker symbol. Subscripts in Eq. (5.7) and Eq. (5.8) follow the Einstein notation. From Eq. (5.7) and Eq. (5.8), the diagonal component of the stress tensor can be expressed as:

$$\sigma_{zz}^{el} = E_1(\varepsilon_{33} - \frac{1}{3}\delta_{33}\varepsilon_{kk}) + E_2\varepsilon_{kk}\delta_{33} = E_1\frac{\partial u_z}{\partial z} + \left(E_2 - \frac{E_1}{3}\right)\left(\frac{\partial u_x}{\partial x} + \frac{\partial u_y}{\partial y} + \frac{\partial u_z}{\partial z}\right) \quad (5.9)$$

$$\sigma_{zz}^{dis} = \eta_1(\dot{\varepsilon}_{33} - \frac{1}{3}\delta_{33}\dot{\varepsilon}_{kk}) + \eta_2\dot{\varepsilon}_{kk}\delta_{33} = \eta_1\frac{\partial \dot{u}_z}{\partial z} + \left(\eta_2 - \frac{\eta_1}{3}\right)\left(\frac{\partial \dot{u}_x}{\partial x} + \frac{\partial \dot{u}_y}{\partial y} + \frac{\partial \dot{u}_z}{\partial z}\right) \quad (5.10)$$

where u_x , u_y , and u_z denote the x-, y-, and z- direction displacement field of the classic Hertz contact problem. \dot{u}_x , \dot{u}_y , and \dot{u}_z denote the time derivative of the displacement field in the x-, y-, and z- directions, respectively. σ_{zz}^{el} has the known solution for the Hertz contact problem (Landau and Lifshitz, 1959).

$$\sigma_{zz}^{el} = E_1\frac{\partial u_z}{\partial z} + \left(E_2 - \frac{E_1}{3}\right)\left(\frac{\partial u_x}{\partial x} + \frac{\partial u_y}{\partial y} + \frac{\partial u_z}{\partial z}\right) = p_0\left(1 - \frac{x^2}{a^2} - \frac{y^2}{a^2}\right)^{1/2} \quad (5.11)$$

where $a = \sqrt{dR_b}$ denotes the radius of contact area and $p_0 = 3F_N/(2\pi a^2)$ denotes the

maximum contact pressure, F_N is the total elastic force, acting by the surface (in normal direction) on the polishing pad:

$$F_N = \frac{2}{3} \frac{Y}{(1-\nu^2)} R_b^{1/2} d^{3/2} \quad (5.12)$$

$\sigma_{zz}^{el}(E_1 \leftrightarrow \eta_1; E_2 \leftrightarrow \eta_2)$ was derived by Brilliantov and Poschel (1998) and Brilliantov et al. (1996) using the technique of coordinate transformation. However, Zheng et al. (2011) noted inappropriate equality in their derivation and obtained $\sigma_{zz}^{el}(E_1 \leftrightarrow \eta_1; E_2 \leftrightarrow \eta_2)$ directly based on the principles of contact mechanics as described by Johnson and Johnson (1987).

$$\sigma_{zz}^{el}(E_1 \leftrightarrow \eta_1; E_2 \leftrightarrow \eta_2) = -\frac{(1-2\nu)(1+\nu)}{Y} (2\eta_2 + \eta_1/3) P_0 \left(1 - \frac{x^2}{a^2} - \frac{y^2}{a^2}\right)^{1/2} \quad (5.13)$$

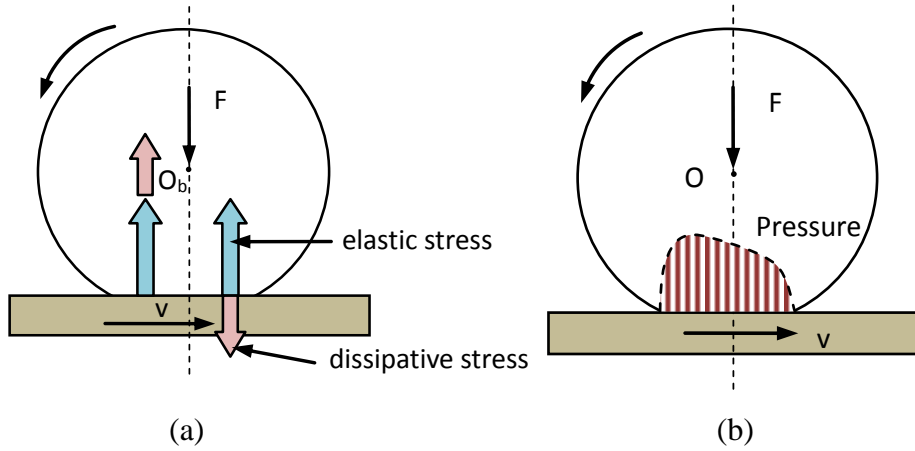


Figure 5.3 Sketch of pressure distribution for the rolling bonnet

A kinematic equation is used to describe the displacement velocity distribution,

$$\dot{u}(x, y, z) = (\vec{\Omega} \cdot \vec{r} \times \vec{\nabla}) \vec{u}(x, y, z) = -\omega \cos \varphi (z \partial_x - x \partial_z) \vec{u}(x, y, z) + \omega \sin \varphi (x \partial_y - y \partial_x) \vec{u}(x, y, z) \quad (5.14)$$

where $\vec{\Omega} = \{0, -\omega \cos \varphi, \omega \sin \varphi\}$, ω is the angular velocity and φ is the inclined angle.

Eq. (5.14) coupled with the definitions of the elastic part and dissipative part of

the stress tensor is used to obtain the dissipative part of the stress tensor as follows

(Brilliantov and Poschel, 1998; Landau and Lifshitz, 1959):

$$\begin{aligned} \sigma_{zz}^{dis} &= \omega \sin \varphi (x \partial y - y \partial x) \sigma_{zz}^{el} (E_1 \leftrightarrow \eta_1; E_2 \leftrightarrow \eta_2) - \omega \cos \varphi (z \partial x - x \partial z) \\ &\cdot \sigma_{zz}^{el} (E_1 \leftrightarrow \eta_1; E_2 \leftrightarrow \eta_2) + (\eta_2 - \eta_1 / 3) \omega \cos \varphi \partial z u_x - (\eta_2 + 2\eta_1 / 3) \omega \\ &\cdot \cos \varphi \partial x u_z + (\eta_2 - \eta_1 / 3) \omega \sin \varphi \partial y u_x - (\eta_2 - \eta_1 / 3) \omega \sin \varphi \partial x u_y \end{aligned} \quad (5.15)$$

where $\partial x = \frac{\partial}{\partial x}$, $\partial y = \frac{\partial}{\partial y}$, $\partial z = \frac{\partial}{\partial z}$; $\vec{u}(x, y, z) = (u_x, u_y, u_z)$ and $E_1 \leftrightarrow \eta_1, E_2 \leftrightarrow \eta_2$,

etc. u_z is the surface displacements in the normal and radial direction and can be expressed as:

$$u_z = (1 - \nu^2) \pi p_0 (2a^2 - x^2 - y^2) / (4Ya) \quad (5.16)$$

Similar to Brilliantov and Poschel (1998), some terms can be omitted by calculation of the relative magnitude. Eq. (5.15) can be written as:

$$\begin{aligned} \sigma_{zz}^{dis} &= -\frac{(1-2\nu)(1+\nu)}{Y} \cdot \frac{\omega \cos \varphi (2\eta_2 + \eta_1 / 3) p_0 x z}{a^2} \cdot \left(1 - \frac{x^2}{a^2} - \frac{y^2}{a^2}\right)^{-1/2} \\ &+ \frac{(1-\nu)^2}{Y} \cdot \frac{\omega \cos \varphi (2\eta_2 + \eta_1 / 3) \pi p_0 x}{2a} \end{aligned} \quad (5.17)$$

As a result, the pressure distribution at the polishing contact area can be expressed by:

$$\begin{aligned} P(x, y) &= \sigma_{zz}^{el} + \sigma_{zz}^{dis} = p_0 \left(1 - \frac{x^2}{a^2} - \frac{y^2}{a^2}\right)^{1/2} - \frac{(1-2\nu)(1+\nu)}{Y} \\ &\cdot \frac{\omega \cos \varphi (2\eta_2 + \eta_1 / 3) p_0 x z}{a^2} \cdot \left(1 - \frac{x^2}{a^2} - \frac{y^2}{a^2}\right)^{-1/2} + \frac{(1-\nu)^2}{Y} \cdot \frac{\omega \cos \varphi (2\eta_2 + \eta_1 / 3) \pi p_0 x}{2a} \end{aligned} \quad (5.18)$$

5.2.3. Single-particle Wear Model

The yield load, W_y , is calculated as a function of the particle radius, R_p , and the mechanical properties of the workpiece based on Hertzian analysis and the Tresca

criterion (Saka et al., 2008):

$$W_y = \frac{\pi^3 H_w^3}{48 E_w^2} R_p^2 \quad (5.19)$$

where E_w and H_w are the Young's modulus and hardness of the workpiece, respectively. As shown in Fig. 5.4(a), an abrasive particle, assumed to be spherical and rigid with the radius of R_p , is dragged across the surface in plastic contact which flows under an indentation pressure p_n . It forms a groove on the target surface and some proportion of the material is removed by the particle. Since the depth of indentation, δ_p , is much smaller than the radius of the abrasive, the depth is related to the radius of the projected circle of contact, a_p , by:

$$\delta_p = \frac{a_p^2}{2R_p} \quad (5.20)$$

For a polishing process, the particle is moving with relative velocity, V_r , and hence in contact only over its front surface; the force applied on an abrasive, W_p is expressed as:

$$W_p = \frac{\pi a_p^2 p_n}{2} = \pi \delta_p R_p p_n \approx \pi \delta_p R_p H_w \quad (5.21)$$

If a fraction η of the material displaced from the groove is actually removed as wear debris, then the volume (Vol_p') removed by this abrasive particle per unit time is

$$Vol_p' = \eta \delta_p a_p V_r = \frac{\sqrt{2}}{\pi^{3/2}} \frac{\eta V_r}{R_p} \left(\frac{W_p}{H_w} \right)^{3/2} \quad (5.22)$$

As can be seen in Figure 5.4(b), an abrasive particle was idealized as a cone of semiangle α . The depth of indentation, δ_p , is related to the radius of the projected circle of contact, a_p , by:

$$a_p = \delta_p \tan \alpha \quad (5.23)$$

For the cone particle, Eq. (5.21) can be rewritten as:

$$W_p = \frac{\pi a_p^2 p_n}{2} = \frac{\pi \delta_p^2 (\tan \alpha)^2 p_n}{2} \approx \frac{\pi \delta_p^2 (\tan \alpha)^2 H_w}{2} \quad (5.24)$$

Hence, the volume of wear debris produced by the cone particle per unit time is expressed by:

$$Vol_p'' = \eta \delta_p a_p V_r = \eta \delta_p^2 \tan \alpha V_r = \frac{2\eta W_p V_r}{\pi H_w \tan \alpha} \quad (5.25)$$

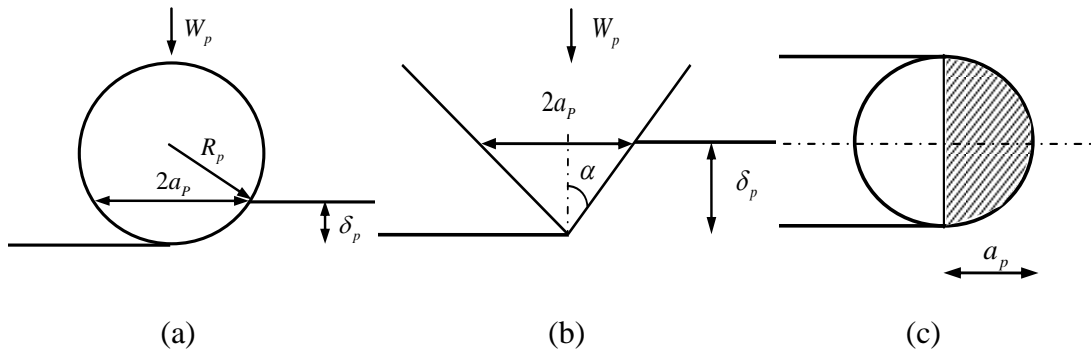


Figure 5.4 Geometry of contact between an abrasive particle and a surface: (a) and (b) in elevation; (c) in plan view

From the above analysis, the wear rate of a single abrasive particle depends heavily on the particle's shape. However, the angularity of abrasive particles is difficult to be defined and this is largely due to the difficulty of identifying and quantifying the features of a complex three-dimensional shape causing its abrasivity. Since angular particles cause more material removal than spherical particles (Hutchings, 1992), cone particles are commonly used in the polishing process.

5.2.4. Active Number of Abrasive Particles

The slurry particles involved in material removal are those that are embedded in the surface of the compliant polishing pad and are dragged across the polished surface by the relative velocity between the two surfaces, and the active number of these particles is generally related to the particle size distribution, the hydrodynamics condition between the polishing pad and the workpiece as well as the surface topography of the polishing pad and target surface. To simplify the theoretical modelling, the pad-particle-workpiece contact is assumed to be solid-solid contact neglecting the effect of the fluid flow, and the particle size is assumed to be a constant.

According to Luo and Dornfeld (2001), the abrasive particles engaged in two-body abrasion are regarded as only agents of effective material removal. The effective contact area between the polishing pad and the entrained particle is approximately equal to πR_p^2 , and hence the force applied on an abrasive, W_p , can be expressed by:

$$W_p = \pi R_p^2 P(x, y) \quad (5.26)$$

Since the polishing pad tends to deteriorate in the polishing process, the modelling of the surface topography of the polishing pad is very hard. Statistical theories were used to model the surface topography of the polishing pad assessed by the pad asperity radius R_a and the standard deviation of asperity heights σ_z (Greenwood and Williamson, 1966; Kim et al., 2014). For relatively soft pad and low abrasive concentration, the active number of abrasive particles tends to be

proportional to the real contact area and the slurry concentration (Fu et al., 2001; Luo and Dornfeld, 2003). As a result, the active number of abrasive particles (N_{ac}) can be expressed by:

$$N_{ac} = K_{ac} \frac{V_c t}{R_p^2} \left(\frac{R_a}{\sigma_z} \right)^{1/2} \quad (5.27)$$

where K_{ac} is the coefficient related to the particle size distribution and the hydrodynamics condition, t is the polishing time, V_c is the volume fraction, R_a is the radius of the pad asperities, and σ_z is the standard deviation of asperity heights.

As a result, the material removal rate (Vol_{mmr}) can be predicted by:

$$Vol_{mmr} = N_{ac} Vol_p = \frac{2\eta K_{ac} V_c t V_r(x, y) P(x, y)}{H_w \tan \alpha} \left(\frac{R_a}{\sigma_z} \right)^{1/2} \quad (5.28)$$

As a result, the model of the material removal characteristics developed in this study attempts to relate to the slurry concentration, particle shape, polishing depth, tool size, head speed, polishing time, pad topography, and hardness of the polishing pad and polished surface. It reveals some insights into the contact mechanics and the wear mechanisms of the bonnet polishing process. It suggests that the material removal rate is proportional to the slurry concentration, polishing time, velocity, and pressure distribution, and is inversely proportional to the hardness of the polished surface. The velocity distribution is proportional to the head speed while the pressure distribution is proportional to the applied load and hence this proportional relation agrees well with Preston's equation.

Moreover, the model reveals that both the polishing depth (the down force) and rotational speed have obvious effects on the pressure distribution in the polishing area

for bonnet polishing. Hence, the calculation of the pressure in the model taking into account the hardness of the polishing pad can explain the asymmetric pressure distribution in the X-cross-section due to the strong time-dependence of the mechanical properties of the polishing bonnet. According to the proposed model, a larger radius of the pad asperities and a smaller standard deviation of asperity heights imply a higher material removal rate.

5.3 Surface Generation Model

In practice, polishing is a multi-step process conducted by repeatedly running particular designed polishing cycles until the expected surface finish and form error are obtained. Within each cycle, the polishing tool sweeps through the polished surface following the adopted polishing tool path and desired dwell time map. Hence, an important part of the surface generation model is dwell time and tool path planning (Tam et al., 1999) as well as considering time efficiency and surface quality improvement.

Based on the experimental results of section 3.5.2.3, bonnet polishing appears to be a relative and cumulative polishing process for various materials and the surface generation, ΔZ_i , of bonnet polishing can be assumed to be a linearly cumulative effect of dwell time, T_0 , together with the material removal rate, MRR_{ij} , under the same polishing conditions as follows:

$$\Delta Z_i = \sum_{j=1}^N MRR_{ij} \cdot T_0, \quad (i = 1, 2, 3 \dots M) \quad (5.29)$$

where M is the sample point number, N is the number of trajectory points along

the polishing path and MRR_{ij} is the material removal of j th sample point when the i th trajectory point along the polishing path is polished by the bonnet. The value of MRR_{ij} depends on the material removal rate and the contract area of the bonnet. It will be non-zero if the j th sample point is located within the contract area of the i th trajectory point, and will be zero if the sample point is located outside the contract area.

In this study, raster polishing was used to understand the surface generation mechanisms and verify the effectiveness of the surface generation model. The polishing conditions in all the paths are assumed to be constant and hence the tool influence function is stable and constant, and the polishing paths are also assumed to be evenly spaced straight lines on a flat surface as can be seen in Figure 5.5.

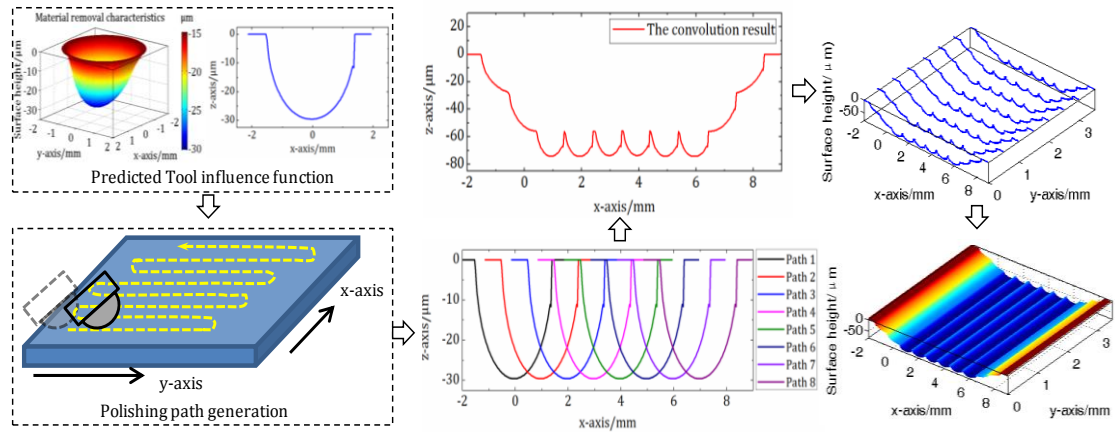


Figure 5.5 Schematic diagram of the surface generation model in raster polishing

When the predicted influence function follows straight path lines with a constant surface feed rate, the removal profile is constant along each and all the path lines. Hence, the material removal distribution is constant along the path line direction and waves in the orthogonal direction arising from the overlapping of the removal profiles affiliated with adjacent polishing path lines for the raster polishing. In this case, the

surface generation may be simplified to be a 2D problem which can be solved numerically for a given polishing path spacing and path number. The polishing path spacing represents the translation distance of removal profile along the orthogonal direction and the feed rate determines the dwell time of each polished spot and hence the surface height of removal profile along the path line direction.

5.4 Results and Discussion

In the present study, prototypes of the multi-scale material removal model and the surface generation model for bonnet polishing were purposely developed using the MATLAB programming software package. Basically, the experimental verification is divided into two parts, spot polishing tests and pattern test. Spot polishing tests were conducted to verify the feasibility of the theoretical model under various polishing conditions; while a pattern test was performed to experimentally evaluate the performance of the surface generation model. A Zeeko IRP 200 ultra-precision freeform polishing machine was used to conduct the experiments. All samples were polished using Al₂O₃ slurry and the surfaces of the samples were measured by a Zygo Nexview 3D Optical Surface Profiler.

5.4.1. Experimental Verification of the Multi-scale Material Removal Model

The multi-scale material removal model for bonnet polishing was verified through a series of simulation and polishing experiments. The predictions of material

removal characteristics of bonnet polishing were accomplished by using a prototype of the multi-scale material removal model purposely built using the MATLAB software package. In this study, a bonnet with a radius of 20 mm was assembled on the main spindle, while the workpiece made of steel (S136) was fixed on the C axis. All samples were polished by a LP-66 (Cerium oxide D'27) polishing pad with a slurry comprising 2.066 vol. % of Al₂O₃ abrasives with an average size of 3.22 μm with a constant machining time of 60 seconds. A series of simulations based on the multi-scale material removal model was conducted under various polishing conditions as shown in Table 5.1, while the coefficients used in the simulations are shown in Table 5.2.

Table 5.1 The process parameters of polishing experiments

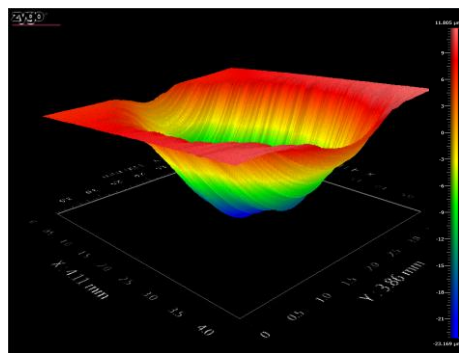
Sample No.	Tool pressure	Tool offset	Head speed	<i>Precess</i> angle	Slurry concentration
A1	1.2 bar	0.12 mm	1200 rpm	10 °	1:12
A2	1.2 bar	0.12 mm	1200 rpm	15 °	1:12
A3	1.2 bar	0.12 mm	1200 rpm	20 °	1:12
B1	1.2 bar	0.1 mm	900 rpm	15 °	1:12
B2	1.2 bar	0.1 mm	1200 rpm	15 °	1:12
B3	1.2 bar	0.1 mm	1500 rpm	15 °	1:12
C1	1.2 bar	0.08 mm	1200 rpm	15 °	1:12
C2	1.2 bar	0.13 mm	1200 rpm	15 °	1:12
C3	1.2 bar	0.18mm	1200 rpm	15 °	1:12
D1	1.2 bar	0.09 mm	1200 rpm	15 °	1:12
D2	1.2 bar	0.09 mm	1200 rpm	15 °	1:9
D3	1.2 bar	0.09 mm	1200 rpm	15 °	1:6

Table 5.2 Parameters used in the present simulation

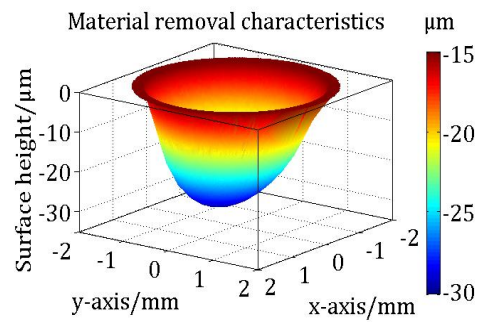
Variable	Symbol	Base value
Young's modulus	Y	2 Mpa
Poisson's ratio	ν	0.3
Viscosity coefficient	η_1	5×10^{-4} Mpa s
Viscosity coefficient	η_2	0 Mpa s
Semiangle of cone particle	α	45°
Hardness of workpiece	H_w	509 Mpa
Radius of pad asperities	R_a	23.5 μm
Standard deviation	σ_z	4.4 μm

Figure 5.6(a) shows the experimental data of polished spot measured by a Zygo Nexview 3D Optical Surface Profiler, while Figure 5.6(b) shows the predicted 3D topography of the material removal characteristics for the case of B3. It was found that the predicted result of the theoretical model shows a good correlation in surface shape with the experimental data. The cross-section curve of the X-Z profile and Y-Z profile of the measured experimental data passing the deepest point were used to verify the theoretical model as shown in Figure 5.6(c) and Figure 5.6(d), respectively. It is turned out that the simulated result by the theoretical model agree reasonably well with the measured data. It is interesting to note that the width of the X-Z profile was significantly larger than that for the Y-Z profile and hence the real contact area was not a circle. This may be due to the deformation of the polishing bonnet and/or the swing of the main spindle.

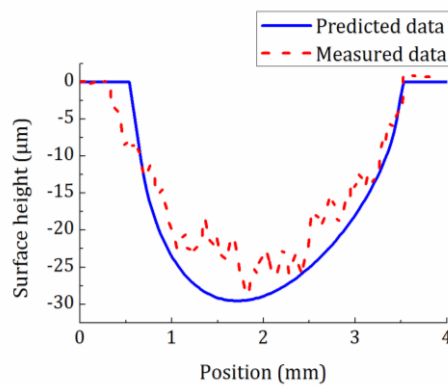
Due to the new calculation method for pressure distribution, the theoretical model was found to be able to explain the asymmetry of the X-Z profile and Y-Z profile of the polished spot. This implies that the contact mechanics and kinetics theory proposed in this study can provide an explanation for the polishing mechanisms in bonnet polishing. Moreover, the hydrodynamics condition and abrasive distribution in the contact area of the removal process should be further studied to enhance the prediction accuracy of the theoretical modelling and better understand the polishing mechanisms in the bonnet polishing process.



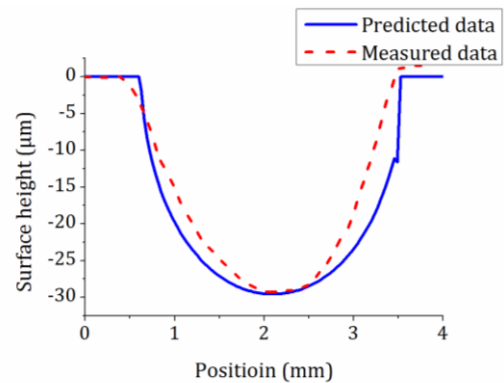
(a) Measured 3D topography data



(b) Predicted 3D influence function



(c) X-Z profile of TIF



(d) Y-Z profile of TIF

Figure 5.6 Results of the simulation and experiment in terms of 3D topography, X-Z profile and Y-Z profile (for the case of B3)

To further verify the theoretical model, four sets of simulation and polishing experiments were conducted under different *precess* angle, head speed, tool offset, and slurry concentration. Figure 5.7(a) shows that the amount of material removal increases with increasing *precess* angle. This is due to the fact that a higher *precess* angle means a higher velocity distribution in the contact area and hence a higher material removal rate is obtained. It can be explained reasonably well by the theoretical model.

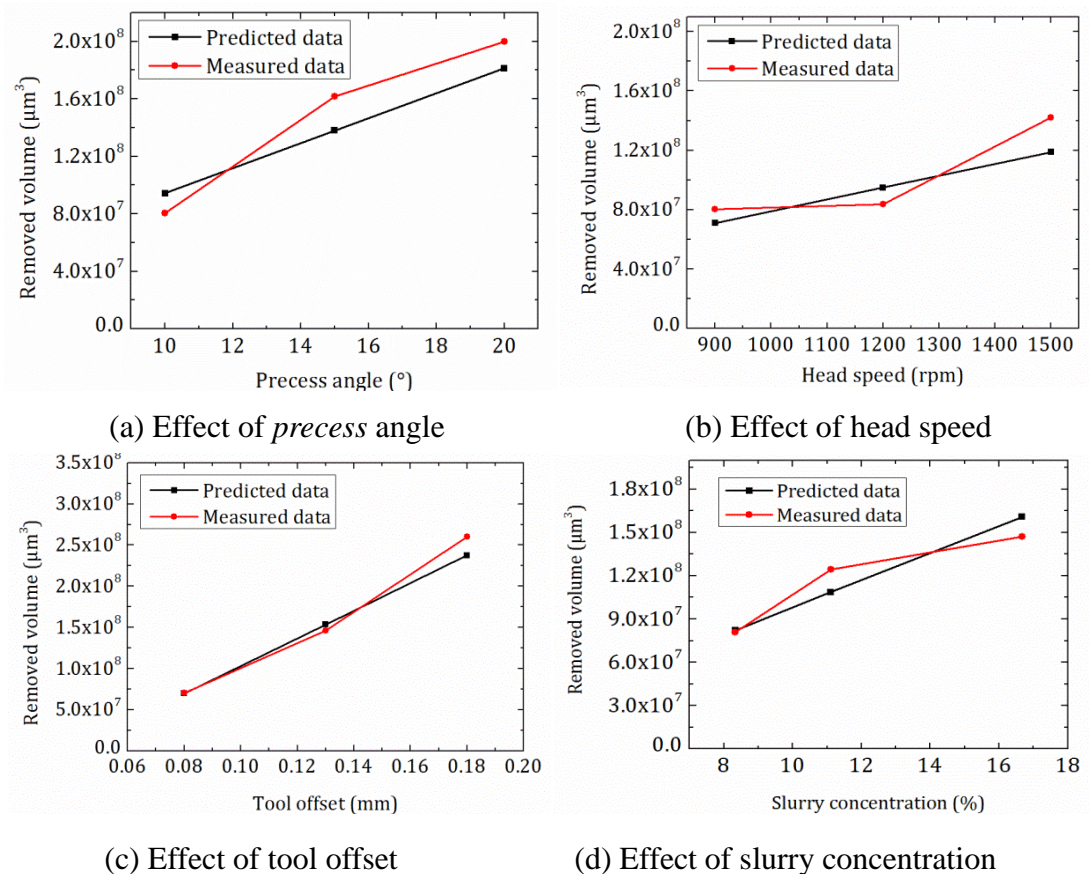


Figure 5.7 Comparison of experimental data and predicted data under different polishing conditions

Figure 5.7(b) shows that the volumetric material removal rate increases linearly with increasing head speed and this is predicted well by the theoretical modelling. Both the experimental and predicted results in Figure 5.7(c) show that the volumetric material removal increases as the tool offset increases. This can be explained by a larger tool offset presenting a larger contact area and a higher contact pressure and hence a higher material removal rate. Figure 5.7(d) shows that the amount of material removal depends linearly on the slurry concentration. This is due to the fact that a higher slurry concentration means a larger number of abrasive particles involved in the material removal in bonnet polishing and this can be explained reasonably well by the theoretical modelling.

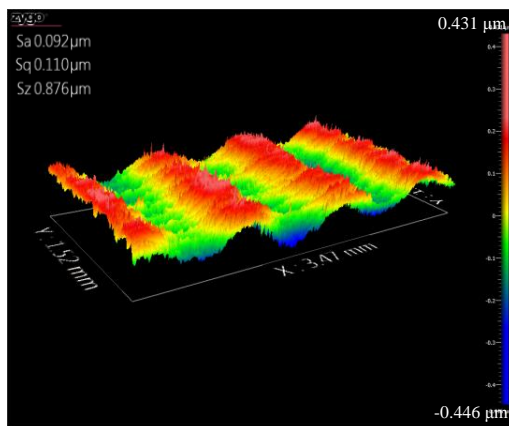
5.4.2. Experimental Verification of the Surface Generation Model by the Pattern Test

A raster polishing experiment was designed to validate the proposed surface generation model. The polishing strategies used for generating the designed surface pattern are shown in Table 5.3, while the surface generation model was purposely built and programmed using the MATLAB software package. Figure 5.8 shows a comparison between the measured and simulated results in the pattern test. It is found that the simulated surface pattern by the surface generation model agrees well with that for the experimental results. The peak-to-valley value (PV) value and the root-mean-squared (RMS) value are determined for the measured surface data and the predicted ones. The PV value of the predicted data is $0.803\mu\text{m}$ and the RMS value is

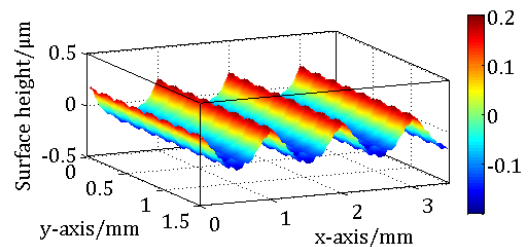
229 nm, while the PV value and RMS value of the measured surface data are 0.876 μm and 110 nm, respectively. It is interesting to note that the parametric values are of the same order of magnitude. This further validates that the surface generation model can help to explain and predict the relative and cumulative polishing process and the linearly cumulative effect of dwell time together with the constant material removal rate under the identical polishing condition in surface generation of bonnet polishing.

Table 5.3 Parameters for generating surface pattern

Workpiece Material	Steel (S136)	Polishing mode	Raster
Surface feed	20 mm/min	Polishing cloth	LP-66
Polishing spacing	1 mm	Head speed	1200 rpm
Polishing depth	0.2 mm	<i>Precess</i> angle	15 °
Tool pressure	1.2 bar	Slurry concentration	1:12
Tool radius	20 mm	Particle property	3.22 μm (Al_2O_3)



(a) Experimental data



(b) Predicted data

Figure 5.8 Comparison between the measured and simulated results of the pattern test

To further verify the effectiveness of the surface generation model, a least-squares-based surface matching method was used to evaluate the deviation of the measured surface from the corresponding simulated surface (Ren et al., 2012a). Due to the misalignment between the coordinate frames of the coordinate frames of the measured surface and the simulated surface, surface matching is required to search for an optimal Euclidean motion for the measured surface so that it is well aligned with the simulated surface as closely as possible. After that, the deviation of the simulated surface and the measured surface is considered to be the prediction error of the proposed model as shown in Figure 5.9. It turned out that the peak-to-valley value (PV) of the prediction error was $0.4231\ \mu\text{m}$ and the root-mean-squared value (RMS) was $64.8\ \text{nm}$. The result reveals that the surface generation model can be successfully used for predicting and better explaining the surface generation in bonnet polishing. This further validates the technical feasibility and effectiveness of the surface generation model in bonnet polishing.

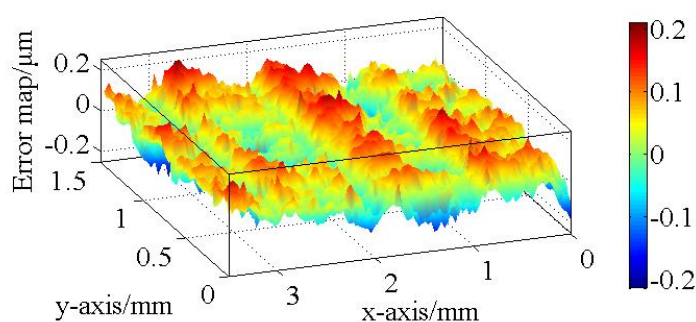


Figure 5.9 Evaluated prediction error of the testing pattern for bonnet polishing

5.5 Conclusions

Due to the complex machining mechanism, it is still difficult to model the material removal characteristics and surface generation in bonnet polishing (BP). This chapter presents a theoretical and experimental investigation which attempts to achieve better scientific understanding of the material removal characteristics and surface generation mechanisms in bonnet polishing. The major findings are summarized as follows:

(i) A multi-scale material removal model was built for predicting and characterizing the material removal characteristics in bonnet polishing based on the study of contact mechanics, kinematics theory, and abrasive wear mechanism. Specifically, the velocity and pressure distributions were determined based on the kinematics theory and contact mechanics at macro scale, and the pad topography which affects the contact ratio and hence the material removal rate at micro scale, and the micro- or nano-sized abrasive particles scratch the surface at the nano scale. The model developed in this work captures much of the basic physics of the polishing process including the tool radius, polishing depth, head speed, precess angle, pad topography, polishing time, particle shape, slurry concentration, and the mechanical properties of the pad and workpiece.

(ii) The calculation of the pressure in the model taking into account the strong time-dependence of the mechanical properties of the polishing bonnet reveals that both polishing depth (the down force) and rotational speed have significant effects on the pressure distribution in the polishing area, and hence this can explain the asymmetry of the material removal characteristics in the X-cross-section and

Y-cross-section. It is also found that the X-Z width of the polished spot is larger than the Y-Z width.

(iii) A surface generation model was also built to take account of the relative and cumulative removal process together with the predicted material removal characteristics.

(iv) A series of spot and pattern polishing tests as well as simulation experiments was conducted. The results show that the theoretical model predicts the amount of material removal well which not only increases with increasing *precess* angle and tool offset, but also depends linearly on the head speed and slurry concentration. Through the experimental study and theoretical analysis by the surface generation model, it is also found that a relative and cumulative process is proven to be a key surface generation mechanism in bonnet polishing.

CHAPTER 6 OVERALL CONCLUSIONS

Computer Controlled Ultra-precision Polishing (CCUP) based on fluid jet polishing (FJP) and bonnet polishing (BP) with multi-axis machining is an enabling technology which is capable of fabricating ultra-precision surfaces with sub-micrometre form accuracy and surface roughness in the nanometre range. This is particularly useful for machining difficult-to-machine and ferrous materials, which are not amenable for other ultra-precision machining technologies such as single-point diamond turning and ultra-precision raster milling. Most previous research on the polishing process was based on achieving super mirror finished surfaces without focusing on achieving high form accuracy.

Since CCUP is a complex process that exhibits multidisciplinary and multi-scale complexity, our understanding of the material removal characteristics, surface generation, and the factors affecting the surface generation of CCUP is still far from complete. As a result, the research study aimed to conduct extensive experimental and theoretical investigations on the material removal characteristics and surface generation mechanisms in CCUP.

To gain a better understanding of the deterministic polishing process, a comprehensive analysis of the material removal characteristics in CCUP was conducted. The Taguchi design of experiments was used to determine the optimal operational parameters and the significance of the important parameters for the volumetric material rate in fluid jet polishing and bonnet polishing. The results of the Taguchi trials show that pressure has the largest effect on the material removal rate

and the standoff distance has the smallest effect in fluid jet polishing, while the *precess* angle, head speed, particle diameter, tool offset, slurry concentration, and tool pressure are the significant factors in order of declining effect on the material removal rate in bonnet polishing. It is also found that the maximum depth as well as the volumetric removal increases with increasing polishing time and slurry concentration linearly while it increases non-linearly with increasing slurry pressure, slurry distance and particle size, while it increases first then decreases with increasing impingement angle.

The material removal and surface generation mechanisms of bonnet polishing were also studied through a series of polishing experiments. Although the material removal is shared by the abrasive particles and the pad asperities in the designed experiments, the abrasive wear observed in bonnet polishing was found to be dominated significantly by the plastic removal mode of abrasive particles, while the material removal caused by the polishing pad should be mitigated in order to obtain super mirror finished surfaces without pad scratches. The experimental results imply that there exists a critical polishing depth which if exceeded leads to the breaking of the hydrodynamic lubrication condition in the high pressure area of the polished spot which causes the pad scratching. Moreover, the results also reveal that the surface generation of bonnet polishing is a linearly cumulative effect of dwell time together with the constant material removal rate for the identical polishing condition.

Through the investigation of the material removal characteristics and surface generation mechanisms in fluid jet polishing, it was found that the amount of material

removed by the fluid jet depends on the flow conditions of the jet slurry and the abrasive particles' erosion mechanism, while the surface generation can be considered as the convolution of the influence function and the dwell time map along the pre-specified tool path. Based on these studies, a theoretical model was built for predicting and characterizing the material removal characteristics and surface generation in FJP. Computational Fluid Dynamics (CFD), statistical theory and erosion mechanisms were used to establish a material removal model for FJP, while the polishing strategy was determined by the desired surface integrity of the optical surface to be generated by using the data on the material removal characteristics.

Through a comparison between the actual polishing experiments and the theoretical results, the material removal model was found to satisfactorily predict the amount of material removal which increases with increasing pressure, and depends linearly on the polishing time and the abrasive particle concentration, while the theoretical model predicts the surface generation well under various polishing conditions. With a constant material removal rate and under identical polishing conditions, it was revealed that the surface generation in FJP is a linearly cumulative function of the dwell time. The proposed prediction model not only helps to provide an important means for better understanding and predicting the effect of process parameters on the polishing process, but also contributes significantly to improving the predictability for the achievement of corrective polishing and deterministic machining using the FJP technology.

For the bonnet polishing process, a multi-scale theoretical model for the

prediction and simulation of the material removal characteristics and surface generation was established based on the study of contact mechanics, kinematics theory, and wear mechanisms, as well as the relative and cumulative removal process of the surface generation. Specifically, the pressure and velocity distributions were determined based on the kinematics theory while contact mechanics were used to model at the macro scale. The pad topography affects the contact ratio and hence the material removal rate at the micro scale, and the micro- or nano-sized abrasive particles scratch the surface at the nano scale.

The multi-scale theoretical model developed in the present study captures much of the basic physics of the polishing process including the tool radius, polishing depth, head speed, *precess* angle, pad topography, polishing time, particle shape, slurry concentration, and the mechanical properties of the pad and workpiece. It reveals that both the polishing depth (the down force) and rotational speed have significant effects on the pressure distribution in the polishing area, and hence this can explain the asymmetry of the material removal characteristics in the X-cross-section and Y-cross-section. It was also found that the X-Z width of the polished spot is larger than the Y-Z width. A series of spot and pattern polishing tests as well as simulation experiments was conducted. The results show that the theoretical model predicts the amount of material removal well which not only increases with increasing *precess* angle and tool offset, but also depends linearly on the head speed and slurry concentration. Through the experimental study and theoretical analysis by the surface generation model, it was also found that a relative and cumulative process is proven to

be a key surface generation mechanism in bonnet polishing. The successful development of the theoretical model helps to make the bonnet polishing process more predictive, thereby optimizing the manufacturing process, and forms the theoretical basis for better understanding of the polishing mechanisms in bonnet polishing.

CCUP based on FJP or BP is a complex multi-stage process which relies heavily on the planning of the process steps in terms of the use of the polishing conditions and polishing fluid on the specific materials being cut. The polishing mechanisms of the CCUP process usually exhibit multidisciplinary and multi-scale complexity, and are affected by many factors such as process parameters, slurry property, work materials, workpiece geometry, and so on. Nowadays, the generation of a desired surface integrity of high-performance optical surface still depends largely on the experience and skill of the machine operator through an expensive trial-and-error approach.

On the whole, the experimental and theoretical investigation reported in this thesis contributes significantly to the advancement of the scientific understanding of the materials removal characteristics and surface generation mechanisms in CCUP based on FJP and BP. Moreover, this was a novel attempt in which the deterministic models were successfully built which acquire much of the basic physics of the polishing process. This is essential for further improving the performance of ultra-precision machines. The successful development of the theoretical models for the prediction of the material removal and surface generation provides an important means to make the CCUP process more predictable and efficient. They help to explain

quantitatively the effect of different factors which affect the material removal and hence the surface generation in CCUP without the need for costly trial and error cutting tests.

CHAPTER 7 SUGGESTIONS FOR FUTURE RESEARCH

The present research work presented in this thesis provides an important means for better understanding the effect of polishing parameters, material removal characteristics and surface generation mechanisms in computer controlled ultra-precision polishing (CCUP) which make CCUP more predictable in terms of the prediction and simulation of the material removal characteristics and surface generation. However, there are some topics which are worth further study as follows:

- (i) The material removal model would be further enhanced by taking into account the effect of curvature on the material removal characteristics. This is important for better predicting the form accuracy of ultra-precision surfaces being polished. Moreover, the established theoretical models of the material removal characteristics will be incorporated into the capability of the tool path planning and the optimization of the dwell time. They will be integrated into the model-based simulation system for the simulation and optimization of the surface generation in the CCUP process. There is a need for further research into the model-based simulation system in order to further enhance the capability of the models and systems so that they are able to cater for more factors which affect the surface generation. For example, a comprehensive and precise model needs to take into account factors such as tool path generation and planning, the geometry of the machined surface, materials factors, and the dynamic factors involved in the machining process.

- (ii) To gain a better understanding of the polishing process, a monitoring system should be constructed for further study of the slurry distributions with the use of tactile sensors so as to measure the stress-strain behaviour during the polishing. The material removal of FJP is caused by the repeated impact of abrasive particles and hence the study of the spatial distribution and trajectories of abrasive particles will make FJP more deterministic, while the measurement of pressure distribution in the contact area and spatial distribution of active abrasive particles embedded in the polishing area are crucial for better understanding the material removal distribution of polished spots in bonnet polishing.
- (iii) To further understand the material removal mechanisms in the polishing process, more fundamental experiments need to be conducted, such as indentation or scratch tests for various materials to determine the experimental coefficients to improve the established theoretical models, and to better understand the material properties associated with the manufacturing process such as the ductile-brittle critical conditions and subsurface damage.

Since the ultimate performance of the polishing processes can be assessed by their achievable surface finish, form accuracy and resulting surface integrity, a comprehensive analysis method should be developed to assess the polished surface under various polishing conditions.

- (iv) To polish super hard and brittle materials in a more efficient and productive way, hybrid processes can be applied for CCUP, such as chemical reaction, plasma

assisted action, electric and magnetic field-assisted operation, etc. This will also improve the stability of the influence function in the polishing process through decreasing the deterioration of the polishing tool.

- (v) It is interesting to note that polishing is a multi-stage process conducted by repeatedly running particular designed polishing cycles until the expected surface finish and form accuracy are obtained. In other words, surface generation is usually realized by a series of polishing process steps. The surface generation in the current polishing process step will be affected by that of the previous polishing process steps. However, most of the previous studies focus mainly on individual polishing processes while the effect of the interaction of each different process and step has received relatively little attention. As a result, process chain modelling and analysis for computer controlled ultra-precision polishing of optical freeform surfaces should be further studied to optimize the polishing process.

REFERENCES

Allen, L. N. (1995). Progress in ion figuring large optics. *Laser-Induced Damage in Optical Materials: 1994*, 2428, 237-247.

Allen, L. N., and Keim, R. E. (1989). *An ion figuring system for large optic fabrication*. Paper presented at the 33rd Annual Technical Symposium.

Andre, D., Iordanoff, I., Charles, J. L., and Neauport, J. (2012). A Quantitative Discrete Element Model to Investigate Sub-Surface Damage Due to Surface Polishing. *Proceedings of the Asme 11th Biennial Conference on Engineering Systems Design and Analysis, Vol 4*, 577-585.

Annoni, M., Arleo, F., and Malmassari, C. (2014). CFD aided design and experimental validation of an innovative Air Assisted Pure Water Jet cutting system. *Journal of Materials Processing Technology*, 214(8), 1647-1657.

Ansys. (2010a). *Fluent 13.0 Theory Guide*. Canonsburg, USA Ansys Inc

Ansys. (2010b). *Fluent 13.0 User's Guide*. Canonsburg, USA: Ansys Inc.

Archard, J. (1953). Contact and rubbing of flat surfaces. *Journal of Applied Physics*, 24(8), 981-988.

Aurich, J. C., Linke, B., Hauschild, M., Carrella, M., and Kirsch, B. (2013). Sustainability of abrasive processes. *CIRP Annals - Manufacturing Technology*, 62(2), 653-672.

Balz, R., Mokso, R., Narayanan, C., Weiss, D. A., and Heiniger, K. C. (2013). Ultra-fast X-ray particle velocimetry measurements within an abrasive water jet. *Experiments in Fluids*, 54(3).

-
- Beaucamp, A., and Namba, Y. (2013). Super-smooth finishing of diamond turned hard X-ray molding dies by combined fluid jet and bonnet polishing. *Cirp Annals-Manufacturing Technology*, 62(1), 315-318.
- Beaucamp, A., Namba, Y., and Charlton, P. (2014a). Corrective finishing of extreme ultraviolet photomask blanks by precessed bonnet polisher. *Appl Opt*, 53(14), 3075-3080.
- Beaucamp, A., Namba, Y., and Charlton, P. (2015). Process mechanism in shape adaptive grinding (SAG). *Cirp Annals-Manufacturing Technology*, 64(1), 305-308.
- Beaucamp, A., Namba, Y., Combrinck, H., Charlton, P., and Freeman, R. (2014b). Shape adaptive grinding of CVD silicon carbide. *Cirp Annals-Manufacturing Technology*, 63(1), 317-320.
- Beaucamp, A., Namba, Y., and Freeman, R. (2012). Dynamic multiphase modeling and optimization of fluid jet polishing process. *Cirp Annals-Manufacturing Technology*, 61(1), 315-318.
- Beaucamp, A., Namba, Y., Messelink, W., Walker, D., Charlton, P., and Freeman, R. (2014c). Surface Integrity of Fluid Jet Polished Tungsten Carbide. *Procedia CIRP*, 13(0), 377-381.
- Beaucamp, A. T. H., Freeman, R. R., Matsumoto, A., and Namba, Y. (2011). Fluid Jet and Bonnet Polishing of Optical Moulds for Application from Visible to X-Ray. *Optical Manufacturing and Testing IX*, 8126.
- Beckstette, K., Kuchel, M., and Heynacher, E. (1989). Large Mirror Figuring and Testing. *Astrophysics and Space Science*, 160(1-2), 207-214.

- Bennett, J. M., Shaffer, J. J., Shibano, Y., and Namba, Y. (1987). Float Polishing of Optical-Materials. *Applied Optics*, 26(4), 696-703.
- Bingham, R. G., Walker, D. D., Kim, D. H., Brooks, D., Freeman, R., and Riley, D. (2000). A novel automated process for aspheric surfaces. *Current Developments in Lens Design and Optical Systems Engineering*, 4093, 445-450.
- Binnig, G., Quate, C. F., and Gerber, C. (1986). Atomic force microscope. *Physical Review Letters*, 56(9), 930.
- Bitter, J. G. A. (1963a). A study of erosion phenomena part I. *Wear*, 6(1), 5-21.
- Bitter, J. G. A. (1963b). A study of erosion phenomena: Part II. *Wear*, 6(3), 169-190.
- Blunn, G. W., Joshi, A. B., Minns, R. J., Lidgren, L., Lilley, P., Ryd, L., . . . Walker, P. S. (1997). Wear in retrieved condylar knee arthroplasties - A comparison of wear in different designs of 280 retrieved condylar knee prostheses. *Journal of Arthroplasty*, 12(3), 281-290.
- Booij, S. M., Fahnle, O. W., Meeder, M., Wons, T., and Braat, J. J. M. (2003). Jules Verne - a new polishing technique related to FJP. *Optical Manufacturing and Testing V*, 5180, 89-100.
- Booij, S. M., van Brug, H., Braat, J. J. M., and Fahnle, O. W. (2002). Nanometer deep shaping with fluid jet polishing. *Optical Engineering*, 41(8), 1926-1931.
- Booij, S. M., van Brug, H., Singh, M., and Braat, J. J. M. (2001). Nanometer accurate shaping with fluid jet polishing. *Optical Manufacturing and Testing Iv*, 4451, 222-232.
- Bridgman, P. W., and Šimon, I. (1953). Effects of very high pressures on glass. *Journal of Applied Physics*, 24(4), 405-413.

- Brilliantov, N. V., and Poschel, T. (1998). Rolling friction of a viscous sphere on a hard plane. *Europhysics Letters*, 42(5), 511-516.
- Brilliantov, N. V., Spahn, F., Hertzsch, J. M., and Poschel, T. (1996). Model for collisions in granular gases. *Phys Rev E Stat Phys Plasmas Fluids Relat Interdiscip Topics*, 53(5), 5382-5392.
- Brinksmeier, E. (1989). State-of-the-art of non-destructive measurement of sub-surface material properties and damages. *Precision Engineering*, 11(4), 211-224.
- Brinksmeier, E., Aurich, J. C., Govekar, E., Heinzl, C., Hoffmeister, H. W., Klocke, F., Wittmann, M. (2006). Advances in modeling and simulation of grinding processes. *Cirp Annals-Manufacturing Technology*, 55(2), 667-696.
- Brinksmeier, E., Cammett, J. T., König, W., Leskovar, P., Peters, J., and Tönshoff, H. K. (1982). Residual stresses—measurement and causes in machining processes. *Cirp Annals-Manufacturing Technology*, 31(2), 491-510.
- Brinksmeier, E., Gläbe, R., and Schönemann, L. (2012). Review on diamond-machining processes for the generation of functional surface structures. *CIRP Journal of Manufacturing Science and Technology*, 5(1), 1-7.
- Brinksmeier, E., Mutlugunes, Y., Klocke, F., Aurich, J. C., Shore, P., and Ohmori, H. (2010). Ultra-precision grinding. *Cirp Annals-Manufacturing Technology*, 59(2), 652-671.
- Bull, S. J. (2006). Using work of indentation to predict erosion behavior in bulk materials and coatings. *Journal of Physics D-Applied Physics*, 39(8), 1626-1634.
- Cambou, B., Chaze, M., and Dedecker, F. (2000). Change of scale in granular materials.

European Journal of Mechanics-A/Solids, 19(6), 999-1014.

Cao, Z. C., and Cheung, C. F. (2014). Theoretical modelling and analysis of the material removal characteristics in fluid jet polishing. *International Journal of Mechanical Sciences*, 89(0), 158-166.

Challen, J. M., and Oxley, P. L. B. (1979). An explanation of the different regimes of friction and wear using asperity deformation models. *Wear*, 53(2), 229-243.

Chaves-Jacob, J., Linares, J. M., and Sprauel, J. M. (2013). Improving tool wear and surface covering in polishing via toolpath optimization. *Journal of Materials Processing Technology*, 213(10), 1661-1668.

Chen, R., Liang, M., Luo, J., Lei, H., Guo, D., and Hu, X. (2011). Comparison of surface damage under the dry and wet impact: Molecular dynamics simulation. *Applied Surface Science*, 258(5), 1756-1761.

Chen, X., McLaury, B. S., and Shirazi, S. A. (2004). Application and experimental validation of a computational fluid dynamics (CFD)-based erosion prediction model in elbows and plugged tees. *Computers & Fluids*, 33(10), 1251-1272.

Chen, Y. (2007). Polishing of polycrystalline diamond composites.

Cheung, C. F., Ho, L. T., Charlton, P., Kong, L. B., To, S., and Lee, W. B. (2010a). Analysis of surface generation in the ultraprecision polishing of freeform surfaces. *Proceedings of the Institution of Mechanical Engineers Part B-Journal of Engineering Manufacture*, 224(B1), 59-73.

Cheung, C. F., Kong, L. B., Ho, L. T., and To, S. (2011). Modelling and simulation of structure surface generation using computer controlled ultra-precision polishing.

Precision Engineering-Journal of the International Societies for Precision Engineering and Nanotechnology, 35(4), 574-590.

Cheung, C. F., Kong, L. B., Ren, M. J., Whitehouse, D., and To, S. (2012). Generalized form characterization of ultra-precision freeform surfaces. *Cirp Annals-Manufacturing Technology*, 61(1), 527-530.

Cheung, C. F., Lee, W. B., Charlton, P., and To, S. (2010b). A Study of Wear Characteristics of Superpolished Orthopaedic Implant Materials Using Ultra-precision Polishing. *Advanced Precision Engineering*, 447-448, 111-115.

Cheung, C. F., Li, H. F., Lee, W. B., To, S., and Kong, L. B. (2007). An integrated form characterization method for measuring ultra-precision freeform surfaces. *International Journal of Machine Tools & Manufacture*, 47(1), 81-91.

Cundall, P. A., and Strack, O. D. L. (1979). A discrete numerical model for granular assemblies. *Geotechnique*, 29, 47-65.

Curodeau, A., Sachs, E., and Caldarise, S. (2000). Design and fabrication of cast orthopedic implants with freeform surface textures from 3-D printed ceramic shell. *Journal of Biomedical Materials Research*, 53(5), 525-535.

Des Ruisseaux, N. R., and Zerkle, R. (1970). Thermal analysis of the grinding process. *Journal of Manufacturing Science and Engineering*, 92(2), 428-433.

Dong-Fang, G., Takeuchi, Y., and Asakawa, N. (1995, 21-27 May 1995). *Dexterous polishing of overhanging sculptured surfaces with a 6-axis control robot*. Paper presented at the Robotics and Automation, 1995. Proceedings., 1995 IEEE International Conference on.

- Drueding, T. W., Bifano, T. G., and Fawcett, S. C. (1995). Contouring Algorithm for Ion Figuring. *Precision Engineering-Journal of the American Society for Precision Engineering*, 17(1), 10-21.
- Dumas, P. (2005). Magnetorheological finishing (optics).
- Dunn, C. R., and Walker, D. D. (2008). Pseudo-random tool paths for CNC sub-aperture polishing and other applications. *Optics Express*, 16(23), 18942-18949.
- Edwards, J. K., McLaury, B. S., and Shirazi, S. A. (2001). Modeling solid particle erosion in elbows and plugged tees. *Journal of Energy Resources Technology-Transactions of the Asme*, 123(4), 277-284.
- Enomoto, T., Satake, U., Miyake, T., and Tabata, N. (2011). A newly developed polishing pad for achieving high surface flatness without edge roll off. *CIRP Annals - Manufacturing Technology*, 60(1), 371-374.
- Evans, A. (2011). Abrasive wear in ceramics: an assessment. *Lawrence Berkeley National Laboratory*.
- Evans, C. J., Paul, E., Dornfeld, D., Lucca, D. A., Byrne, G., Tricard, M., . . . Mullany, B. A. (2003a). Material Removal Mechanisms in Lapping and Polishing. *CIRP Annals - Manufacturing Technology*, 52(2), 611-633.
- Evans, C. J., Paul, E., Dornfeld, D., Lucca, D. A., Byrne, G., Tricard, M., . . . Mullany, B. A. (2003b). Material removal mechanisms in lapping and polishing. *Cirp Annals-Manufacturing Technology*, 52(2), 611-633.
- Fahnle, O. W., and van Brug, H. (1999a). Finishing of optical materials using fluid jet polishing. *Proceedings of the Fourteenth Annual Meeting of the American Society for*

Precision Engineering, 509-512.

Fahnle, O. W., and van Brug, H. (1999b). Fluid Jet Polishing: removal process analysis.

Optical Fabrication and Testing, 3739, 68-77.

Fahnle, O. W., van Brug, H., and Frankena, H. J. (1998). Fluid jet polishing of optical surfaces. *Applied Optics*, 37(28), 6771-6773.

Fang, F. Z., Zhang, X. D., Weckenmann, A., Zhang, G. X., and Evans, C. (2013). Manufacturing and measurement of freeform optics. *Cirp Annals-Manufacturing Technology*, 62(2), 823-846.

Fang, H., Guo, P., and Yu, J. (2006a). Surface roughness and material removal in fluid jet polishing. *Appl Opt*, 45(17), 4012-4019.

Fang, H., Guo, P. J., and Yu, J. C. (2006b). Optimization of the material removal in fluid jet polishing. *Optical Engineering*, 45(5).

Fang, L., Zhao, J., Sun, K., Zheng, D. G., and Ma, D. X. (2009). Temperature as sensitive monitor for efficiency of work in abrasive flow machining. *Wear*, 266(7-8), 678-687.

Fillot, N., Iordanoff, I., and Berthier, Y. (2007). Modelling third body flows with a discrete element method—a tool for understanding wear with adhesive particles. *Tribology International*, 40(6), 973-981.

Finnie, I. (1960). Erosion of surfaces by solid particles. *Wear*, 3(2), 87-103.

Finnie, I. (1995). Some Reflections on the Past and Future of Erosion. *Wear*, 186(1), 1-10.

Finnie, I., and McFadden, D. H. (1978). On the velocity dependence of the erosion of

- ductile metals by solid particles at low angles of incidence. *Wear*, 48(1), 181-190.
- Fu, G. H., Chandra, A., Guha, S., and Subhash, G. (2001). A plasticity-based model of material removal in chemical-mechanical polishing (CMP). *Ieee Transactions on Semiconductor Manufacturing*, 14(4), 406-417.
- Gee, A. E. (1996). Modelling the mechanics of free particulate abrasive polishing from the viewpoint of single-point processes. *Specification, Production, and Testing of Optical Components and Systems*, 2775, 611-618.
- Gnanavelu, A., Kapur, N., Neville, A., and Flores, J. F. (2009). An integrated methodology for predicting material wear rates due to erosion. *Wear*, 267(11), 1935-1944.
- Gnanavelu, A., Kapur, N., Neville, A., Flores, J. F., and Ghorbani, N. (2011). A numerical investigation of a geometry independent integrated method to predict erosion rates in slurry erosion. *Wear*, 271(5-6), 712-719.
- Greenwood, J., and Williamson, J. (1966). Contact of nominally flat surfaces. *Proceedings of the Royal Society of London. Series A. Mathematical and Physical Sciences*, 295(1442), 300-319.
- Griffiths, B. (2001). *Manufacturing surface technology: surface integrity and functional performance*: Elsevier.
- Han, X. (2007). Study micromechanism of surface planarization in the polishing technology using numerical simulation method. *Applied Surface Science*, 253(14), 6211-6216.
- Han, X., and Gan, Y. X. (2011). Analysis the complex interaction among flexible

- nanoparticles and materials surface in the mechanical polishing process. *Applied Surface Science*, 257(8), 3363-3373.
- Harris, D. C. (2011). History of Magnetorheological Finishing. *Window and Dome Technologies and Materials Xii*, 8016.
- Heyliger, P., and McMeeking, R. (2001). Cold plastic compaction of powders by a network model. *Journal of the Mechanics and Physics of Solids*, 49(9), 2031-2054.
- Hilerio, I., Mathia, T., and Alepee, C. (2004). 3D measurements of the knee prosthesis surfaces applied in optimizing of manufacturing process. *Wear*, 257(12), 1230-1234.
- Ho, L. T., Cheung, C. F., and To, S. (2012). An experimental investigation of surface generation using an integrated ultra-precision polishing process and different polishing trajectories. *Proceedings of the Institution of Mechanical Engineers Part B-Journal of Engineering Manufacture*, 226(B2), 203-220.
- Hoover, W. G. (2012). *Computational statistical mechanics*: Elsevier.
- Hu, Z. F., Mao, J. W., and Luo, Y. (2012). Research on LED Lighting Secondary Light Distribution by Using a Freeform Lens. *Advances in Precision Instrumentation and Measurement*, 103, 138-141. doi: DOI 10.4028/www.scientific.net/AMM.103.138
- Huang, C. K., Chiovelli, S., Minev, P., Luo, J. L., and Nandakumar, K. (2008). A comprehensive phenomenological model for erosion of materials in jet flow. *Powder Technology*, 187(3), 273-279.
- Hutchings, I. M. (1976). The ricochet of spheres and cylinders from the surface of water. *International Journal of Mechanical Sciences*, 18(5), 243-247.
- Hutchings, I. M. (1977). Deformation of metal surfaces by the oblique impact of square

- plates. *International Journal of Mechanical Sciences*, 19(1), 45-52.
- Hutchings, I. M. (1992). Tribology: friction and wear of engineering materials.
- Hutchings, I. M. (1993). Mechanisms of Wear in Powder Technology - a Review. *Powder Technology*, 76(1), 3-13.
- Hutchings, I. M., Macmillan, N. H., and Rickerby, D. G. (1981). Further studies of the oblique impact of a hard sphere against a ductile solid. *International Journal of Mechanical Sciences*, 23(11), 639-646.
- Hutchings, I. M., and O'Brien, T. J. (1981). Normal impact of metal projectiles against a rigid target at low velocities. *International Journal of Mechanical Sciences*, 23(5), 255-261.
- Ikawa, N., Shimada, S., Tanaka, H., and Ohmori, G. (1991). An atomistic analysis of nanometric chip removal as affected by tool-work interaction in diamond turning. *Cirp Annals-Manufacturing Technology*, 40(1), 551-554.
- Inasaki, I., Tönshoff, H. K., and Howes, T. D. (1993). Abrasive Machining in the Future. *CIRP Annals - Manufacturing Technology*, 42(2), 723-732.
- Iordanoff, I., Battentier, A., Neauport, J., and Charles, J. L. (2008). A discrete element model to investigate sub-surface damage due to surface polishing. *Tribology International*, 41(11), 957-964.
- Iordanoff, I., Fillot, N., and Berthier, Y. (2005). Numerical study of a thin layer of cohesive particles under plane shearing. *Powder Technology*, 159(1), 46-54.
- Jacobs, S. D. (2007). Manipulating mechanics and chemistry in precision optics finishing. *Science and Technology of Advanced Materials*, 8(3), 153-157.

-
- Jacobs, S. D., Golini, D., Hsu, Y., Puchebner, B. E., Strafford, D., Prokhorov, I. V., . . .
- Kordonski, W. I. (1995). *Magnetorheological finishing: a deterministic process for optics manufacturing*.
- Jafar, R. H. M., Spelt, J. K., and Papini, M. (2013a). Numerical simulation of surface roughness and erosion rate of abrasive jet micro-machined channels. *Wear*, 303(1-2), 302-312.
- Jafar, R. H. M., Spelt, J. K., and Papini, M. (2013b). Surface roughness and erosion rate of abrasive jet micro-machined channels: Experiments and analytical model. *Wear*, 303(1-2), 138-145.
- Jawahir, I. S., Brinksmeier, E., M'Saoubi, R., Aspinwall, D. K., Outeiro, J. C., Meyer, D., Jayal, A. D. (2011). Surface integrity in material removal processes: Recent advances. *CIRP Annals - Manufacturing Technology*, 60(2), 603-626.
- Jeng, Y. R., and Huang, P. Y. (2005). A material removal rate model considering interfacial micro-contact wear behavior for chemical mechanical polishing. *Journal of Tribology-Transactions of the Asme*, 127(1), 190-197.
- Johnson, K. L., and Johnson, K. L. (1987). *Contact mechanics*: Cambridge university press.
- Jones, R. A., and Plante, R. L. (1987). Rapid Fabrication of Large Aspheric Optics. *Precision Engineering-Journal of the American Society for Precision Engineering*, 9(2), 65-70.
- Jones, R. A., and Rupp, W. J. (1990). Rapid Optical Fabrication with Ccos. *Advanced Optical Manufacturing and Testing*, 1333, 34-43.

- Kakinuma, Y., Igarashi, K., Katsura, S., and Aoyama, T. (2013). Development of 5-axis polishing machine capable of simultaneous trajectory, posture, and force control. *Cirp Annals-Manufacturing Technology*, 62(1), 379-382.
- Kanaoka, M., Liu, C., Nomura, K., Ando, M., Takino, H., Fukuda, Y., . . . Yamauchi, K. (2008). Processing efficiency of elastic emission machining for low-thermal-expansion material. *Surface and Interface Analysis*, 40(6-7), 1002-1006.
- Kasai, T., Horio, K., and Kobayashi, A. (1990). Improvement of Conventional Polishing Conditions for Obtaining Super Smooth Surfaces of Glass and Metal Works. *CIRP Annals - Manufacturing Technology*, 39(1), 321-324.
- Keating, A., and Nestic, S. (2001). Numerical prediction of erosion-corrosion in bends. *Corrosion*, 57(7), 621-633.
- Kim, S., Saka, N., and Chun, J.-H. (2014). The Effect of Pad-asperity Curvature on Material Removal Rate in Chemical-mechanical Polishing. *Procedia CIRP*, 14(0), 42-47.
- Kim, S., Saka, N., Chun, J. H., and Shin, S. H. (2013). Modeling and mitigation of pad scratching in chemical–mechanical polishing. *CIRP Annals - Manufacturing Technology*, 62(1), 307-310.
- Klocke, F. (2003). *Modelling and simulation of grinding processes*. Paper presented at the 1st European conference on Grinding.
- Komanduri, R., Chandrasekaran, N., and Raff, L. M. (1999). Some aspects of machining with negative-rake tools simulating grinding: a molecular dynamics simulation approach. *Philosophical Magazine B-Physics of Condensed Matter*

-
- Statistical Mechanics Electronic Optical and Magnetic Properties*, 79(7), 955-968.
- Komanduri, R., Lucca, D. A., and Tani, Y. (1997). Technological Advances in Fine Abrasive Processes. *CIRP Annals - Manufacturing Technology*, 46(2), 545-596.
- Kordonski, W., Shorey, A. B., and Sekeres, A. (2004). *New magnetically assisted finishing method: material removal with magnetorheological fluid jet*.
- Kordonsky, W. I., Prokhorov, I. V., Gorodkin, S. R., Gorodkin, G. R., Gleb, L. K., and Kashevsky, B. E. (1995). Magnetorheological polishing devices and methods: Google Patents.
- Landau, L. D., and Lifshitz, E. M. (1959). *Theory of Elasticity*: Pergamon Press.
- Larsen-Basse, J., and Liang, H. (1999). Probable role of abrasion in chemo-mechanical polishing of tungsten. *Wear*, 233, 647-654.
- Lawn, B., and Wilshaw, R. (1975). Indentation Fracture - Principles and Applications. *Journal of Materials Science*, 10(6), 1049-1081.
- Lawn, B. R., Evans, A., and Marshall, D. (1980). Elastic/plastic indentation damage in ceramics: the median/radial crack system. *Journal of the American Ceramic Society*, 63(9-10), 574-581.
- Lawn, B. R., and Evans, A. G. (1977). A model for crack initiation in elastic/plastic indentation fields. *Journal of Materials Science*, 12(11), 2195-2199.
- Leach, R. (2014). *Fundamental principles of engineering nanometrology*: Elsevier.
- Li, H., Walker, D., Yu, G., and Zhang, W. (2013). Modeling and validation of polishing tool influence functions for manufacturing segments for an extremely large telescope. *Appl Opt*, 52(23), 5781-5787.

- Li, H. Y., Yu, G. Y., Walker, D., and Evans, R. (2011). Modelling and measurement of polishing tool influence functions for edge control. *Journal of the European Optical Society-Rapid Publications*, 6.
- Li, Z., Li, S., Dai, Y., and Peng, X. (2010). Optimization and application of influence function in abrasive jet polishing. *Appl Opt*, 49(15), 2947-2953.
- Lian, J., and Shima, S. (1994). Powder assembly simulation by particle dynamics method. *International journal for numerical methods in engineering*, 37(5), 763-775.
- Liu, G. L., Huang, Z. R., Liu, X. J., and Jiang, D. L. (2010). Removal Behaviors of Different SiC Ceramics during Polishing. *Journal of Materials Science & Technology*, 26(2), 125-130.
- Liu, H., Wang, J., Kelson, N., and Brown, R. J. (2004). A study of abrasive waterjet characteristics by CFD simulation. *Journal of Materials Processing Technology*, 153-154, 488-493.
- Lonardo, P., Trumpold, H., and De Chiffre, L. (1996). Progress in 3D surface microtopography characterization. *Cirp Annals-Manufacturing Technology*, 45(2), 589-598.
- Loth, E. (2008). Drag of non-spherical solid particles of regular and irregular shape. *Powder Technology*, 182(3), 342-353.
- Luedtke, W., and Landman, U. (1994). Stability and collapse of metallic structures on surfaces. *Physical Review Letters*, 73(4), 569.
- Luedtke, W. D., and Landman, U. (1992). Solid and liquid junctions. *Computational Materials Science*, 1(1), 1-24.

- Luo, J. F., and Dornfeld, D. A. (2001). Material removal mechanism in chemical mechanical polishing: Theory and modeling. *Ieee Transactions on Semiconductor Manufacturing*, 14(2), 112-133.
- Luo, J. F., and Dornfeld, D. A. (2003). Effects of abrasive size distribution in chemical mechanical planarization: Modeling and verification. *Ieee Transactions on Semiconductor Manufacturing*, 16(3), 469-476.
- Maekawa, K., and Itoh, A. (1995). Friction and Tool Wear in Nano-Scale Machining - a Molecular-Dynamics Approach. *Wear*, 188(1-2), 115-122.
- Marshall, D. B., Lawn, B. R., and Evans, A. G. (1982). Elastic Plastic Indentation Damage in Ceramics - the Lateral Crack System. *Journal of the American Ceramic Society*, 65(11), 561-566.
- Martin, H. M., Anderson, D. S., Angel, J. R. P., Nagel, R. H., West, S. C., and Young, R. S. (1990). Progress in the Stressed-Lap Polishing of a 1.8-M F/1 Mirror. *Advanced Technology Optical Telescopes Iv, Pts 1 and 2*, 1236, 682-690.
- Matsumura, T., Muramatsu, T., Fueki, S., and Hoshi, T. (2011). Abrasive water jet machining of glass with stagnation effect. *Cirp Annals-Manufacturing Technology*, 60(1), 355-358.
- Menter, F. R. (1994). Two-equation eddy-viscosity turbulence models for engineering applications. *AIAA journal*, 32(8), 1598-1605.
- Mori, Y., Ikawa, N., Okuda, T., and Yamagata, K. (1976). Numerically Controlled Elastic Emission Machining. *Technology Reports of the Osaka University*, 26, 283-294.
- Mori, Y., Yamauchi, K., and Endo, K. (1987). Elastic Emission Machining. *Precision*

- Engineering-Journal of the American Society for Precision Engineering*, 9(3), 123-128.
- Mori, Y., Yamauchi, K., and Endo, K. (1988). Mechanism of Atomic Removal in Elastic Emission Machining. *Precision Engineering-Journal of the American Society for Precision Engineering*, 10(1), 24-28.
- Mori, Y., Yamauchi, K., Endo, K., Ide, T., Toyota, H., Nishizawa, K., and Hasegawa, M. (1990). Evaluation of Elastic Emission Machined Surfaces by Scanning Tunneling Microscopy. *Journal of Vacuum Science & Technology a-Vacuum Surfaces and Films*, 8(1), 621-624.
- Namba, Y., and Tsuwa, H. (1977). Ultra-Fine Finishing of Sapphire Single Crystal. *CIRP Annals - Manufacturing Technology*, 26(1), 325-329.
- Namba, Y., and Tsuwa, H. (1978). Mechanism and Some Applications of Ultra-Fine Finishing. *CIRP Annals - Manufacturing Technology*, 27(1), 511-516.
- Namba, Y., and Tsuwa, H. (1980). Surface Properties of Polished Stainless Steel. *CIRP Annals - Manufacturing Technology*, 29(1), 409-412.
- Namba, Y., Tsuwa, H., Wada, R., and Ikawa, N. (1987). Ultra-Precision Float Polishing Machine. *CIRP Annals - Manufacturing Technology*, 36(1), 211-214.
- Namba, Y., Wada, R., Unno, K., Tsuboi, A., and Okamura, K. (1989). Ultra-Precision Surface Grinder Having a Glass-Ceramic Spindle of Zero-Thermal Expansion. *CIRP Annals - Manufacturing Technology*, 38(1), 331-334.
- Nanz, G., and Camilletti, L. E. (1995). Modeling of Chemical-Mechanical Polishing - a Review. *Ieee Transactions on Semiconductor Manufacturing*, 8(4), 382-389.
- Neilson, J. H., and Gilchrist, A. (1968). Erosion by a stream of solid particles. *Wear*,

II(2), 111-122.

Obikawa, T., and Yamaguchi, M. (2015). Suppression of notch wear of a whisker reinforced ceramic tool in air-jet-assisted high-speed machining of Inconel 718. *Precision Engineering*, 39(0), 143-151.

Olsson, E., Kreiss, G., and Zahedi, S. (2007). A conservative level set method for two phase flow II. *Journal of Computational Physics*, 225(1), 785-807.

Papini, M., and Dhar, S. (2006). Experimental verification of a model of erosion due to the impact of rigid single angular particles on fully plastic targets. *International Journal of Mechanical Sciences*, 48(5), 469-482.

Papini, M., and Spelt, J. K. (2000a). Impact of rigid angular particles with fully-plastic targets Part I: Analysis. *International Journal of Mechanical Sciences*, 42(5), 991-1006.

Papini, M., and Spelt, J. K. (2000b). Impact of rigid angular particles with fully-plastic targets Part II: Parametric study of erosion phenomena. *International Journal of Mechanical Sciences*, 42(5), 1007-1025.

Preston, F. W. (1927). The theory and design of plate glass polishing machines. *J. Soc. Glass Technol.*, 11, 214-256.

Qin, S., Wright, D. K., Kang, J., and Prieto, P. A. (2006). Use of three-dimensional body motion to free-form surface design. *Proceedings of the Institution of Mechanical Engineers Part B-Journal of Engineering Manufacture*, 220(2), 335-339.

Rabinowicz, E. (1965). *Friction and wear of materials*: Wiley.

Rapaport, D. C. (2004). *The art of molecular dynamics simulation*: Cambridge

university press.

Redanz, P., and Fleck, N. A. (2001). The compaction of a random distribution of metal cylinders by the discrete element method. *Acta Materialia*, 49(20), 4325-4335.

Ren, M. J., Cheung, C. F., and Kong, L. B. (2012a). A task specific uncertainty analysis method for least-squares-based form characterization of ultra-precision freeform surfaces. *Measurement Science & Technology*, 23(5).

Ren, M. J., Cheung, C. F., Kong, L. B., and Jiang, X. Q. (2012b). Invariant-Feature-Pattern-Based Form Characterization for the Measurement of Ultraprecision Freeform Surfaces. *Ieee Transactions on Instrumentation and Measurement*, 61(4), 963-973.

Rentsch, R., and Inasaki, I. (1994). Molecular dynamics simulation for abrasive processes. *Cirp Annals-Manufacturing Technology*, 43(1), 327-330.

Rentsch, R., and Inasaki, I. (1995). Investigation of surface integrity by molecular dynamics simulation. *Cirp Annals-Manufacturing Technology*, 44(1), 295-298.

Roswell, A., Xi, F., and Liu, G. (2006). Modelling and analysis of contact stress for automated polishing. *International Journal of Machine Tools and Manufacture*, 46(3-4), 424-435.

Ruff, A. W., and Wiederhorn, S. (1979). Erosion by solid particle impact: DTIC Document.

Runnels, S. R. (1994). Feature-Scale Fluid-Based Erosion Modeling for Chemical-Mechanical Polishing. *Journal of the Electrochemical Society*, 141(7), 1900-1904.

- Runnels, S. R., and Eyman, L. M. (1994). Tribology Analysis of Chemical-Mechanical Polishing. *Journal of the Electrochemical Society*, 141(6), 1699-1701.
- Saka, N., Eusner, T., and Chun, J. H. (2008). Nano-scale scratching in chemical–mechanical polishing. *CIRP Annals - Manufacturing Technology*, 57(1), 341-344.
- Saka, N., Eusner, T., and Chun, J. H. (2010). Scratching by pad asperities in chemical–mechanical polishing. *CIRP Annals - Manufacturing Technology*, 59(1), 329-332.
- Schinhaerl, M., Rascher, R., Stamp, R., Smith, G., Smith, L., Pitschke, E., and Sperber, P. (2007). Filter algorithm for influence functions in the computer controlled polishing of high-quality optical lenses. *International Journal of Machine Tools and Manufacture*, 47(1), 107-111.
- Schinhaerl, M., Rascher, R., Stamp, R., Smith, L., Smith, G., Sperber, P., and Pitschke, E. (2008a). Utilisation of time-variant influence functions in the computer controlled polishing. *Precision Engineering-Journal of the International Societies for Precision Engineering and Nanotechnology*, 32(1), 47-54.
- Schinhaerl, M., Smith, G., Stamp, R., Rascher, R., Smith, L., Pitschke, E., . . . Geiss, A. (2008b). Mathematical modelling of influence functions in computer-controlled polishing: Part I. *Applied Mathematical Modelling*, 32(12), 2888-2906.
- Schinhaerl, M., Smith, G., Stamp, R., Rascher, R., Smith, L., Pitschke, E., . . . Geiss, A. (2008c). Mathematical modelling of influence functions in computer-controlled polishing: Part II. *Applied Mathematical Modelling*, 32(12), 2907-2924.

- Sheldon, G. L., and Kanhere, A. (1972). An investigation of impingement erosion using single particles. *Wear*, 21(1), 195-209.
- Shi, C. Y., Yuan, J. H., Wu, F., Hou, X., and Wan, Y. J. (2010). Material removal model of vertical impinging in fluid jet polishing. *Chinese Optics Letters*, 8(3), 323-325.
- Shi, C. Y., Yuan, J. H., Wu, F., and Wan, Y. J. (2011). Ultra-precision figuring using submerged jet polishing. *Chinese Optics Letters*, 9(9).
- Shimada, S., Ikawa, N., Inamura, T., Takezawa, N., Ohmori, H., and Sata, T. (1995). Brittle-ductile transition phenomena in microindentation and micromachining. *Cirp Annals-Manufacturing Technology*, 44(1), 523-526.
- Shiou, F. J., and Asmare, A. (2015). Parameters optimization on surface roughness improvement of Zerodur optical glass using an innovative rotary abrasive fluid multi-jet polishing process. *Precision Engineering*, 42, 93-100.
- Slikkerveer, P. J., Bouten, P. C. P., Veld, F. H. I., and Sholten, H. (1998). Erosion and damage by sharp particles. *Wear*, 217(2), 237-250.
- Song, J. F., Yao, Y. G., Xie, D. G., Gao, B., and Yuan, Z. J. (2008). Effects of Polishing Parameters on Material Removal for Curved Optical Glasses in Bonnet Polishing. *Chinese Journal of Mechanical Engineering*, 21(5), 29-33.
- Sousa, F. (2014). Polishing. In L. Laperrière and G. Reinhart (Eds.), *CIRP Encyclopedia of Production Engineering* (pp. 957-962): Springer Berlin Heidelberg.
- Stroud, M. F., and Wilman, H. (1962). The proportion of the groove volume removed as wear in abrasion of metals. *British Journal of Applied Physics*, 13(4), 173.
- Su, C. T., Wong, J. T., and Tsou, S. C. (2005). A process parameters determination

- model by integrating artificial neural network and ant colony optimization. *Journal of the Chinese Institute of Industrial Engineers*, 22(4), 346-354.
- Su, Y. T., Liu, S. H., and Chen, Y. W. (2001). A preliminary study on smoothing efficiency of surface irregularities by hydrodynamic polishing process. *Wear*, 249(9), 808-820.
- Sun, J., Zhang, L. C., Mai, Y. W., Payor, S., and Hogg, M. (2000). Material removal in the optical polishing of hydrophilic polymer materials. *Journal of Materials Processing Technology*, 103(2), 230-236.
- Sundararajan, G. (1991). An Analysis of the Erosion-Oxidation Interaction Mechanisms. *Wear*, 145(2), 251-282.
- Tam, H. Y., Cheng, H., and Dong, Z. (2013). Peano-like paths for subaperture polishing of optical aspherical surfaces. *Appl Opt*, 52(15), 3624-3636.
- Tam, H. Y., and Cheng, H. B. (2010). An investigation of the effects of the tool path on the removal of material in polishing. *Journal of Materials Processing Technology*, 210(5), 807-818.
- Tam, H. Y., Lui, O. C. H., and Mok, A. C. K. (1999). Robotic polishing of free-form surfaces using scanning paths. *Journal of Materials Processing Technology*, 95(1-3), 191-200.
- Thompson, T. L., and Clark, N. N. (1991). A Holistic Approach to Particle Drag Prediction. *Powder Technology*, 67(1), 57-66.
- Thornton, C., and Antony, S. (1998). Quasi-static deformation of particulate media. *Philosophical Transactions of the Royal Society A: Mathematical, Physical and*

Engineering Sciences, 2763-2782.

Tichy, J., Levert, J. A., Shan, L., and Danyluk, S. (1999). Contact mechanics and lubrication hydrodynamics of chemical mechanical polishing. *Journal of the Electrochemical Society*, 146(4), 1523-1528.

Toshiro, K. D. (2006). Polishing Technology *Handbook of Lapping and Polishing*: CRC Press.

Tsai, F. C., Yan, B. H., Kuan, C. Y., and Huang, F. Y. (2008). A Taguchi and experimental investigation into the optimal processing conditions for the abrasive jet polishing of SKD61 mold steel. *International Journal of Machine Tools & Manufacture*, 48(7-8), 932-945.

Tsai, M. J., Huang, J. F., and Kao, W. L. (2009). Robotic polishing of precision molds with uniform material removal control. *International Journal of Machine Tools & Manufacture*, 49(11), 885-895.

van Brug, H., Dorrepaal, N., and Saunders, I. (2003). Polishing robot based on FJP with in-situ monitoring system. *Optical Manufacutring and Testing V*, 5180, 101-106.

van Brug, H., Groeneveld, M., Booij, S. M., and Braat, J. J. M. (2002). In-process measurements of material removal in fluid jet polishing. *Interferometry Xi: Applications*, 4778, 243-250.

Venkatesh, V., Inasaki, I., Toenshof, H., Nakagawa, T., and Marinescu, I. (1995). Observations on polishing and ultraprecision machining of semiconductor substrate materials. *Cirp Annals-Manufacturing Technology*, 44(2), 611-618.

Vora, H., Orent, T., and Stokes, R. (1982). Mechanochemical polishing of silicon

nitride. *Journal of the American Ceramic Society*, 65(9), c140-c141.

Walker, D. D., Beaucamp, A. T. H., Brooks, D., Freeman, R., King, A., McCavana, G., . . . Simms, J. (2002a). Novel CNC polishing process for control of form and texture on aspheric surfaces. *Current Developments in Lens Design and Optical Engineering Iii*, 4767, 99-105.

Walker, D. D., Brooks, D., Freeman, R., King, A., McCavana, G., Morton, R., . . . Simms, J. (2001). The first aspheric form and texture results from a production machine embodying the Precession Process. *Optical Manufacturing and Testing Iv*, 4451, 267-276.

Walker, D. D., Freeman, R., McCavana, G., Morton, R., Riley, D., Simms, J., . . . King, A. (2002b). The Zeeko/UCL process for polishing large lenses and prisms. *Large Lenses and Prism*, 4411, 106-111.

Wallace, M. S., Dempster, W. M., Scanlon, T., Peters, J., and McCulloch, S. (2004). Prediction of impact erosion in valve geometries. *Wear*, 256(9-10), 927-936.

Wang, C., Wang, Z., Yang, X., Sun, Z., Peng, Y., Guo, Y., and Xu, Q. (2014a). Modeling of the static tool influence function of bonnet polishing based on FEA. *International Journal of Advanced Manufacturing Technology*, 74(1-4), 341-349.

Wang, C., Yang, W., Wang, Z., Yang, X., Hu, C., Zhong, B., . . . Xu, Q. (2014b). Dwell-time algorithm for polishing large optics. *Appl Opt*, 53(21), 4752-4760.

Wang, C. J., Yang, W., Guo, Y. B., Wang, Z. Z., and Zheng, M. J. (2012). Research on Parameters of Bonnet Polishing Based on FEA. *Mems, Nano and Smart Systems, Pts 1-6*, 403-408, 486-490.

- Wang, G. J., and Chou, M. H. (2005). A neural-Taguchi-based quasi time-optimization control strategy for chemical-mechanical polishing processes. *International Journal of Advanced Manufacturing Technology*, 26(7-8), 759-765.
- Wang, J., Nguyen, T., and Pang, K. L. (2009a). Mechanisms of microhole formation on glasses by an abrasive slurry jet. *Journal of Applied Physics*, 105(4), 044906-044906.
- Wang, M. H., Huang, C. U., Nandakumar, K., Minev, P., Luo, J., and Chiovelli, S. (2009b). Computational fluid dynamics modelling and experimental study of erosion in slurry jet flows. *International Journal of Computational Fluid Dynamics*, 23(2), 155-172.
- Wang, Y. T., and Wang, C. P. (1999, 1999). *Development of a polishing robot system*. Paper presented at the Emerging Technologies and Factory Automation, 1999. Proceedings. ETFA '99. 1999 7th IEEE International Conference on.
- West, S. C., Martin, H. M., Nagel, R. H., Young, R. S., Davison, W. B., Trebisky, T. J., . . . Hille, B. B. (1994). Practical Design and Performance of the Stressed-Lap Polishing Tool. *Applied Optics*, 33(34), 8094-8100.
- Whitehouse, D. J. (1994). *Handbook of surface metrology*: CRC Press.
- Withers, P. J., Turski, M., Edwards, L., Bouchard, P. J., and Buttle, D. J. (2008). Recent advances in residual stress measurement. *International Journal of Pressure Vessels and Piping*, 85(3), 118-127.
- Wu, B., and Wang, J.-J. J. (2009). A neuro-fuzzy approach to generating mold/die polishing sequences. *Journal of Materials Processing Technology*, 209(7), 3241-3250.
- Xi, F. F., and Zhou, D. (2005). Modeling surface roughness in the stone polishing

- process. *International Journal of Machine Tools & Manufacture*, 45(4-5), 365-372.
- Xie, Y. S., and Bhushan, B. (1996). Effects of particle size, polishing pad and contact pressure in free abrasive polishing. *Wear*, 200(1-2), 281-295.
- Yan, B. H., Tsai, F. C., Sun, L. W., and Hsu, R. T. (2008). Abrasive jet polishing on SKD61 mold steel using SiC coated with Wax. *Journal of Materials Processing Technology*, 208(1-3), 318-329.
- Yongqi, F., and Bryan, N. K. A. (2000). Investigation of 3D microfabrication characteristics by focused ion beam technology in silicon. *Journal of Materials Processing Technology*, 104(1-2), 44-47.
- Yu, Y. F., Liu, X. R., Wu, J. H., and Meng, H. B. (2010). Comparison among Turbulence Models for a Novel Static Circulating Jet Mixer. *Advanced Mechanical Engineering, Pts 1 and 2*, 26-28, 382-385.
- Zeng, S. Y., and Blunt, L. (2014). Experimental investigation and analytical modelling of the effects of process parameters on material removal rate for bonnet polishing of cobalt chrome alloy. *Precision Engineering-Journal of the International Societies for Precision Engineering and Nanotechnology*, 38(2), 348-355.
- Zhang, Z., and Kleinstreuer, C. (2003). Low-Reynolds-number turbulent flows in locally constricted conduits: A comparison study. *AIAA journal*, 41(5), 831-840.
- Zhao, J., Zhan, J. M., Jin, R. C., and Tao, M. Z. (2000). An oblique ultrasonic polishing method by robot for free-form surfaces. *International Journal of Machine Tools & Manufacture*, 40(6), 795-808.
- Zhao, Y., and Chang, L. (2002). A micro-contact and wear model for

chemical–mechanical polishing of silicon wafers. *Wear*, 252(3–4), 220-226.

Zheng, Q. J., Zhu, H. P., and Yu, A. B. (2011). Finite element analysis of the rolling friction of a viscous particle on a rigid plane. *Powder Technology*, 207(1-3), 401-406.

Zum Gahr, K. H. (1988). Modelling of two-body abrasive wear. *Wear*, 124(1), 87-103.

Zum Gahr, K. H. (1981). Formation of Wear Debris by the Abrasion of Ductile Metals. *Wear*, 74(2), 353-373.